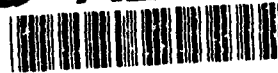AD-A257 511

SUPERLATTICES FOR INFRARED DETECTORS

R.H. MILES

Hughes Research Laboratories

3011 Malibu Canyon Road

Malibu, California 90265

October 1992

Final Report

Contract N00014-89-C-0203

September 1989 through October 1992

DTIC
ELECTE
NOV16 1992
S E D

100 92-28942

92

REPORT DOCUMENTATION PAGE

Form Approved
OMB No. 0704-0188

1a. REPORT SECURITY CLASSIFICATION Unclassified		1b. RESTRICTIVE MARKINGS			
2a. SECURITY CLASSIFICATION AUTHORITY		3. DISTRIBUTION / AVAILABILITY OF REPORT			
2b. DECLASSIFICATION / DOWNGRADING SCHEDULE					
4. PERFORMING ORGANIZATION REPORT NUMBER(S) N00014-89-C-0203		5. MONITORING ORGANIZATION REPORT NUMBER(S)			

6a. NAME OF PERFORMING ORGANIZATION Hughes Research Laboratories	6b. OFFICE SYMBOL (If applicable)	7a. NAME OF MONITORING ORGANIZATION Office of Naval Research
6c. ADDRESS (City, State, and ZIP Code) 3011 Malibu Canyon Road Malibu, CA 90265		7b. ADDRESS (City, State, and ZIP Code) Department of the Navy 800 N. Quincy Arlington, VA 22217-5000
8a. NAME OF FUNDING / SPONSORING ORGANIZATION	8b. OFFICE SYMBOL (If applicable)	9. PROCUREMENT INSTRUMENT IDENTIFICATION NUMBER

8c. ADDRESS (City, State, and ZIP Code)	10. SOURCE OF FUNDING NUMBERS			
	PROGRAM ELEMENT NO.	PROJECT NO.	TASK NO.	WORK UNIT ACCESSION NO.

11. TITLE (Include Security Classification)

SUPERLATTICES FOR INFRARED DETECTORS

12. PERSONAL AUTHOR(S)
Miles, R.H.

13a. TYPE OF REPORT Final	13b. TIME COVERED FROM 9/89 TO 10/92	14. DATE OF REPORT (Year, Month, Day) 10/30/92	15. PAGE COUNT 93

16. SUPPLEMENTARY NOTATION

17.	COSATI CODES		18. SUBJECT TERMS (Continue on reverse if necessary and identify by block number)
FIELD	GROUP	SUB-GROUP	infrared, detector, stained layer, superlattice

19. ABSTRACT (Continue on reverse if necessary and identify by block number)

GaInSb/InAs superlattices have been grown and analyzed for use as high performance, high operating temperature 8 to 12 μm infrared detectors. Optical and transport properties favorable for long wavelength IR detection have been measured, and preliminary photoconductive and photovoltaic device structures have been fabricated and tested. Our results underscore the considerable potential of GaInSb/InAs superlattices to achieve detectivities comparable to HgCdTe at considerably higher operating temperatures. Such an improvement would be of significant benefit, both in reduced cost and complexity, to high performance DoD IR sensing systems.

Molecular beam epitaxial (MBE) growth techniques were developed, yielding superlattices of exceptionally high structural quality, with uncompensated background doping in the low-to-mid 10^{15} cm^{-3} range,

20. DISTRIBUTION / AVAILABILITY OF ABSTRACT ☐ UNCLASSIFIED / UNLIMITED ☒ SAME AS RPT. ☐ DTIC USERS	21. ABSTRACT SECURITY CLASSIFICATION	
22a. NAME OF RESPONSIBLE INDIVIDUAL Larry Cooper	22b. TELEPHONE (Include Area Code) (703) 696-4215	22c. OFFICE SYMBOL

DD Form 1473, JUN 86   Previous editions are obsolete   SECURITY CLASSIFICATION OF THIS PAGE

UNCLASSIFIED

19. (continued)

n-type. Methods for silicon doping the superlattices were established, allowing n-on-p and p-on-n photojunctions to be grown. Superlattice energy gaps were shown to span the infrared, and a 10-μm absorption coefficient comparable to that of HgCdTe was measured, in agreement with theory. Initial unpassivated photovoltaic test devices show $R_0A = 0.1$ Ω-cm^2 at 77K, for a 12-μm cutoff.

Accesion For		
NTIS CRA&I	☒	
DTIC TAB	☐	
Unannounced	☐	
Justification		
By		
Distribution /		
Availability Codes		
Dist	Avail and / or Special	
A-1		

Statement A per Telecon
Larry Cooper ONR/Code 1114
Arlington, VA 22217-5000

NWW 11-16-92

CONTENTS

CONTENTS (Continued)

ILLUSTRATIONS

ILLUSTRATIONS (continued)

Section 1
INTRODUCTION AND OVERVIEW

1.1 PROGRAM MOTIVATION AND GOALS

It was the goal of this program to demonstrate the feasibility of GaInSb/InAs superlattices for infrared detector applications in the 8-12 μm region of the spectrum. At the inception of the program, calculations had shown these to be promising structures for long wavelength applications requiring high detectivity and/or operating temperature,[1,2] but no such superlattices had been grown, and no devices had been demonstrated. Under this and the coupled Caltech program (No. N00014-89-J-3196), GaInSb/InAs superlattices were to be grown, their optical and electronic properties examined and compared with theory, and preliminary detector structures fabricated and tested.

Interest in long wavelength infrared (LWIR) detectors based on GaInSb/InAs superlattices derives from several predicted benefits:[3]

- increased operating temperature relative to current technology

- performance equivalent to, or superior to, current state-of-the-art

- cutoff wavelength selectable over 8-20+ μm

- compatibility with mainline III-V electronics

- robust material

- uniformity superior to that of other tunable detectors

While this potential will not be achieved without considerable further development, the improvements over current technology exceed those promised by any competing advanced IR detector structure.

Expected increases in the ultimate operating temperature and/or performance of GaInSb/InAs superlattice -based detectors come from a suppression of intrinsic impact ionization noise processes in these structures and a reduction in tunneling leakage currents. Recent calculations[4] have shown Auger lifetimes in 10 μm GaInSb/InAs superlattices to be approximately 10^3 longer than in HgCdTe (e.g. for p-type structures doped at 3×10^{16} cm^{-3}, @ 77 K). Such a difference implies that performance obtainable in Auger-limited (state-of-the-art) HgCdTe detectors operating at 120 K could be achieved at room temperature in ideal GaInSb/InAs superlattice detectors. Although this improvement in operating temperature will only be realized in structures of substantially higher quality than presently obtainable, the potential of this system exceeds that of any other presently under consideration. Further performance benefits are to be derived from

the considerable magnitude of the electron effective masses in these superlattices,[5] which are approximately 0.02-0.05 m_e. These values exceed the 0.0088 m_e effective mass of 10 μm HgCdTe, and should suppress tunnel noise currents in a photovoltaic detector under an applied bias.

Improvements in material uniformity have been predicted for GaInSb/InAs superlattices,[3] based upon the precise layer thickness control afforded by molecular beam epitaxy (MBE). These gains are increasingly significant at longer wavelengths; for a given uniformity specification, GaInSb/InAs superlattices with gaps beyond 12 μm can tolerate variations in growth fluxes >10 times as great as can be tolerated in HgCdTe.

Last, the benefits of fabricating detectors from a robust III-V semiconductor are considerable. These superlattices promise improved stability under thermal cycling, and offer the possibility of direct integration of a detector with III-V readout electronics. Compatibility with a mature III-V processing technology is also expected to be of benefit during development of an effective detector pixel delineation and passivation process.

1.2 RELEVANCE TO DoD SYSTEMS

LWIR detectors based on GaInSb/InAs superlattices offer several significant advantages for infrared imaging applications at 8-12 μm and beyond. Brought to maturity, these detectors would relieve or eliminate the stringent cooling requirements of current HgCdTe or extrinsic systems. If realized, such an improvement would dramatically lower the cost and complexity of high performance IR systems, and would enable numerous applications currently precluded by the size, weight, or power requirements of thermoelectric coolers. Further, GaInSb/InAs superlattices offer hope for a single technology spanning the LWIR and VLWIR spectral regions, superceding both HgCdTe and extrinsic detector systems in most applications (the exceptions are those applications demanding the uniformity of response afforded by extrinsic detectors, of fixed cutoff wavelength).

Of practical importance to large area staring arrays is the uniformity intrinsic to GaInSb/InAs superlattices, relative to other tunable detectors. Order-of-magnitude gains in uniformity translate into improved array yield and reduced complexity for non-uniformity correction electronics, and would allow application of these detectors at wavelengths longer than those practically accessible to HgCdTe.

1.3 PROGRAM APPROACH

Efforts to develop GaInSb/InAs superlattice detectors at Hughes were closely coupled to Caltech's superlattice growth and modeling program. Initially, structures grown at Caltech were characterized by structural, electrical, and optical experiments at Hughes. When Caltech's

growth studies yielded high-quality (100) superlattices on GaAs substrates, growth technology was transferred to Hughes. Further material development and characterization was performed at Hughes, and initial photoconductive and photovoltaic device structures were fabricated and tested.

1.4 KEY RESULTS

Under the coupled Hughes/Caltech DARPA/ONR contracts, we became the first group to successfully grow GaInSb/InAs superlattices, and have played the leading role in the structural and doping studies that have ensued. To date, we have grown almost 90 GaInSb/InAs superlattices; on GaSb, InP, and GaAs substrates. We have demonstrated growth of structurally ideal superlattices showing negligible interdiffusion, a high degree of regularity, and submonolayer uniformity control, and have established the essentially dislocation-free nature of structures grown on GaSb substrates.[6] This represents, to our knowledge, the first time that any semiconductor superlattice with this level of strain (2%) has been grown with this degree of structural perfection. We have also shown that the superlattices can be readily and controllably doped n-type with Si, by doping only the InAs layers within a superlattice.[7] (P-type doping with Be is well established in these materials.) Doping levels as high as the 10^{18}'s are readily achieved. Our doping work has enabled us to grow GaInSb/InAs superlattice photojunctions.

Ours are the first experimental studies of the long wavelength properties of GaInSb/InAs superlattices. Photoconductivity, photoluminescence, optical transmission, and Hall measurements[8,9] have been used to enumerate the dependences of energy band gap on layer thicknesses and compositions, and to establish that 8-12 μm gaps can be obtained for modest layer thicknesses and strains. We have measured the optical absorption coefficient to be comparable to that of HgCdTe in the 8-12 μm region. Our contract effort in this area has been complemented by modeling and basic work carried out under IR&D funds, which has enabled us to correlate experimental band structure results with theory. Predictions of favorable effective masses in this system (small enough to allow good perpendicular transport, but sufficiently large to greatly suppress noise derived from electron tunneling currents) have been confirmed; we have obtained measurements of electron effective masses of approximately 0.03 m_e, in a collaborative effort with the Naval Research Laboratory.[5]

Our long wavelength superlattices are routinely analyzed by fabricating and evaluating individual photoconductive devices. Recently, we have begun to apply expertise in the passivation of III-V detectors to the development of competitive photovoltaic devices. We are examining differences in the performances of unpassivated and nitride- or oxide-passivated 8-12 μm photojunctions, and are analyzing characteristics of detectors fabricated by both wet and dry processes. In addition, we have pursued ion implantation studies that promise both pixel

delineation in planar devices, and effective alternative doping schemes; we have demonstrated n-type conductivity with implanted Si, and p-type conductivity with implanted Be. We anticipate that our efforts will lead to substantial improvements over the R_oA of 0.1 Ohm-cm^2 measured at 80K in initial unpassivated 12 μm devices.

1.5 FUTURE WORK

Further development of detectors based on these superlattices is planned under a new DARPA/ONR contract. The ultimate goal of this program is to develop a 128×128 detector array, sensitive in the 8-12 μm spectral region. The program consists of three tasks, directed towards improving the properties and uniformity of the materials, tailoring the performance of individual detectors, and developing a focal plane array fabrication process.

Section 2
MBE GROWTH OF GaInSb/InAs SUPERLATTICES

2.1 GROWTH

All of the superlattices studied in this program were grown by MBE. Samples were grown in similar Perkin Elmer 430 systems at Hughes and Caltech, and, more recently, in a new VG VATH 80 MK II system dedicated to antimonide heterostructures at HRL. Each of the growth systems was equipped with both arsenic and antimony crackers. Measurements of substrate temperature were obtained using a thermocouple, which was in contact either with a molybdenum block (in the case of indium-soldered substrates), or a heat diffuser (in the case of indium-free substrate mounts). In either case, thermocouple readings were calibrated to optical pyrometer readings above 500°C. At lower substrate temperatures, a transition in the GaSb surface reconstruction under an Sb_2 flux from 1×3 to 1×5 was used as a point of calibration for thermocouple readings. Nominal growth rates were calibrated via bulk film thickness measurements and RHEED oscillations measured during homoepitaxial growth of GaAs and InAs. A "nude" ion gauge was used to monitor the Sb_2 and As_2 fluxes.

Table I lists GaInSb/InAs superlattices grown and/or characterized at HRL, and buffer layers fabricated under this contract. Characterization techniques applied to each sample are summarized in the table. 89 superlattices were grown in all, with $Ga_{1-x}In_xSb$ compositions of $x=0.0-0.35$, typical GaInSb layer thicknesses of 25 Å, and InAs layers 25-55 Å thick.

Superlattices were grown on (100)-oriented GaAs, InP, and GaSb substrates. Growth of superlattices on GaAs or InP wafers required buffer layer schemes to relax stresses derived from the lattice mismatch between the substrates and superlattices. Initially, some superlattices grown on GaAs wafers employed relaxed InAs buffer layers. However, GaSb buffers were found to yield superior structural quality, and were used exclusively after the first several growths, regardless of the substrate. Figure 1 illustrates typical layer schemes employed in growth of the superlattices.

Growth of samples on GaAs wafers commenced with deposition of 1000-3000 Å of GaAs, at a substrate temperature of 600°C. A highly strained, short period superlattice was then grown. Such a procedure has been shown previously to improve buffer layer quality in some instances.[10,11] Initially, a five period, 2 monolayer / 2 monolayer $In_{0.7}Ga_{0.3}As$/GaAs short period superlattice was grown at 520°C, followed by a 0.5 μm thick InAs buffer grown at 450-520°C. However, GaSb buffers were ultimately found to yield better structural quality than

5

TABLE I. List of samples grown by molecular beam epitaxy under contract and IR&D funding. Ex situ characterization techniques used on each sample are listed, including: x-ray diffraction (XRD), temperature dependent Hall (Hall), transmission electron microscopy (TEM), photoluminescence (PL), spectral photoconductivity (PC), spectral photovoltaic (PV), optical transmission (a), and current-voltage (I-V). A brief description of the purpose for growth of each sample is also listed.

Sample ID	Ex situ Characterization	Purpose
III-204	XRD,Hall,PL,PC,TEM	GaSb/InAs superlattice standard for comparison
III-207	XRD	GaInSb/InAs superlattice, determine growth params
III-209	XRD	Determine superlattice growth parameters
III-212	XRD	Determine superlattice growth parameters
III-215	XRD	Determine superlattice growth parameters
III-235	XRD	Determine superlattice growth parameters
III-241	XRD	Determine superlattice growth parameters
III-244	XRD	Determine superlattice growth parameters
III-245	XRD	Determine superlattice growth parameters
III-247	XRD	Determine superlattice growth parameters
III-250	XRD	Determine superlattice growth parameters
III-262	XRD, Hall, PL, PC, TEM	Determine superlattice growth params, 1st success
III-270	XRD, PL, PC	Demonstrate 8-12 micron energy gap
III-291	XRD, PC	Demonstrate 15+ micron energy gap
III-309	XRD	GaInSb/InAs superlattice on In-free substrate
III-314	XRD, PC	GaInSb/InAs superlattice on In-free substrate
III-322	XRD, PC, a	Determine absorption coefficient
III-354	XRD, PC, Hall	$Ga_{1-x}In_xSb$/InAs superlattice on InP with higher x
III-366	XRD, PC, Hall	$Ga_{1-x}In_xSb$/InAs superlattice with higher x
III-367	XRD	$Ga_{1-x}In_xSb$/InAs superlattice with higher x
TCH533	XRD	First GaSb growth at HRL
TCH534	XRD	First GaSb growth on InP at HRL
TCH538	XRD, Hall	First GaInSb/InAs superlattice at HRL
TCH542	XRD	Determine superlattice growth parameters
TCH544	XRD	Determine superlattice growth parameters
TCH546	XRD	Determine superlattice growth parameters
TCH564	XRD	Det. growth params, 1st 8-12 micron sls at HRL
TCH566	XRD, Hall, PC	8-12 micron sls
TCH571	XRD	Work on GaSb buffer structural quality
TCH573	XRD	Work on GaSb buffer structural quality
TCH574	XRD	8-12 micron sls
TCH579	XRD, Hall	First superlattice growth on GaSb substrate

Table I. List of samples grown by molecular beam epitaxy (Continued)

Sample ID	*Ex situ* Characterization	Purpose
TCH581	XRD	Work on GaSb buffer structural quality
TCH582	XRD, Hall	Work on GaSb buffer structural quality
TCH588	XRD, Hall	1st silicon doped superlattice (n-type)
TCH601	XRD, I-V	1st GaInSb/InAs superlattice pn junction
TCH618	XRD, I-V, PV	GaInSb/InAs superlattice pn junction
TCH619	XRD	Work on GaSb buffer structural quality
TCH631	XRD, Hall,TEM	Calibration sls
TCH632	XRD	Work on GaSb buffer structural quality
TCH646	XRD	Work on GaSb buffer structural quality
TCH661	XRD, Hall	calibration sls
TCH680	XRD	calibration sls
III-397	XRD, Hall	RHEED studies
TCH697	XRD	calibration sls
TCH717	XRD	calibration sls
TCH721	XRD, Hall	AlGaSb capped sls
TCH732	XRD	calibration sls
TCH749	XRD, Hall	thin, silicon doped sls
TCH750	XRD	1st superlattice on radiatively heated GaSb
TCH756	XRD, Hall	superlattice with half InSb-like interfaces
TCH757	XRD	determine sls growth params on rad. heat GaSb
TCH761	XRD, Hall	sls with all InSb-like interfaces
TCH762	XRD, Hall, TEM	superlattice on rad. heat GaSb (high structural qual.)
TCH768	XRD, Hall	sls with all GaInAs-like interfaces
TCH775	XRD, Hall	silicon doped sls on GaSb substrate
TCH794	XRD, Hall	sls with half InSb-like, half GaInAs-like interfaces
TCH795	XRD, Hall	opposite of TCH794
TCH806	XRD, Hall, PL, PC	sls, working on lowering background doping
TCH823	XRD, Hall	reduced strain interfaces
TCH834	XRD, Hall	sls, working on lowering background doping
TCH836	XRD, Hall	reduced strain interfaces
III-413	XRD	RHEED studies
TCH865	XRD, Hall	sls, system problem during growth
TCH887	XRD, Hall	calibration sls
TCH890	XRD, Hall	sls grown with GaSb cap layer
TCH893	XRD, Hall	repeat of TCH890 (reproducibility check)
TCH899	XRD, Hall	sls grown without growth interrupts at interfaces

Table I. List of samples grown by molecular beam epitaxy (Concluded)

Sample ID	*Ex situ* Characterization	Purpose
TCH901	XRD, Hall	sls, working on lowering background doping
TCH902	XRD, Hall	sls with GaInAs-like interfaces and GaSb cap
TCH903	XRD, Hall	sls with As-soak at each interface
III-430	XRD, Hall	RHEED studies
III-432	XRD, Hall	RHEED studies
III-433	XRD, Hall	RHEED studies
III-437	XRD, Hall	RHEED studies
III-451	XRD, Hall	RHEED studies
Sb012	XRD, Hall	determine superlattice growth params on VG system
Sb016	XRD, Hall	calibration sls
Sb018	XRD, Hall ,a	thick sls for optical transmission measurements
Sb021	XRD, I-V	superlattice pn junction with AlGaSb(p) cap layer
Sb022	XRD, I-V	superlattice pn junction with GaSb(p) cap layer
Sb025	XRD, I-V	superlattice pn junction with GaSb(p) cap layer
Sb026	XRD, Hall	sls, GaInSb layers doped with silicon
Sb027	XRD, Hall	superlattice with AlGaSb(p) cladding layers
Sb028	XRD, Hall	sls, working on lowering background doping
Sb030	XRD, Hall, a	thick sls for optical transmission measurement
Sb031	XRD, Hall	thick sls with InSb-like interfaces
Sb033	XRD, Hall	sls with nearly InSb-like interfaces
Sb036	XRD, Hall	sls with InSb-like interfaces
Sb043	XRD, Hall	calibration sls
Sb045	XRD, Hall	reproducibility check and calibration sls
Sb046	XRD, Hall	sls, working on lowering background doping
Sb048	XRD, Hall	sls with InSb-like interfaces
Sb053	XRD, I-V	GaSb pn junction
Sb055	XRD, Hall	sls, working on lowering background doping
Sb057	XRD, Hall	superlattice with GaSb spacer layers
Sb061	XRD, Hall	sls, GaInSb layers doped with silicon
Sb062	XRD	GaSb on GaSb(n) substrate (test pregrowth prep)
Sb063	XRD	superlattice with GaSb spacer layers
Sb065	XRD, I-V	superlattice n on p junction

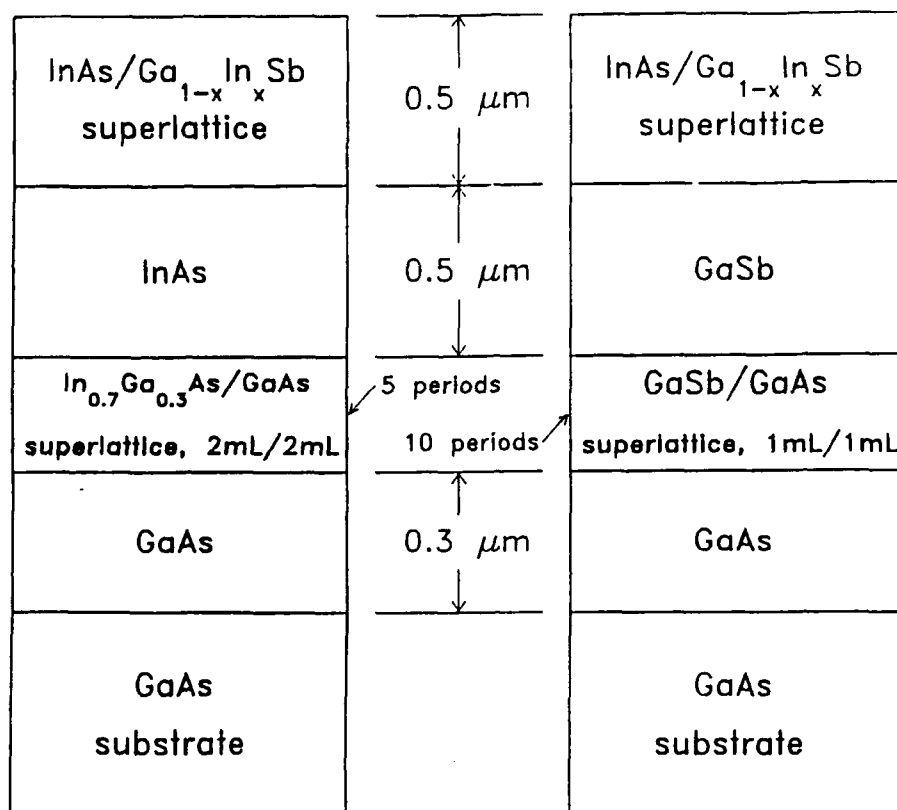| Left structure		Right structure
InAs/Ga$_{1-x}$In$_x$Sb superlattice	0.5 μm	InAs/Ga$_{1-x}$In$_x$Sb superlattice
InAs	0.5 μm	GaSb
In$_{0.7}$Ga$_{0.3}$As/GaAs superlattice, 2mL/2mL	5 periods 10 periods	GaSb/GaAs superlattice, 1mL/1mL
GaAs	0.3 μm	GaAs
GaAs substrate		GaAs substrate

Figure 1. Schematic layer diagram, illustrating buffer layer schemes used to grow GaInSb/InAs superlattices on (100) GaAs substrates.

InAs. For these buffers, the short period superlattice was achieved through a ten period, 1 monolayer / 1 monolayer, GaSb/GaAs growth sequence, at 520°C. The GaSb buffer overlying this superlattice was grown to a typical thickness of 0.5-1.0 μm. Gradual lowering of the substrate temperature, from 450-420°C, was found to yield the best structural quality for the buffer.

Superlattices grown on InP wafers employed the same layer sequence as those grown on GaAs substrates, with the exception that the first buffer layer deposited was Ga$_{0.47}$In$_{0.53}$As, rather than GaAs, grown at a temperature of 520°C. The elaborate layered buffer scheme was unnecessary for samples grown on GaSb substrates; these superlattices were grown on GaSb buffers overlying the substrates without intervening layers. The choice of GaSb as a top buffer layer material, regardless of the substrate, was made because of the intermediate value of the lattice constant of GaSb with respect to the two constituent materials of the Ga$_{1-x}$In$_x$Sb/InAs superlattice.

Samples grown on lattice mismatched substrates displayed spotty RHEED patterns, indicative of a three-dimensional growth mode, almost immediately upon commencement of the short period buffer superlattice. However, streaky RHEED patterns were recovered within the first 100 Å of growth of the overlying 0.5 μm GaSb buffer. A 1×3 RHEED pattern was observed ʰhroughout the deposition of the GaSb buffer layers, which were observed to be stress relaxed (free standing) as determined by x-ray diffraction.

Growth was completed by deposition of a $Ga_{1-x}In_xSb/InAs$ superlattice on top of the buffer layer. Substrate temperatures ranging from 350°C to 450°C were explored for the $Ga_{1-x}In_xSb/InAs$ superlattices, with best results obtained at approximately 380-390°C. Above 370°C, $Ga_{1-x}In_xSb$ and InAs displayed 1×3 and 1×2 surface reconstructions, respectively, as observed via RHEED patterns during growth of the superlattices. For substrate temperatures below approximately 370°C, a transition to a 1×5 RHEED pattern was observed during growth interrupts (in an Sb flux) on $Ga_{1-x}In_xSb$ surfaces. By providing a readily observed reference point, this transition allowed superlattice growth temperatures to be set reproducibly from one growth to another, in a temperature regime inaccessible in practice to an optical pyrometer.

Superlattices grown at higher temperatures showed two problems: above 400°C, smooth growth fronts deteriorated, leaving hazy, rough surfaces; and as growth temperature increased, As incorporation was found to rise to appreciable levels. The requirement of low growth temperatures to avoid morphological problems in the superlattices may be a consequence of strain and/or interdiffusion in these structures; InAs and $Ga_{1-x}In_xSb$ films with excellent surface morphologies can be grown at temperatures as high as 525 and 450°C, respectively. By contrast, As incorporation in the antimonide layers appears to be a bulk phenomenon. GaSb films grown (using a cracked Sb source) in an As background produced by a hot, shuttered, As cracker, showed substantial cross-incorporation (7-30%) of As over the substrate temperature range 450-530°C. Lower substrate temperatures were found to yield lesser degrees of As-incorporation; at a substrate temperature of approximately 425°C, as was virtually eliminated from the GaSb. These results suggest that:

(i) increased coverage of Sb on the GaSb surface occurs as the substrate temperature is lowered, and

(ii) the As-sticking coefficient is more strongly dependent on surface composition (Sb-coverage) than substrate temperature over the temperature range studied here.

The effects of increased Sb-surface coverage would be enhanced if As_4 molecules dominate the As-background pressure when the As shutter is closed, since adjacent lattice sites are required for incorporation of As_4 into GaAs.[12,13] Based upon the structural analysis described in Section 3.1,

we estimate the cross-incorporation of arsenic in the $Ga_{1-x}In_xSb$ layers of typical superlattices to be no greater than 1%.

In addition to examining growth conditions for superlattices of particular layer thicknesses and compositions, control of the interfacial chemistry in these structures was explored. Two types of interfaces are possible in, e.g., a (100) GaSb/InAs superlattice: an "InSb-like" interface, in which planes of atoms are stacked in the growth direction as follows:

• • • Ga Sb Ga **Sb In** As In As In As **In Sb** Ga Sb Ga • • •

or a "GaAs-like" interface:

• • • Ga Sb **Ga As** In As In As In As In **As Ga** Sb Ga • • •

Control of the interfacial chemistry was examined by using different shuttering sequences and interrupts during growth. In this study, all of the superlattices consisted nominally of 8 monolayers (25 A) of $Ga_{0.75}In_{0.25}Sb$ and 13 monolayers (39 A) of InAs. 80 period superlattices were grown, yielding samples roughly 0.5 μm thick. Superlattices with these parameters, in which growth was interrupted (no group-III flux) in an Sb_2 flux for 5 seconds at each interface, had previously been shown to have energy gaps near 110 meV (11 μm).

Figure 2 depicts the shutter sequences used to produce superlattices with $Ga_{0.75}In_{0.25}As$-like and InSb-like interfaces. In the case of $Ga_{0.75}In_{0.25}As$-like interfaces, deposition of each 13 monolayer thick InAs layer was followed by a 5 second "soak" in As in an attempt to terminate the layer with As atoms. A 1×2 RHEED pattern was observed during both the InAs layer and As soak. Next, the As shutter was closed, and the Ga and In shutters opened (without an accompanying group-V flux) for the time required for deposition of one monolayer of $Ga_{0.75}In_{0.25}$. This step resulted in a transformation of the RHEED pattern to 4×4 (presumably a metal rich surface reconstruction). The Sb shutter was then opened for the time needed to deposit 6 monolayers of $Ga_{0.75}In_{0.25}Sb$ (nominally resulting in 6 ML of $Ga_{0.75}In_{0.25}$ separating 7ML of Sb), and closed again for the time required for a single monolayer of $Ga_{0.75}In_{0.25}$. The characteristic 1×3 RHEED pattern observed during growth of the $Ga_{0.75}In_{0.25}Sb$ layer was transformed to a 4×1 pattern (again due to a metal rich reconstruction) when the Sb shutter was closed. The sample was then soaked for 5 seconds in an As flux, resulting in a 1×3 RHEED pattern, prior to the next 13 monolayer InAs deposition.

In the case of InSb-like interfaces, deposition of each 8 monolayer thick $Ga_{0.75}In_{0.25}Sb$ layer was followed by a 5 second soak in Sb. A transformation from 1×3 to 1×5 in surface reconstruction was observed during the Sb soak. Next, the Sb shutter was closed, and the In
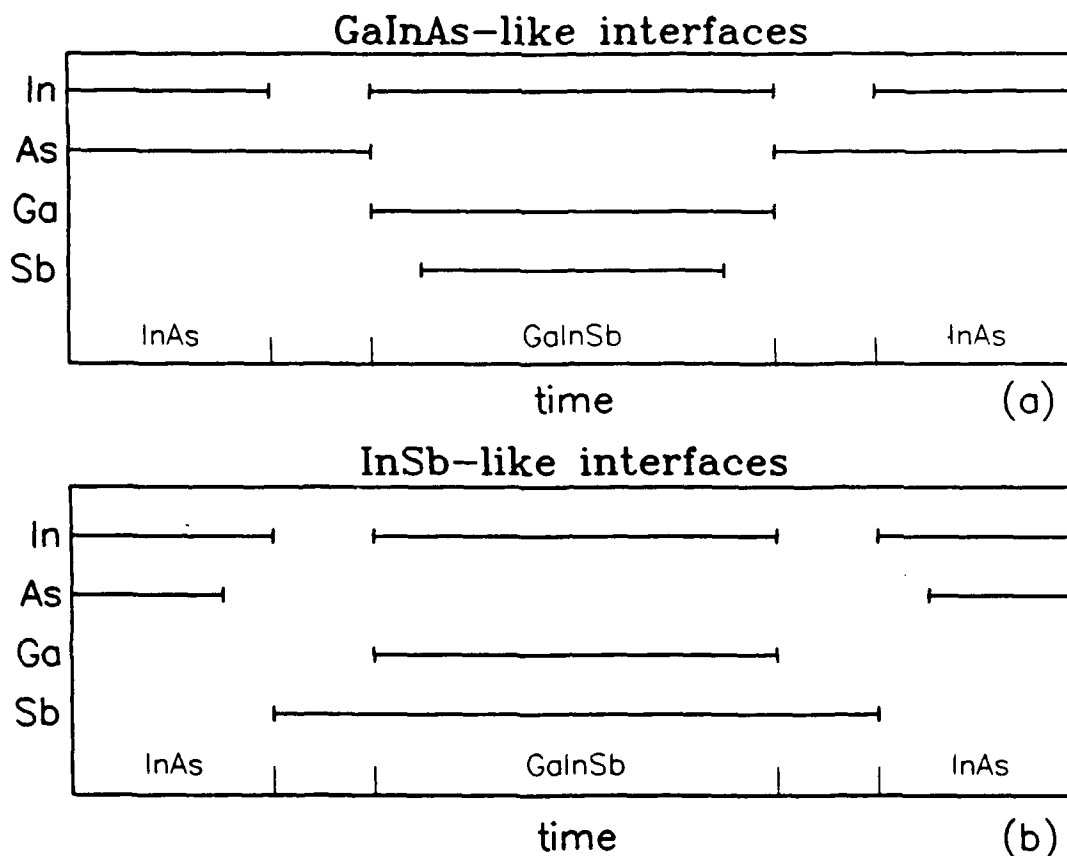
11

GaInAs-like interfaces

(a)

InSb-like interfaces

(b)

Figure 2. MBE shutter sequences used to fabricate (a) GaInAs-like interfaces, and (b) InSb-like interfaces. Solid bars indicate time periods during which shutters were open.

shutter opened for the time needed to deposit a monolayer of In, resulting in a return to a 1×3 RHEED pattern. The As shutter was then opened for the time needed to deposit 11 monolayers of InAs (nominally resulting in 11 monolayers of In separating 12 monolayers of As), and closed again for the time required for a single monolayer of In. The 1×2 RHEED pattern observed during growth of the InAs layer was transformed to a 2×4 pattern when the As shutter was closed. The sample was then soaked for 5 seconds in an Sb flux, resulting in a 1×3 RHEED pattern, prior to the next 8 monolayer $Ga_{0.75}In_{0.25}Sb$ deposition.

In addition to $Ga_{1-x}In_xSb/InAs$ superlattices with all InSb-like interfaces and all $Ga_{1-x}In_xAs$-like interfaces, samples were grown to have InSb-like GaInSb on InAs interfaces, and GaInAs-like InAs on GaInSb interfaces, and vice versa (i.e., GaInAs-like interfaces for GaInSb layers grown on InAs, and InSb-like interfaces at the termination of InAs layers). A superlattice with an intermediate interfacial composition was also grown, by depositing group-III monolayers of average composition at the interfaces (e.g., by sandwiching 0.5 ML of In and 0.5 ML of $Ga_{0.75}In_{0.25}$ between Sb-terminated $Ga_{0.75}In_{0.25}Sb$ and As-terminated InAs layers).

The total group-III deposition time was preserved in all cases in this sample set, ensuring that the number of monolayers in each superlattice period was unaffected by the choice of interfacial composition. As described in Section 3.1, these interfacial schemes each proved to influence the interfacial chemistry, and allowed the sensitivities of superlattice properties to the nature of the interfaces to be isolated.

2.2 DOPING

The ability to dope an infrared material both p-type and n-type is necessary for the realization of photovoltaic detectors. III-V semiconductors benefit considerably from the availability of well-behaved substitutional impurity dopants. For III-V MBE growth, silicon and beryllium are by far the most popular dopants. Silicon has been demonstrated to be a well behaved p-type dopant for GaSb,[14] while it is an n-type dopant for InAs. Beryllium is known to be an acceptor for all of the conventional III-V compounds. Hence, it should be possible to dope $Ga_{1-x}In_xSb/InAs$ superlattices p-type by codeposition of Be during growth of either or both constituent layers, or by codeposition of Si during growth of $Ga_{1-x}In_xSb$ layers only (assuming that the diffusion of Si atoms is limited). Conversely, codeposition of Si during growth of InAs layers should result in an n-type superlattice. We have observed well-behaved n-type doping of $Ga_{1-x}In_xSb/InAs$ superlattices via this in situ Si technique at levels up to 10^{18} cm^{-3}. Higher levels of n-type doping have not yet been attempted, and are probably unnecessary for photovoltaic detectors.

Although intentional doping in $Ga_{1-x}In_xSb/InAs$ superlattices is straightforward, achieving low background (unintentional) carrier concentrations has required more study. Low carrier concentrations are highly desirable as Auger lifetimes and depletion lengths are strong functions of carrier densities. In superlattices grown in the Perkin Elmer MBE machines at Hughes and Caltech, we consistently observed background p-type doping, with carrier concentrations of approximately 5×10^{16} cm^{-3} at low temperatures. We speculate that the Perkin Elmer -grown superlattices suffer from p-type centers derived from arsenic cell impurities. Superlattices grown in HRL's VG machine now routinely attain uncompensated background doping levels of 4×10^{15} cm^{-3}, n-type. While HgCdTe can be grown in the 10^{14} cm^{-3} -range, the larger Auger cross-sections in the bulk II-VI material more than compensate for this advantage of lower background doping levels. Additional reductions in the background carrier concentrations of the GaInSb/InAs superlattices should further reduce impact ionization rates below those of HgCdTe; this is the subject of ongoing work.

Several photojunctions have been grown to date, employing a variety of schemes to achieve a built-in electric field. Characteristics of these samples are described in Section 4.1.

13

Section 3
# PHYSICAL CHARACTERIZATION
OF GaInSb/InAs SUPERLATTICES

3.1 STRUCTURAL PROPERTIES

Thorough x-ray diffraction analysis was applied to each of the GaInSb/InAs superlattices grown under this contract, yielding extensive information on layer thicknesses and compositions, strain levels, interdiffusion, and crystallinity. Structural data derived from this technique were, in some cases, supplemented by optical and transmission electron microscopy.

Structural characterization was essential in identifying conditions under which high quality GaInSb/InAs superlattices could be grown. In particular, the growth conditions described in Section 2.1 yielded structures which were highly planar, regular, and uniform across a 2 in. wafer (although the latter property is more often dependent on MBE architecture than growth conditions). No evidence of interdiffusion was found in samples grown at these low temperatures. Consistent with the extensive literature describing growth on lattice mismatched substrates, we found threading dislocation densities of 10^7-10^9 cm^{-3} in superlattices grown on GaAs or InP substrates. (To date, we have not found these appreciable dislocation densities to affect electrical or optical properties of the superlattices.) Samples grown on GaSb substrates were of extraordinarily high quality; the observation of Pendellosung fringes in x-ray diffraction spectra and the complete absence of dislocations in plan-view or cross-sectional TEM demonstrate the outstanding structural quality of these superlattices, despite the 2 percent lattice mismatch between $Ga_{0.8}In_{0.2}Sb$ and InAs.

Experimental x-ray rocking curves or theta/two-theta scans were analyzed in two ways. The period and average perpendicular lattice constant of a superlattice was calculated based upon the separation of satellite peaks and the position of the zeroth-order superlattice peak, respectively. Combining this information with the known MBE shutter opening times uniquely specified the layer thicknesses and compositions for a given superlattice. For samples in which cross-incorporation of group-V's was an issue (e.g. incorporation of As in nominally GaInSb layers), or in which the interfacial chemistry was unknown, additional information could be extracted by fitting the experimental diffraction data using a sophisticated kinematical simulation.

Typical $\Theta/2\Theta$ x-ray diffraction data from superlattices grown on GaAs and InP substrates are shown in Figure 3. Peaks are bimodal due to the Cu Kα doublet x-ray source. In addition to the substrate and buffer layer peaks (GaAs and GaSb; and InP, InGaAs, and GaSb), zeroth and higher-order superlattice satellite peaks are clearly visible. The intensities of the superlattice satellite peaks are in excellent agreement with those predicted by a kinematical theory. The

14

(a)

(b)
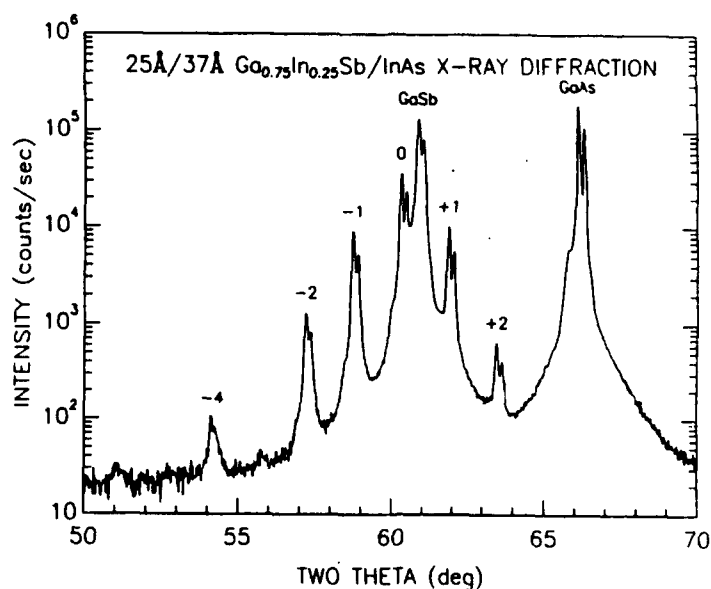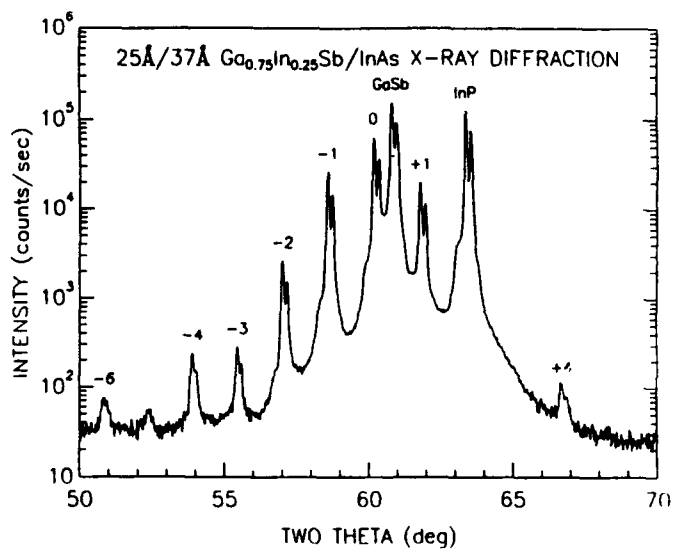
Figure 3. Θ/2Θ x-ray diffraction data from GaInSb/InAs superlattices grown on (a) GaAs and (b) InP substrates.

widths of the peaks are limited by the resolution of the x-ray diffractometer used here, although the washing-out of the $K\alpha_1$ - $K\alpha_2$ doublet indicates the presence of extended structural defects (i.e. threading and misfit dislocations). The intensity and narrowness of higher-order satellite peaks is indicative of highly regular superlattice growth with limited interdiffusion between layers.[15]

A cross-sectional transmission electron micrograph from one of our superlattices is shown in Figure 4. Inset in the figure is a [011] zone axis electron diffraction pattern from the specimen, exhibiting clear superlattice satellites around {200}, {111}, and {022} diffraction spots. The highly planar and regular nature of the layers is apparent from the micrograph, as is the absence of threading or misfit dislocations. Since we were unable to image any dislocations in any cross-sectional micrographs, despite scanning the sample in search of defects, plan-view samples were prepared to obtain an estimate of the dislocation density. The complete absence of dislocations observable in plan-view placed an upper bound of 10^5 cm^{-2} on the dislocation density in this superlattice.

An x-ray rocking curve for one of the superlattices is shown in Figure 5. An envelope of sharp (004)-like superlattice peaks is apparent, in addition to the (004) diffraction peak arising from the GaSb substrate. The outstanding structural quality of the superlattice is evidenced by the considerable amplitude of higher order superlattice peaks, and by the absence of appreciable broadening of the satellites; interdiffusion would broaden and lower the intensity of higher order satellites, while dislocations could be expected to widen each of the observed peaks. An additional indication of high structural quality comes from the presence of Pendellosung fringes, illustrated in Figure 6. These fringes are evident on the 0, ±1, and ±2 superlattice peaks. Those illustrated here are from the zeroth-order peak. Pendellosung fringes are observed only in exceptionally planar and regular heterostructures. This is, to our knowledge, the first observation of finite thickness fringes in a semiconductor heterostructure with this great a lattice mismatch between constituents (1.9 percent).

As shown in Figures 5 and 6, the data are in excellent agreement with a kinematical diffraction model. The calculated diffraction corresponds to a 28 Å/33 Å $Ga_{0.8}In_{0.2}Sb/InAs$ superlattice with a 78 percent InSb character to the interfaces. This fraction yielded the best fit to the data (the calculated diffraction was highly sensitive to the interfacial composition), and was consistent with layer thicknesses in good agreement with those anticipated from independent calibrations of the MBE growth rates. The InSb-rich nature of the interfaces was plausible in this sample, as an Sb flux was maintained during the 5 second interrupt in group-III flux imposed at each of the interfaces.
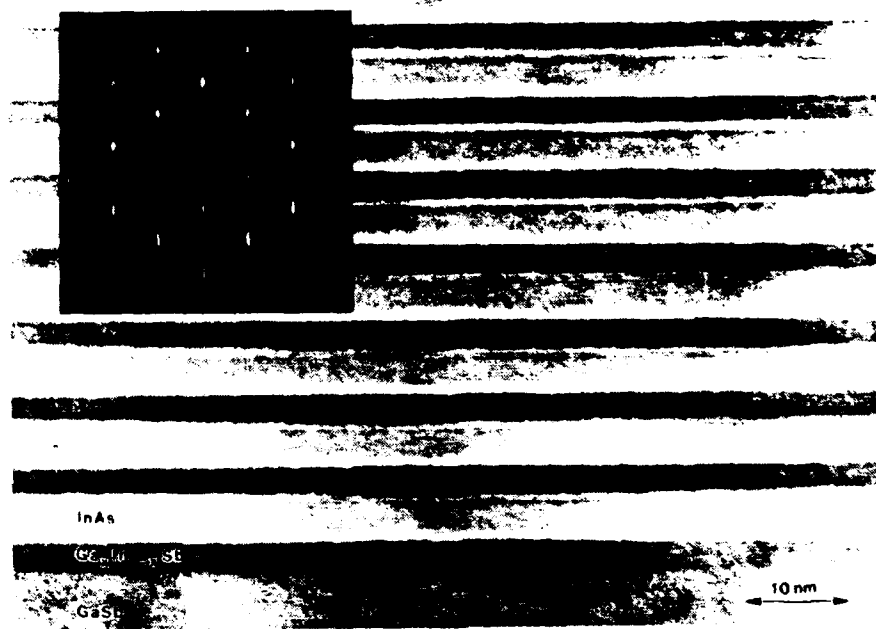
Figure 4. Cross-sectional transmission electron micrograph and electron diffraction from a GaInSb/InAs superlattice, illustrating the uniform and dislocation-free character of the epilayer.
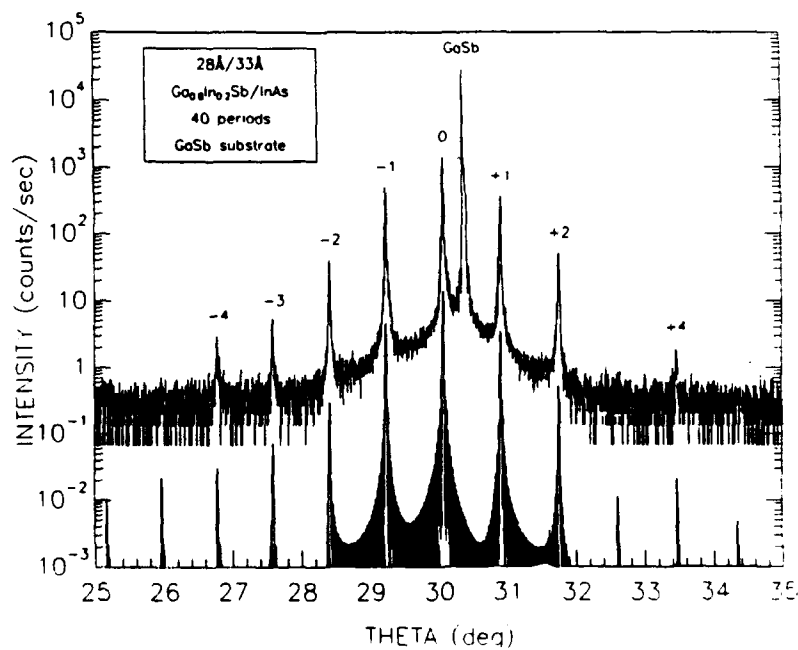

Figure 5. Comparison of experimental and theoretical x-ray rocking curve diffraction from a GaInSb/InAs superlattice grown on a GaSb substrate.
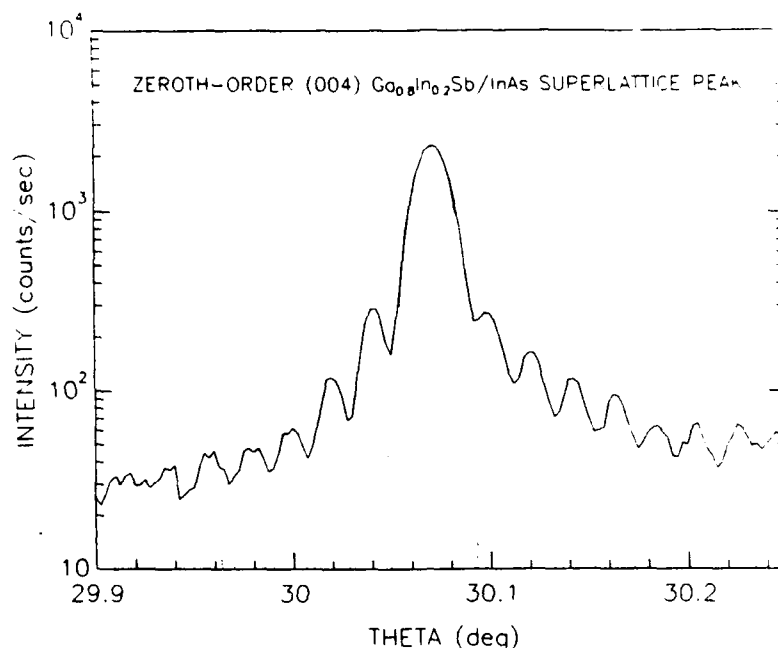
Figure 6. Measured and calculated Pendellossung fringes around the zeroth-order (004)-like superlattice diffraction peak.
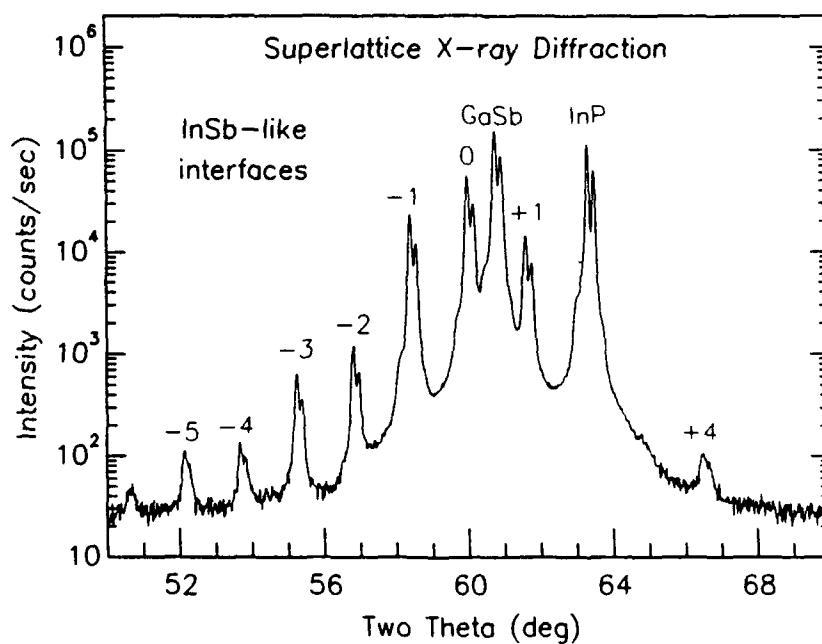
Diffraction from superlattices with GaInAs- and InSb-like interfaces is compared in Figure 7. The striking shift in zeroth-order peak position (observed to be on different sides of the GaSb buffer peak in the two cases) indicates a significant difference in average interatomic spacing in the two superlattices. As the structures were grown to be identical in all respects except interface chemistry, this shift is a direct measure of the effectiveness of growth interrupts and shuttering sequences in determining this chemistry. The plot of zeroth-order lattice constant versus nominal interface composition, shown in Figure 8, illustrates the considerable influence of various growth schemes in determining the nature of the interfaces. Intrinsic differences in the infrared response of these structures are discussed in Section 3.3.

3.2 OPTICAL PROPERTIES

Spectrally resolved photoconductive measurements were made on many of the GaInSb/InAs superlattices grown under this contract. In addition, selected samples were examined by photoluminescence and optical transmission spectroscopy. The experiments were used to enumerate the dependences of energy band gap on layer thicknesses and compositions, and to determine the magnitude and abruptness of the LWIR absorption edges. It was established that 8-12 μm gaps could be readily obtained for modest superlattice layer thicknesses and strains. Crisp absorption thresholds were obtained in these structures, and absorption coefficients comparable to those of HgCdTe were obtained. Our contract effort in this area was
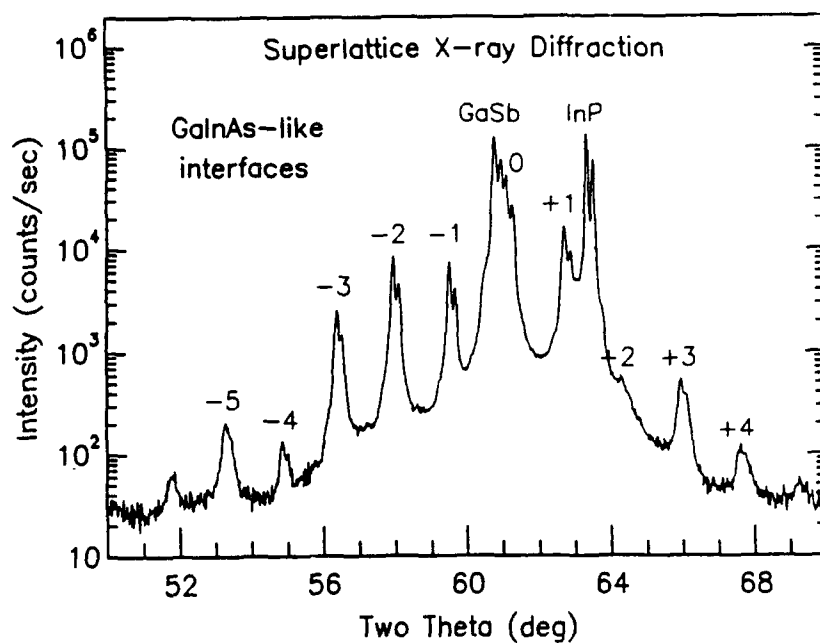
(a)

(b)

Figure 7. Comparison of $\Theta/2\Theta$ x-ray diffraction scans from 8 ml/ 13 ml $Ga_{0.75}In_{0.25}$ Sb/InAs superlattices with (a) GaInAs-like interfaces and (b) InSb-like interfaces.
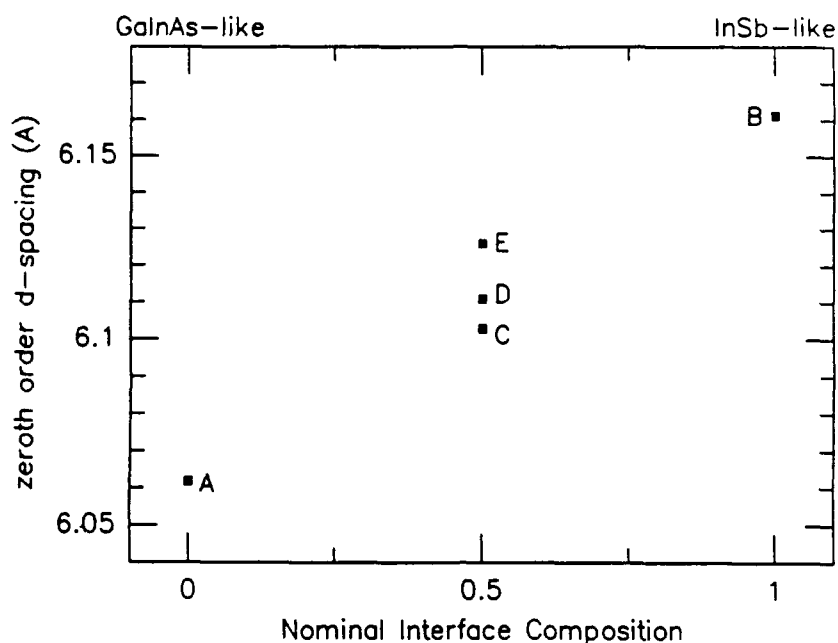
19

Figure 8. Plot of zeroth order d-spacing versus nominal interfacial lattice constant for five GaInSb/InAs superlattices. Sample A = all GaInAs-like interfaces, B = all InSb-like interfaces, C = GaInAs like interfaces for InAs on GaInSb and InSb-like interfaces for GaInSb grown on InAs, D = opposite of sample C, E = intermediate interfacial composition. The data show a clear correlation between average interatomic spacing and nominal interfacial composition.

complemented by modeling work carried out under internal research and development funds, which enabled us to correlate experimental band structure results with theory.

Spectrally resolved measurements were made on a Bomem Fourier Transform Infrared (FTIR) spectrometer. In the case of the photoluminescence experiment, a double modulation technique was necessary to discriminate signals from the substantial 300 K blackbody background.[16] An Ar$^+$ laser or AlGaAs laser diode pump was used for these measurements, modulated at 40 kHz. Signals were detected by an InSb or a HgCdTe detector cooled to 77 K, or by a Si:As detector operating at 4.2 K.

Photoluminescence spectra from three samples are shown in Figure 9. Consistent with previous work on GaSb/InAs superlattices,[17] we associate the prominent luminescence peaks from our samples with transitions across the fundamental conduction to heavy hole valence band gap. In the case of the GaSb/InAs superlattice, luminescence was only detected for high pump power densities (>3500 W/cm^2); the intensity of this optical pump likely contributed to the observed broadening, leading us to associate the energy gap with the low energy luminescence edge. However, in the case of the 25 Å/25 Å Ga$_{0.75}$In$_{0.25}$Sb/InAs superlattice, luminescence was obtained with a 70 mW AlGaAs laser diode pump. The approximately Gaussian shape of the emission peak from this sample suggests a random variation in superlattice parameters, leading

us to associate the band gap with the luminescence peak energy in this sample. Consistent with this interpretation, the 30 meV width of the luminescence peak coincides with the change in superlattice energy gap expected from a single monolayer fluctuation in InAs well thickness (the gap is less sensitive to changes in $Ga_{1-x}In_xSb$ layer thickness). Although we have demonstrated sample-to-sample growth to be reproducibile to better than 0.1 Å in superlattice period, discrete interfacial fluctuations of one monolayer can be expected in samples grown by MBE in a two-dimensional growth mode in which surface atomic mobilities are high.[18]

Energy band gaps were also determined by spectrally resolving the photoconductive responses of these and other GaInSb/InAs superlattices. Mesa structures were patterned using photolithography, with an etch stopping within the superlattice, near the buffer layer interface. Aluminum contacts were evaporated on the top and base of the mesas, and photocurrent measured for backside illumination under an applied bias. Figure 10 illustrates the clear photoconductive thresholds observed in five of the samples.

Photoconductive measurements yielded energy gaps in good agreement with those derived from photoluminescence, and yielded the energy gaps of superlattices not showing clear luminescence. Figure 10 clearly illustrates the dependence of superlattice energy gap on the InSb fraction x, and the thickness of the InAs layers. As shown in the figure, a photoconductive threshold beyond 15 μm was observed in a 45 Å/28 Å $Ga_{0.75}In_{0.25}Sb$/InAs superlattice. Longer wavelengths could be obtained either by further increasing layer thicknesses, or by increasing x,

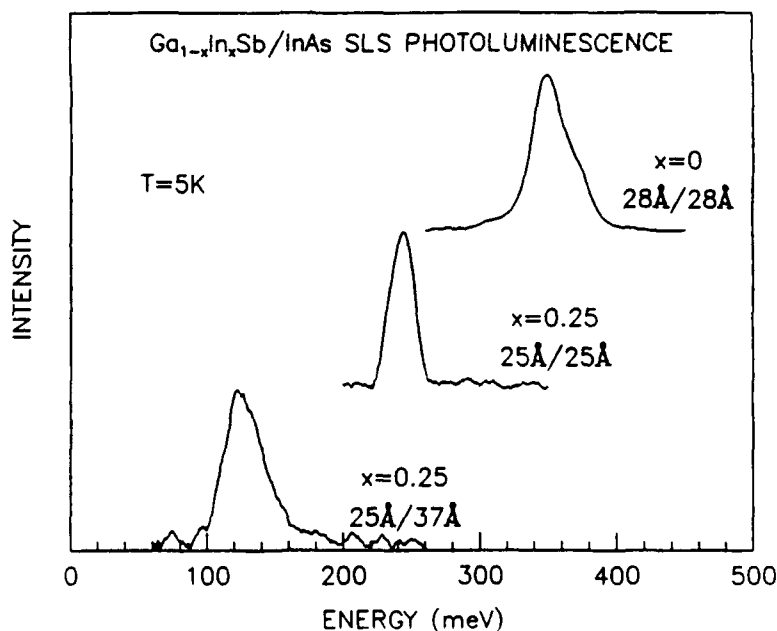Figure 9. Photoluminescence spectra from three $Ga_{1-x}In_x$ Sb/InAs superlattices.

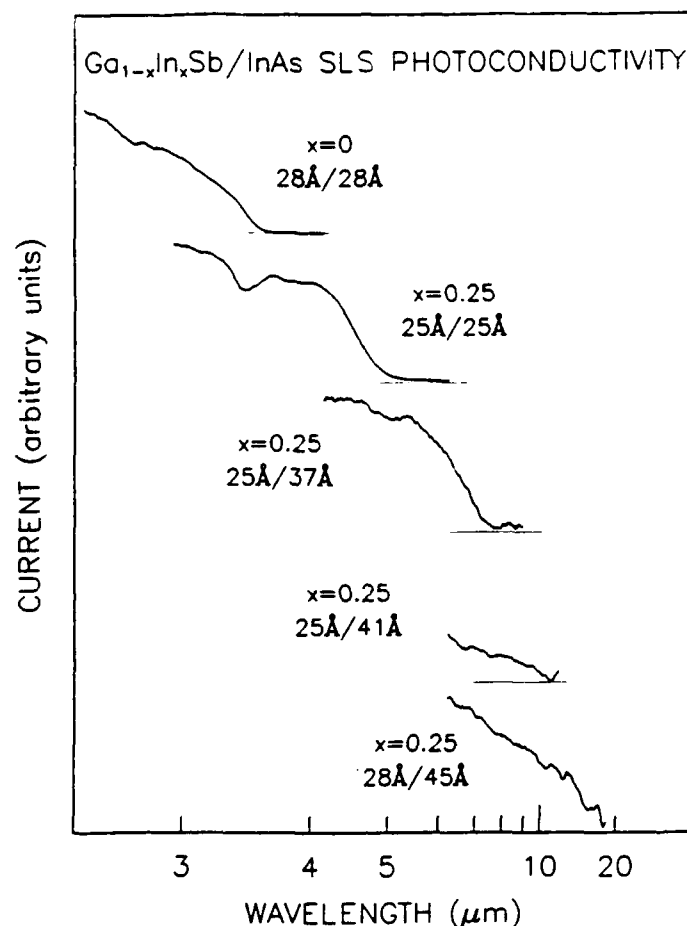Figure 10. Spectrally resolved photoconductivity from Ga$_{1-x}$In$_x$ Sb/InAs superlattice mesa structures.

the In content within the antimonide layers. Experimental confirmation of these long wavelength energy gaps in superlattices of layer thicknesses of 45 Å and less was important as it showed that far infrared response is compatible with thin layers in this material system. As the type-II band alignment localizes electrons and holes in dissimilar layers, large absorption coefficients were only predicted for thin layer structures, in which the electron-hole overlap remains high.

Table 2 compares theoretical and experimental energy gaps of some of the first superlattices grown under this contract. A column has been added to the table to identify the extent of arsenic incorporation in our antimonide layers, which initially posed a problem in the growth of these samples. Superlattice energy gaps derived from photoluminescence are in excellent agreement with those inferred from photoconductivity measurements, and are close to those calculated from a two band k • p model. Reasonable agreement between our experimental results and calculated gaps appears to validate the assumption of a 560 meV InAs/GaSb band offset, and a small InSb/GaSb valence band offset.

22

Table 2. Comparison of energy band gaps derived from photoluminescence, photoconductivity, and theory for the InAs/Ga$_{1-x}$In$_x$Sb superlattices examined here.

Layer Thickness (Å)		x	y	Energy gap (meV)		
InAs	Ga$_{1-x}$In$_x$Sb$_{1-y}$As$_y$			PL	PC	Theory
28	28	0	0.07	330 ± 10	350 ± 10	320
25	25	0.25	0.08	240 ± 10	250 ± 10	280
37	25	0.25	0.05	150 ± 10	170 ± 10	180
41	25	0.25	0	. . .	110 ± 10	110
45	28	0.25	0	. . .	80 ± 10	100

Experimental and theoretical absorption spectra for a 41 Å/25 Å Ga$_{0.75}$In$_{0.25}$Sb/InAs superlattice are shown in Figure 11. The calculated spectrum was derived from a two-band tight-binding model. As is apparent from the figure, both the observed energy gap of 108 meV and the measured absorption coefficient are in excellent agreement with theory. The superlattice absorption edge is abrupt, attaining a value of approximately 2000 cm^{-1} at 10 μm. As this value is comparable to that of bulk HgCdTe with the same gap, it is a promising result for detectors based on Ga$_{1-x}$In$_x$Sb/InAs superlattices. In addition, the magnitude of this absorption is consistent with the prediction that the perpendicular electron effective mass in the superlattice is greater than that of HgCdTe. Although the oscillator strengths in these type-II superlattices are expected to be smaller than those of HgCdTe, comparable absorption coefficients were predicted due to the higher density of states associated with larger effective masses in the superlattices.[19] As described in Section 1.1, these larger effective masses present potential for improved performance over HgCdTe, as they could suppress tunneling responsible for leakage currents in present detectors.

3.3 ELECTRICAL PROPERTIES

Electrical characteristics of GaInSb/InAs superlattices were routinely determined by Hall analysis. Nominally undoped samples grown in the VG MBE machine were typically found to be n-type, with background carrier concentrations in the mid-to-high-10^{15} cm^{-3} range (as low as 3 × 10^{15} cm^{-3}) at low temperatures, and in-plane electron mobilities between 500-6000 cm^2/V-sec. Unintentional background doping in superlattices grown in the Perkin-Elmer systems was usually p-type, in the mid-10^{16} cm^{-3} range, with typical in-plane mobilities of several hundred cm^2/V-sec. Effective n-type substitutional doping of the superlattices to 10^{18} cm^{-3} levels was found to be possible through codeposition of Si during growth of the InAs layers. Last, by examining intrinsic carrier concentrations (i.e. at elevated temperatures), it was possible to estimate superlattice energy gaps. This enabled comparison of energy gaps in superlattices
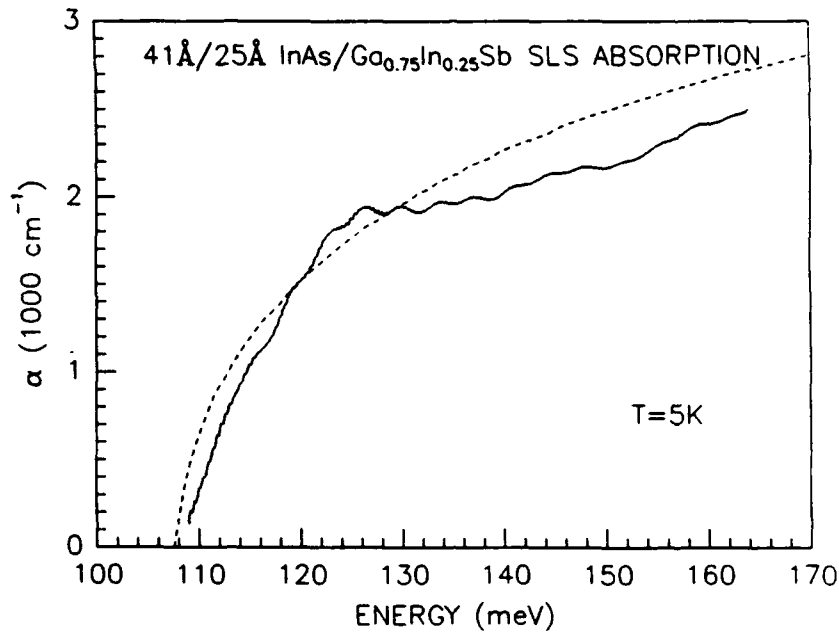
Figure 11. Experimental and theoretical absorption coefficients (solid and broken lines, respectively) for a 25 Å/41Å GaInSb/InAs superlattice.

differing only in interfacial chemistry, confirming a calculated shift to longer wavelengths for structures with InSb-like interfaces.

Hall measurements were performed in a variable temperature cryostat, allowing carrier concentrations and mobilities to be determined over the range 5 - 360 K. Samples were probed in a van der Pauw geometry. Typical data are shown in Figure 12, for an 8 monolayer/ 13 monolayer $Ga_{0.75}In_{0.25}Sb/InAs$ superlattice grown in the VG machine. While carrier freeze-out is not observed at low temperatures, the concentration drops to $\sim 3 \times 10^{15}$ cm^{-3}, n-type. Measurements at higher temperatures continue to be dominated by electrons, despite the presence of holes, due to the substantially greater mobility of electrons.

The narrow energy gaps of GaInSb/InAs superlattices result in intrinsic carrier concentrations in unintentionally doped samples at higher temperatures (>250 K). Examination of the temperature activation of this carrier population yields an estimate of a sample's energy gap. In particular, neglecting the dependences of energy gap and effective density of states on temperature, the number of intrinsic carriers n^i is proportional to $\exp(-E_g/2kT)$, where E_g is the energy gap of the superlattice.
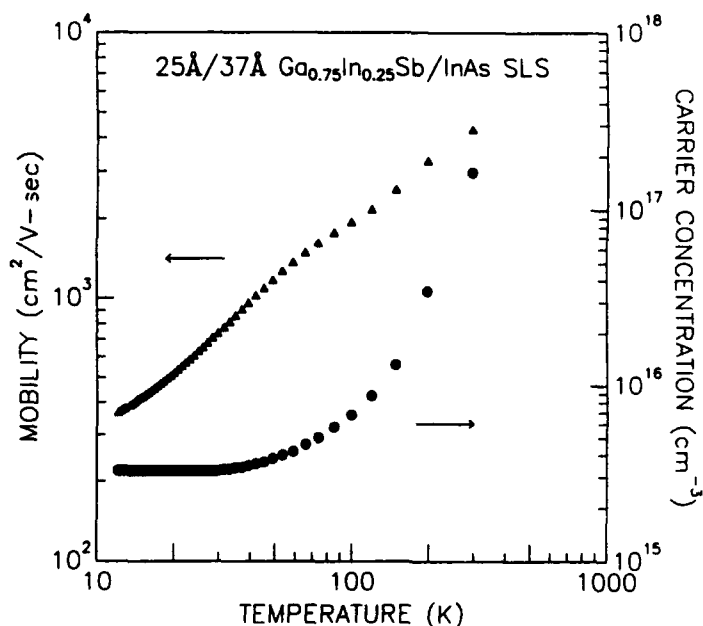
Figure 12. Temperature dependence of carrier concentration and mobility in an 8 ML/13 ML GaInSb/InAs superlattice.

Figure 13 is a semilog plot of measured intrinsic carrier concentration versus 1000/T for GaInSb/InAs superlattices with InSb-like and GaInAs-like interfaces. The data show that a superlattice with InSb-like interfaces has a higher intrinsic carrier concentration than a sample with GaInAs-like interfaces, consistent with a smaller energy gap. Furthermore, the slopes of the two data groups differ by about 20 percent, which is consistent with a difference of 25 meV in energy gap. The observed dependence of energy gap on interfacial chemistry is in accord with intuitive expectations: superlattices with relatively wide gap interfacial compounds (in this case InGaAs) should show larger energy gaps than equivalent structures in which these monolayers are replaced by a narrow gap material (e.g. strained InSb).

While low temperature Hall measurements of GaInSb/InAs superlattices grown in the Perkin-Elmer machine generally revealed unintentional p-type background concentrations in the 10^{16} cm^{-3} range, the superlattice with GaInAs-like interfaces displayed n-type carrier concentrations at low temperatures. Possible explanations for this observation include the formation of a surface inversion layer, or the creation of As antisite defects.
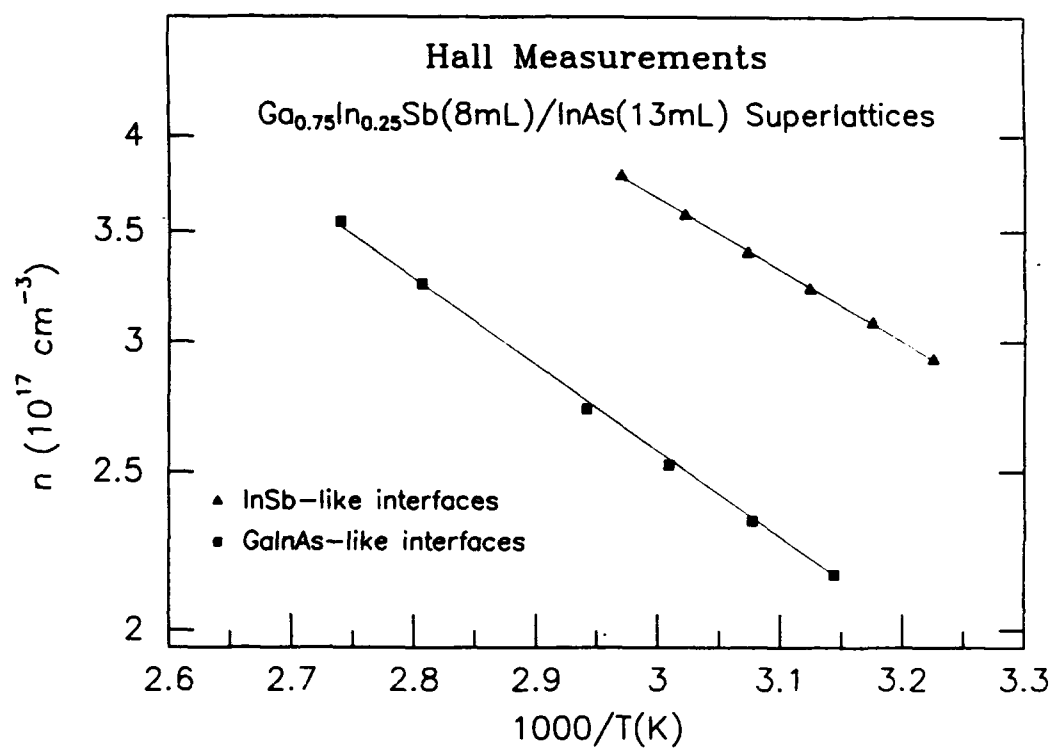
Figure 13. Intrinsic carrier concentration versus 1000/T for superlattices with GaInAs-like interfaces (squares) and InSb-like interfaces (triangles).

Section 4
PHOTOVOLTAIC DETECTOR STRUCTURES

Photovoltaic detectors are attractive for focal plane array applications due to their low power consumption. These devices depend upon a p-n junction formed within the active infrared material, creating a built-in electric field which sweeps minority carriers across the junction. Photogenerated signals near zero bias are then detected with minimal dark current. Rudimentary $Ga_{1-x}In_xSb/InAs$ superlattice photovoltaic detectors have been fabricated under this contract, demonstrating the suitability of these materials for applications requiring these devices.

4.1 PHOTOVOLTAIC SAMPLES

Table 1 includes brief descriptions of seven photovoltaic device structures grown by MBE under this contract (TCH601, TCH618, Sb021, Sb022, Sb025, Sb053, Sb065). All of the samples contain $Ga_{1-x}In_xSb/InAs$ superlattice active layers except Sb053; that sample is a GaSb p-n junction grown as a processing standard. Figure 14 is a schematic layer diagram depicting the layer sequence used for samples TCH601 and TCH618. The active device layers were deposited on thick, undoped GaSb buffer layers atop GaAs substrates. Samples were grown by the method described in Section 2. Although this approach yields $Ga_{1-x}In_xSb/InAs$ superlattices with high threading dislocation densities relative to those grown on GaSb substrates, it has the advantage of providing an optically transparent substrate for backside detector illumination. An n-type $Ga_{1-x}In_xSb/InAs$ superlattice, doped by codepositing silicon during the InAs layers, forms the bottom contact for the structure. This n-type layer is 2500 Å thick, with $n = 1 \times 10^{18}cm^{-3}$. A highly conductive bottom contact layer is important for this device structure to minimize the effects of parasitic in-plane resistance. An undoped, 2500 Å thick $Ga_{1-x}In_xSb/InAs$ superlattice is then deposited on the doped contact layer. The background doping of this layer is approximately $5 \times 10^{16}cm^{-3}$, p-type, in samples TCH601 and TCH618, resulting in a p^--n^+ superlattice junction.

Samples Sb021, Sb022, and Sb025 differ from the structure depicted in Figure 14 in two significant features: (i) the undoped superlattice layer is n-type (approximately $5 \times 10^{15}cm^{-3}$) and is 5000 Å thick, and (ii) a heavily doped p-type $Al_{0.15}Ga_{0.85}Sb$ or GaSb layer is deposited as a cap, forming a p^+-n^- heterojunction between the cap and undoped superlattice layers. Sample Sb065 is an n^- on p^+ heterojunction sample grown by heavily doping the GaSb buffer layer p-type and then depositing an undoped superlattice (background n-type) followed by a heavily n-type doped superlattice.
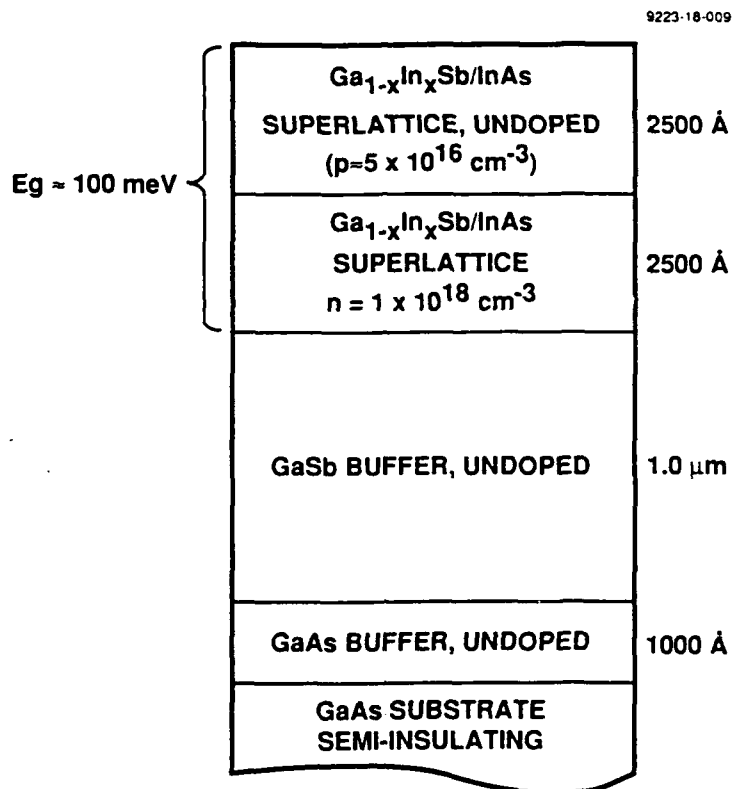
$Ga_{1-x}In_xSb/InAs$ SUPERLATTICE, UNDOPED ($p \approx 5 \times 10^{16}$ cm^{-3})	2500 Å
$Ga_{1-x}In_xSb/InAs$ SUPERLATTICE $n = 1 \times 10^{18}$ cm^{-3}	2500 Å
GaSb BUFFER, UNDOPED	1.0 μm
GaAs BUFFER, UNDOPED	1000 Å
GaAs SUBSTRATE SEMI-INSULATING	

$E_g \approx 100$ meV

Figure 14. Schematic layer diagram for photovoltaic superlattice structures TCH601 and TCH618.

4.2 DEVICE PROCESSING

4.2.1 Chemical Etching

Although the majority of the diode fabrication effort under this contract has been devoted to the development of a dry etching process (described below), some rudimentary devices have been fabricated by wet chemical etching. The procedure used is as follows: (i) an array of 1000 Å thick, gold contacts, ranging in size from 5 × 5 μm to 20 × 20 μm is defined by conventional photolithographic liftoff, (ii) mesas are formed by etching in Br_2:HBr:H_2O (0.5:100:100) for approximately 30 seconds, with the gold contacts acting as a mask for the etch, and (iii) a large area "back"contact is deposited on the etched surface. The targeted etch depth is sufficient to isolate the pn junction without removing a large fraction of the bottom conductive layer. Although this process is useful because of its expediency, it is unsatisfactory in several regards: (i) the etched surface is roughened significantly, (ii) trenching occurs around the mesas, and (iii) there is no sidewall passivation for the diodes.

Devices fabricated by the preceding procedure are suitable for current-voltage testing in a low temperature probe station. A similar procedure has been used to make larger devices (60 × 160 μm) for photovoltaic response measurements. These larger device sizes are required for wirebonding to packages compatible with optical characterization equipment. Figure 15 is a top view photograph of an array of these devices, two of which have been wirebonded for testing. The only distinction between the two procedures is the use of a different mask in defining the gold contacts.

4.2.2 Plasma Etching

A dry etching process is desirable for controllable and reproducible photodiode fabrication. Investigations of CH_4/H_2 plasma etching of $Ga_{1-x}In_xSb/InAs$ superlattices have been performed under this contract, using a PlasmaLab etching system built by Plasma Technology. A variety of masking schemes and etching parameters have been studied. It was determined that aluminum-on-silicon nitride forms an ideal mask for the plasma etch process by simultaneously preventing charging of the wafer surface and metal-semiconductor alloying during etching. Optimal plasma etching was observed for total pressures of 50 mTorr, CH_4/H_2 ratios of 0.5, and a total RF power of 150 W. Figure 16 is a scanning electron microscope photograph of a vertical sidewall produced by this technique. Under the appropriate conditions, etched surfaces remain planar with a nearly constant etch rate. Figure 17 is a plot of mesa height vs. time for a 5000 Å thick $Ga_{0.75}In_{0.25}Sb(8ML)/InAs(13ML)$ superlattice etched in a CH_4/H_2 plasma. The superlattice was grown on a thick GaSb buffer layer, and capped with 1000 Å of GaSb. The figure reveals that the etch rate for GaSb is approximately half that for the superlattice.

Figure 15. Array of photovoltaic superlattice devices. Mesas are 60 × 160 μm in size.

Figure 16. Scanning electron micrograph showing a vertical sidewall achieved by plasma etching.
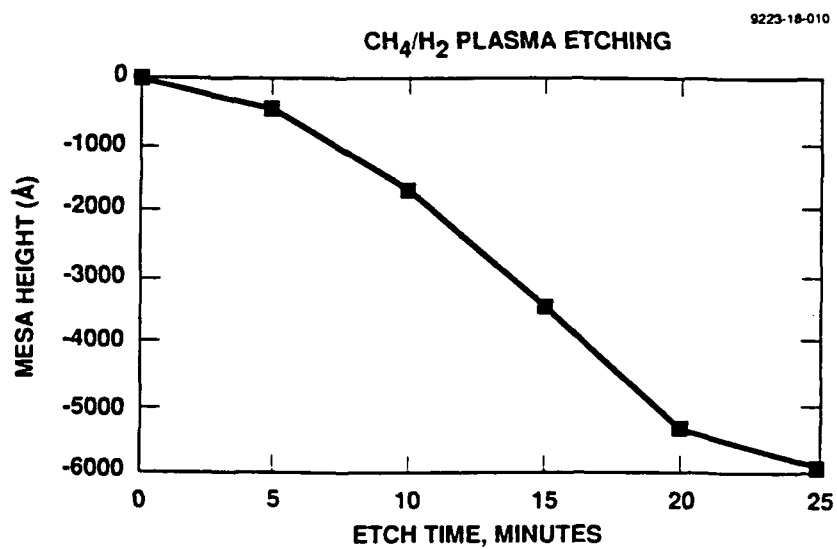

Figure 17. Etch depth vs. time for a GaInSb/InAs superlattice in a CH_4/H_2 plasma.

A photodiode fabrication procedure has been designed, incorporating the CH_4/H_2 plasma etching process: (i) an Al-on-SiN mask is created by evaporation and plasma deposition, respectively, followed by conventional photolithographic patterning and CF_4 plasma etching, (ii) mesas are formed by the CH_4/H_2 plasma etching process, (iii) the Al on SiN mask is removed in HF, (iv) gold contacts are deposited on the mesa tops and etched surfaces by photolithographic liftoff, (v) SiN is deposited and patterned with via holes to the mesa tops and etched surface contacts, (vi) gold contact metal pads are deposited on the SiN, overlapping the via holes, and (vii) a gold "guard" metal contact is deposited. Steps (v) and (vii) of the procedure are intended to provide a means for altering the surface potential along the mesa sidewalls as an investigative tool for surface passivation. These steps may be omitted from the procedure for straightforward low temperature probing measurements.

4.2.3 Ion Implantation

A brief study of doping by ion implantation of silicon into $Ga_{1-x}In_xSb/InAs$ superlattices has been performed under this contract. Figure 18 is a plot of carrier sheet concentration vs. rapid thermal annealing temperature for two different implantation doses into a 2500 Å thick GaInSb/InAs superlattice with a p-type background sheet concentration of $8 \times 10^{11}cm^{-2}$. X-ray diffraction scans revealed no change in superlattice structural quality up to the maximum temperature shown in Figure 18 for annealing times of 30 seconds. At the lower implantation dose, the figure shows nearly ideal implant activation for annealing at 450°C, with an excess of donors generated at 500°C. The data for the higher implantation dose reveals strong p-type doping behavior for the 450°C anneal, with n-type behavior attained at higher annealing temperatures.

4.3 DIODE TESTING

4.3.1 TCH-Series Photodiodes

As discussed previously, background doping levels in the nominally undoped superlattice layers of samples TCH601 and TCH618 were an order of magnitude higher than in photodiode samples grown more recently. Diodes fabricated from these samples by the wet chemical process described in Section 4.2.1 displayed leaky current-voltage behavior down to 77 K (although significant temperature dependence was observed). A strong parasitic resistance effect, due to in-plane transport through the 2500 Å thick bottom contact layer, was observed even for device sizes as small as 5×5 μm. Despite these poor I-V results, it was possible to observe and characterize the photoresponse of 60×160 μm diodes. Figure 19 displays the photovoltaic spectral response observed from a diode fabricated from sample TCH618; the data were obtained by positioning the diode as a detector in the Bomem FTIR spectrometer. The figure shows a photovoltaic threshold near 12 μm, consistent with the energy gap expected in this superlattice.
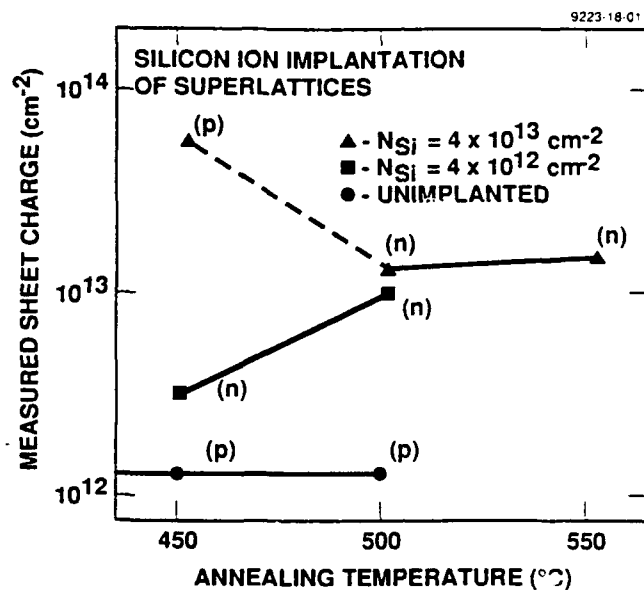
31

Figure 18. Sheet carrier concentration in a 2500 Å GaInSb/InAs superlattice for two implantation doses, as a function of rapid thermal anneal temperature. Dashed lines indicate a change in carrier type.
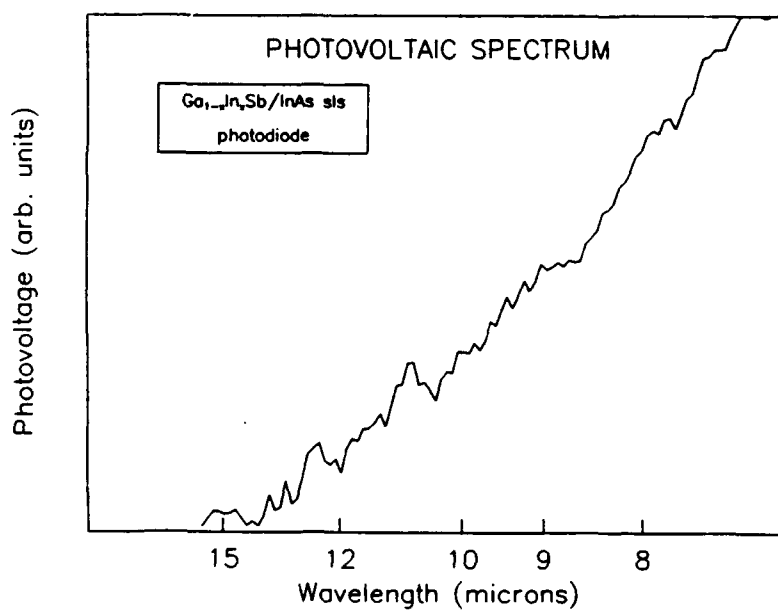

Figure 19. Photovoltaic spectral response from a diode fabricated from superlattice TCH618.

4.3.2 Sb-Series Samples

More recent p-n junction samples (Sb021, Sb022, Sb025, and Sb065) have displayed significantly improved I-V behavior relative to TCH601 and TCH618. The improvement is most likely attributable to a reduction in background doping level in the superlattice active layer, and the addition of a slight heterojunction barrier between p-type GaSb and the n-type superlattice. Figure 20 is an I-V curve taken at 77 K from a 5×5 μm device on sample Sb025. The device was fabricated by the wet chemical etching process described in Section 4.2.1. The curve displays a forward bias threshold near 80 mV, and a reverse bias breakdown voltage greater than 300 mV. R_0A for the device is 0.1 Ω-cm^2, approximately two orders of magnitude lower than state-of-the-art HgCdTe with a 12 μm cutoff wavelength. As noted in Section 4.2.1, the wet chemical process used to fabricate these devices has significant drawbacks (e.g., no passivation); we anticipate dramatic improvements in device performance with the development of a complete fabrication procedure.
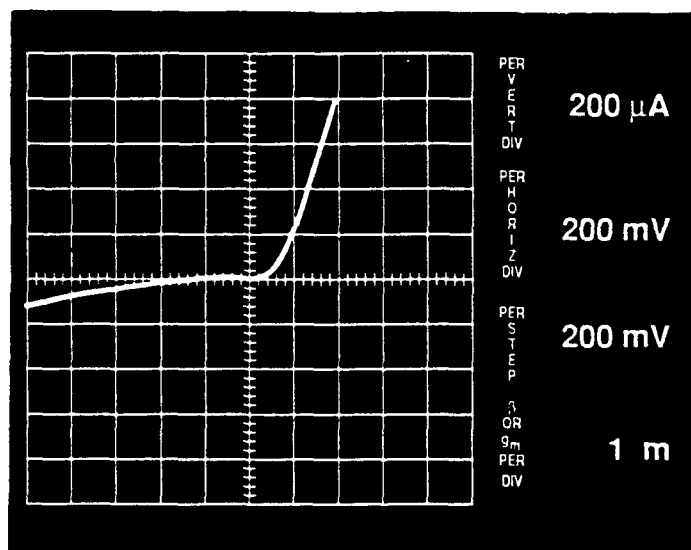

Figure 20. 77K current-voltage characteristic for a 5×5 μm PV device fabricated from sample Sb025. The device showed an R_0A of 0.1 Ωcm^2 and a cutoff wavelength of 12 μm.

Section 5
SUMMARY

In summary, we have grown high-quality $Ga_{1-x}In_xSb/InAs$ superlattices by MBE and have demonstrated their potential for LWIR detector applications. Superlattices grown on GaSb substrates are essentially dislocation-free, show no evidence of interdiffusion, and benefit from submonolayer uniformity control. Our current growth techniques yield n-type background doping in the low-to-mid 10^{15} cm^{-3} range (uncompensated). We have shown that thin layer (25-50 Å) $Ga_{1-x}In_xSb/InAs$ superlattices have cutoff wavelengths spanning the infrared, with absorption coeffients comparable to those of $Hg_{1-x}Cd_xTe$. Predictions of appreciable effective masses in the superlattices are supported by these measurements, and have been confirmed by independent magneto-optical experiments. Initial unpassivated 12 μm photovoltaic devices show R_0A's of 0.1 Ω-cm^2, approximately two orders of magnitude lower than those of comparable HgCdTe. We anticipate that efforts to passivate and further develop the processing of these devices will lead to significantly improved detectors. At present, GaInSb/InAs superlattices appear to be the only innovative IR detector structures offering the tunability and performance of HgCdTe at operating temperatures significantly exceeding current technology. Compounded with benefits derived from a mature III-V processing technology, they promise tremendous savings in both the cost and complexity of LWIR and VLWIR systems tailored to DoD applications.

Section 6
REFERENCES

1. D.L. Smith and C. Mailhiot, J. Appl. Phys. **62**, 2545 (1987).

2. C. Mailhiot and D.L. Smith, J. Vac. Sci. Technol. A **7**, 445 (1989).

3. R.H. Miles, J. N. Schulman, D.H. Chow, and T.C. McGill, to be published in Semicond. Sci. Technol. (See Appendix.)

4. C.H. Grein, P. M. Young, and H. Ehrenreich, submitted to Appl. Phys. Lett.

5. J.P. Omaggio, J.R. Meyer, R. J. Wagner, C.A. Hoffman, M.J. Yang, D.H. Chow, and R. H. Miles, Appl. Phys. Lett. **61**, 207 (1992).

6. R. H. Miles, D. H. Chow, and W. J. Hamilton, J. Appl. Phys. **71**, 211 (1992).

7. D.H. Chow, R. H. Miles, J.N. Schulman, D.A. Collins, and T.C. McGill, Semicond. Sci. Technol. **6**, C47 (1991).

8. R.H. Miles, D.H. Chow, J.N. Schulman, and T.C. McGill, Appl. Phys. Lett. **57**, 801 (1990).

9. D.H. Chow, R.H. Miles, and A.T. Hunter, J. Vac. Sci. Technol. B **10**, 888 (1992).

10. S. Kalem, J.I. Chyi, H. Morkoc, R. Bean, and K. Zanio, Appl. Phys. Lett. **53**, 1648 (1988).

11. J.R. Soderstrom, D.H. Chow, and T.C. McGill, Mat. Res. Soc. Symp. Proc. **145**, 409 (1989).

12. C.T. Foxon and B.A. Joyce, Surface Sci. **50**, 434 (1975).

13. C.T. Foxon and B.A. Joyce, Surface Sci. **64**, 293 (1977).

14. T.M. Rossi, D.A. Collins, D.H. Chow, and T.C. McGill, Appl. Phys. Lett. **57**, 2256 (1990).

15. B.M. Clemens and J.G. Gay, Phys. Rev. B **35**, 9337 (1987).

16. J.P. Baukus, A.T. Hunter, O.J. Marsh, C.E. Jones, G.Y. Wu, S.R. Hetzler, T.C. McGill, and J.-P. Faurie, J. Vac. Sci. Technol. A **4**, 2110 (1986).

17. P. Voisin, G. Bastard, C.E.T. Goncalves da Silva, M. Voos, L.L. Chang, and L. Esaki, Solid State Commun. **39**, 79 (1981).

18. P.M. Petroff, J. Cibert, A. C. Gossard, G.J. Dolan, and C.W. Tu, J. Vac. Sci. Technol. B **5**, 1204 (1987).

19. D.L. Smith and C. Mailhiot, J. Appl. Phys. **62**, 2545 (1987).

APPENDIX A

Electronic band structure of far-infrared Ga₁₋ₓInₓSb/InAs superlattices

R H Miles†, J N Schulman†, D H Chow† and T C McGill‡

† Hughes Research Laboratories, Malibu, CA 90265, USA
‡ California Institute of Technology, Pasadena, CA 91125, USA

Abstract. Results of tight-binding and eight-band $k \cdot p$ calculations of the electronic band structure of long wavelength Ga₁₋ₓInₓSb/InAs superlattices are compared with experimental energy gap and absorption coefficient data. The effective masses, band splittings and absorption coefficients observed in this system illustrate the potential of these structures for application in focal plane array systems demanding high detectivities or relaxed cooling requirements. Comparisons with Hg₁₋ₓCdₓTe, the industry standard, are particularly favourable at longer wavelengths (8–12 μm and beyond), due to both a substantial reduction in tunnel currents and a suppression of impact ionization noise processes. We also find that the InSb- or Ga₁₋ₓInₓAs-like nature of the interfaces should affect the energy gap of a Ga₁₋ₓInₓSb/InAs superlattice, and that substantially larger optical absorption coefficients are to be expected in structures with InSb-like interfaces. Our calculations are in agreement with experimental absorption spectra and with observed dependences of energy gaps on interfacial chemistry, measured in samples in which the nature of the interfaces was controlled through appropriate shuttering sequences and use of interrupts during growth by molecular beam epitaxy.

1. Introduction

Recent work on Ga₁₋ₓInₓSb/InAs superlattices has been motivated by infrared detector applications for these structures [1, 2], particularly in the 8–12 μm atmospheric transmission band. Brought to maturity, detectors based on these superlattices could be expected to achieve background-limited performance at operating temperatures higher than those of HgCdTe-based systems. Such superlattice detectors might also prove to be more readily manufactured and more robust than the II–VIs currently used, owing to compatibility with mainstream III–V processing technology and to the enhanced structural stability of the material, respectively.

While detectors rivaling Hg₁₋ₓCdₓTe have yet to be fabricated from Ga₁₋ₓInₓSb/InAs superlattices, considerable strides have been made in their development over the past couple of years. Molecular beam epitaxial growth conditions yielding superlattices that are essentially structurally ideal [3] have been established [4–6]. Background doping levels, previously in the range 10¹⁶–10¹⁷ cm⁻³ are now routinely in the low 10¹⁵ cm⁻³ [7], and structures with long wavelength energy gaps now yield appreciable photoluminescence [8]. A number of theoretical predictions have been borne out by experiment, including the dependence of the superlattice energy bandgap on layer thicknesses and compositions (up to $x = 0.30$) [9], the magnitude of the optical absorption coefficient in 8–12 μm superlattices [5, 10] and the approximate values of the electron and hole effective masses [11, 12].

In this paper we address the properties of Ga₁₋ₓInₓSb/InAs superlattices with intrinsic photoresponse beyond 12 μm. The considerable magnitude of tunnelling noise currents and the sensitivity of these currents to small variations across a wafer have mitigated against the application of large area Hg₁₋ₓCdₓTe detectors in this spectral region. As a consequence, extrinsic detectors such as those based on doped Si are currently the standard beyond 12 μm, despite the considerable sacrifices in operating temperature or detectivity associated with extrinsic detectors. We predict both a marked reduction in tunnel currents in Ga₁₋ₓInₓSb/InAs superlattice detectors with far-infrared cut-offs, and a comparative insensitivity of these currents to variations across an array, relative to Hg₁₋ₓCdₓTe. These properties derive from the larger effective masses found in these superlattices, and from qualitative differences between the band structures in the two cases. Lastly, we use a tight-binding model to examine effects of interfacial chemistry on the energy gaps and absorption coefficients of these superlattices. We find that the interfaces have a sizable effect on these properties, particularly at longer wavelengths. Our results are consistent with the limited experimental data on this subject.

2. $k \cdot p$ calculations

Two means were used to calculate the electronic band structure of narrow gap Ga₁₋ₓInₓSb/InAs superlattices

A-1
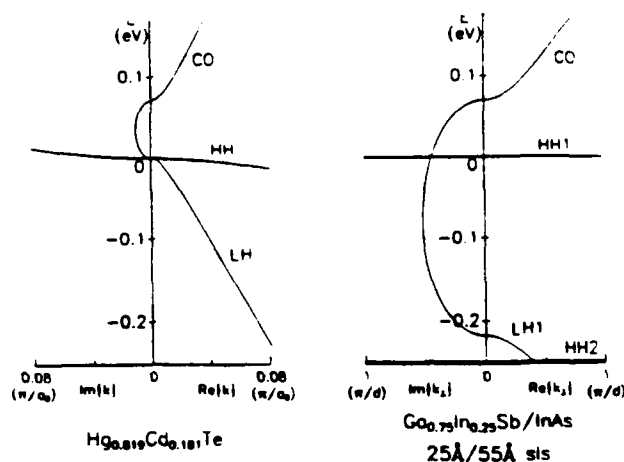
Figure 1. Comparison of $Hg_{1-x}Cd_xTe$ and $Ga_{1-x}In_xSb/InAs$ superlattice electronic band structures, illustrating the considerable magnitude of the imaginary wavevector in the superlattice gap and the shift of the first light-hole state (LH1) more than an energy gap below the heavy hole ground state (HH1). Real wavevectors (Re{k}) are plotted to the right of the energy axes and imaginary wavevectors (Im{k}) to the left. The out-of-plane wavevector ($k_\perp$) is plotted in the case of the superlattice.

An eight-band $k \cdot p$ model was used to determine energy gaps, band splittings and effective masses, neglecting interface effects; and a two-band tight-binding model was applied to estimate the magnitude of effects due to interfaces and the characteristics of the resulting optical absorption spectra. Energy gaps calculated by the two methods are in close agreement when interface effects are neglected in the tight-binding analysis.

The $k \cdot p$ calculation has been described in detail elsewhere [13, 14]. We use a second-order $k \cdot p$ model incorporating spin–orbit splitting and strain. Effects derived from bands outside the basis set (which consists of the two lowest conduction band states and six highest valence band states) are described by Luttinger parameters. Where available, parameters were taken from Lawaetz [15]; the remainder were taken from the Landolt-Börnstein series [16]. Strain is incorporated through a three-parameter deformation potential [17], describing hydrostatic shifts to the energy gap and [100] and [111] uniaxial shifts. We assume an InAs/$Ga_{1-x}In_xSb$ valence band offset of 560 meV [18], regardless of alloy composition, and further assume that hydrostatic strain does not affect this value. Our model yields energy gaps that are in good agreement with those determined from photoconductive thresholds [9], and in-plane effective masses consistent with experimental observations on superlattices with 8–12 μm cut-offs [12].

Figure 1 shows calculated 77 K dispersion curves for a $Hg_{0.819}Cd_{0.181}Te$ alloy and a 25 Å/55 Å $Ga_{0.75}In_{0.25}Sb/InAs$ superlattice. Real wavevectors are plotted to the right of the energy axes, and imaginary wavevectors (corresponding to the reciprocal of the decay length governing tunnelling across a forbidden region) are plotted to the left. Both structures have energy

gaps of 70 meV. We calculate electron effective masses of $m_e^* = 0.00534\, m_e$ and $m_{e,\perp}^* = 0.0215\, m_e$, respectively, for the two cases (we find the electron effective mass in the superlattice to be nearly isotropic). As can be seen from the magnitude of the imaginary wavevectors in the energy gaps, both the zone-centre splitting of the heavy- and light-hole bands and the increased electron effective mass should greatly reduce tunnel currents in the superlattice. The splitting of the valence band states is also predicted to suppress Auger recombination in p-type structures by reducing the phase space available for this process [19]. Initial calculations have shown this to be so [20]. While the effective masses are considerably greater in the superlattice than in the alloy, we also find them to be less sensitive to energy gap fluctuations; a 10 meV reduction in energy gap (corresponding to a 0.6% change in $Hg_{1-x}Cd_xTe$ alloy composition, or a 6.8% change in superlattice layer thickness) results in a 14% reduction in m_e^* for the $Hg_{1-x}Cd_xTe$ alloy (to 0.00460 m_e), but only a 0.9% reduction (to 0.0213 m_e) in the superlattice. These benefits suggest that $Ga_{1-x}In_xSb/InAs$ superlattices are particularly well suited to large area, long wavelength infrared (LWIR) detector applications at wavelengths that have proven inaccessible to $Hg_{1-x}Cd_xTe$ for practical reasons. Furthermore, brought to maturity, such detectors would display higher detectivities and/or higher operating temperatures than $Hg_{1-x}Cd_xTe$ sensors (either would greatly outperform extrinsic detectors in these regards).

3. Effects due to interfaces

Two types of interface are possible in, e.g., a (100) GaSb/InAs superlattice: an 'InSb-like' interface, in which planes of atoms are stacked in the growth direction as follows:

··· Ga Sb Ga Sb In As In As In As In Sb Ga Sb Ga ···

or a 'GaAs-like' interface:

··· Ga Sb Ga As In As In As In As In As Ga Sb Ga ··

Control of the interfacial chemistry, achieved through appropriate shuttering sequences and use of interrupts during growth by molecular beam epitaxy, has been demonstrated previously [21, 22].

We employ a two-band tight-binding model to assess the effects of the interfaces on the electronic properties of these quaternary superlattices. The model allows individual layers of In, Ga, As or Sb atoms (or mixtures thereof) to be identified at each atomic plane. In the wide well and barrier limit, the energy bands and wavefunctions are essentially those of two-band envelope function models. Aside from strain effects, the model has been described previously [23]. The input parameters consist of the bulk bandgaps and band discontinuities for the on-site energy parameters of the
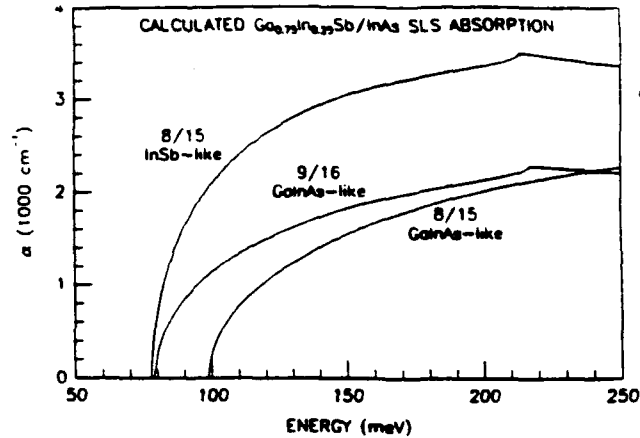
Figure 2. Absorption coefficients calculated for 8 ML/15 ML $Ga_{0.75}In_{0.25}Sb/InAs$ superlattices with InSb- and $Ga_{0.75}In_{0.25}As$-like interfaces and a 9 ML/16 ML structure with $Ga_{0.75}In_{0.25}As$-like interfaces. The 9 ML/16 ML case was chosen to preserve both the 15.5 μm energy gap and the mean level of strain in the superlattice.

model, and the bulk effective masses for the transfer matrix elements.

Strain is included through deformation potentials. 'Local' conduction and valence band edges are found for each atomic bilayer, based on the lattice strain and deformation potentials for the local atomic composition. This determines the on-site parameters. The shifted band edges are then used to find the effective mass in the locally strained material using a three-band $k \cdot p$ formula [24]. The tight-binding transfer matrix elements are then determined from the local effective masses.

An interface atom is treated as having the average of properties of the bulk semiconductor formed by pairing with the atom to its right and those formed by pairing to its left. For example, the on-site interface As parameters at an In–As–Ga–Sb interface were taken to be averages of InAs and GaAs on-site As parameters. Similarly, the Ga parameters were set to be averages of GaAs and GaSb parameters.

Figure 2 shows optical absorption curves derived from our tight-binding model. Three cases are presented: 8 ML/15 ML† $Ga_{0.75}In_{0.25}Sb/InAs$ superlattices with (1) InSb-like interfaces and (2) $Ga_{0.75}In_{0.25}As$-like interfaces, and (3) a 9 ML/16 ML $Ga_{0.75}In_{0.25}Sb/InAs$ superlattice with $Ga_{0.75}In_{0.25}As$-like interfaces (chosen to have approximately the same energy gap and strain level as (1)). The figure illustrates both the shift in energy gap upon changing the interfacial chemistry, and the desirability of InSb-like interfaces for achieving large LWIR absorption coefficients with abrupt thresholds. The magnitude of the energy gap shift is in fair agreement with experiment. A previous study [22] found a shift of 25 meV for a 8 ML/13 ML $Ga_{0.75}In_{0.25}Sb/InAs$ superlattice. While this is somewhat larger than the 15 meV we calculate for this case, we note that small changes in layer thicknesses will significantly alter the
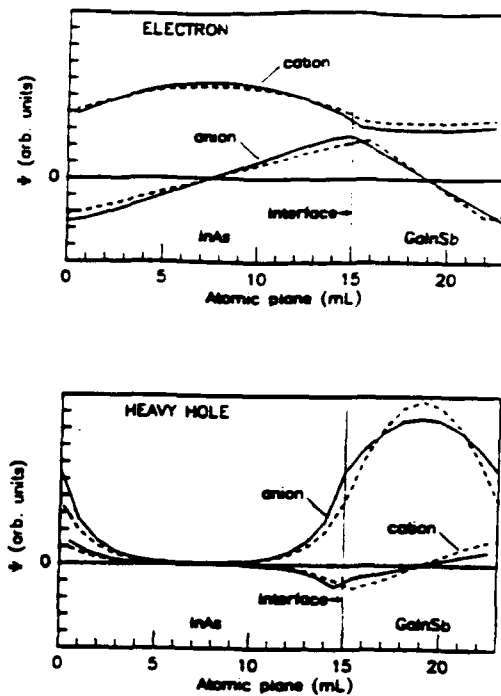
† We adopt the (arbitrary) convention of labelling superlattices by indicating the number of group-III monolayers in each layer of the superlattice.

Figure 3. Zone-centre (a) electron and (b) hole tight-binding wavefunctions for 8 ML/15 ML $Ga_{0.75}In_{0.25}Sb/InAs$ superlattices with InSb-like (full curves) and $Ga_{0.75}In_{0.25}As$-like (broken curves) interfaces. Both cation and anion wavefunctions are plotted.

magnitude of this dependence (as illustrated by the shift of more than 20 meV for the case chosen for figure 2). Our calculations are in excellent agreement with previously published absorption coefficient data [10], assuming InSb-like interfaces. We are not aware of experimental absorption data for samples with $Ga_{1-x}In_xAs$-like interfaces.

Tight-binding wavefunctions for zone-centre states are presented in figure 3. Electron (a) and hole (b) wavefunctions are shown for the 8 ML/15 ML InSb-like and $Ga_{0.75}In_{0.25}Sb$-like cases for which absorption coefficients were given in figure 2. The increased valence-to-conduction band oscillator strength calculated for the former arises from two factors: wavefunction overlap at the interfaces increases on switching from a highly strained monolayer of $Ga_{0.75}In_{0.25}As$ to one of InSb in this region; and the requirement of achieving the same energy gap necessitates wider layers in the $Ga_{0.75}In_{0.25}As$ case, further isolating the electrons and holes in the InAs and $Ga_{0.75}In_{0.25}Sb$ layers, respectively.

Our calculations neglect the possibility of a dependence of the band offsets on interface strain. Such an effect has been predicted in the $InAs/Al_{0.8}Ga_{0.2}As_{0.14}Sb_{0.86}$ superlattice system [25]. A calculation in which a strain-dependent band offset was assumed has yielded a theoretical energy gap in agreement with photoluminescence data from such a super-

lattice. However, the reasonable agreement between our calculations and experiment suggests that these effects are not large in the $Ga_{1-x}In_xSb/InAs$ superlattice system.

4. Conclusion

$Ga_{1-x}In_xSb/InAs$ superlattices currently show considerable promise for 8–12 μm detector applications in which high detectivity is required. While manufacturing issues alone may favour these superlattices over $Hg_{1-x}Cd_xTe$, bringing these superlattice detectors to maturity would also ease cooling requirements for background-limited performance. We find that predicted performance benefits over $Hg_{1-x}Cd_xTe$ are magnified at wavelengths beyond 12 μm. Namely, effective masses remain appreciable for near-zero gap superlattices, which should lead to a reduction in tunnelling noise currents, and the substantial splitting between heavy- and light-hole valence bands should suppress the Auger recombination pathway predominant in p-type $Hg_{1-x}Cd_xTe$, with the result that impact ionization noise associated with this channel should be lowered. Of additional practical importance is the relative insensitivity of the calculated effective masses to fluctuations in layer thicknesses.

Lastly, we have explored the dependence of the electronic band structure of these superlattices upon the choice of InSb-like or $Ga_{1-x}In_xAs$-like interfaces. We find that the choice of interfaces shifts the energy gap of a particular superlattice, with the shift increasing in magnitude at longer wavelengths (both in absolute and relative terms). Our calculations show that large (> 1000 cm^{-1}) absorption coefficients can be obtained in structures with InSb-like interfaces.

Acknowledgments

References

[1] Smith D L and Mailhiot C 1987 J. Appl. Phys. 62 2545
[2] Smith D L and Mailhiot C 1987 J. Appl. Phys. 62 2545
[3] Miles R H, Chow D H and Hamilton W J 1992 J. Appl. Phys. 71 211
[4] Chow D H, Miles R H, J R Söderström and McGill T C 1990 J. Vac. Sci. Technol. B 8 710
[5] Campbell I H, Sela I, Laurich B K, Smith D L, Bolognesi C R, Samoska L A, Gossard A C and Kroemer H 1991 Appl. Phys. Lett. 59 846
[6] Fan W C, Zborowski J T, Golding T D and Shin H D 1992 J. Appl. Phys. 71 2249
[7] Chow D H unpublished
[8] Miles R H unpublished
[9] See, for example, Miles R H, Chow D H and McGill T C 1990 SPIE Proc. 1285 132
[10] Miles R H, Chow D H, Schulman J N and McGill T C 1990 Appl. Phys. Lett. 57 801
[11] Omaggio J P, Meyer J R, Wagner R J, Hoffman C A, Yang M J, Chow D H and Miles R H 1992 Appl. Phys. Lett. to be published
[12] Omaggio J P, Meyer J R, Wagner R J, Hoffman C A, Yang M J, Chow D H and Miles R H 1993 Semicond. Sci. Technol. 8 at press
[13] Kane E O 1966 Semiconductors and Semimetals vol 1, ed R K Willardson and A C Beer (New York: Academic) p 75
[14] Smith D L and Mailhiot C 1986 Phys. Rev. B 33 8345
[19] Smith D L private communication
[20] Ehrenreich H, Grein C, Young P and McGill T C 1992 submitted to the HgCdTe Workshop (October)
[15] Lawaetz P 1971 Phys. Rev. B 4 3460
[16] Landolt-Börnstein New Series 1987 vol III/22a, ed O Madelung (Berlin: Springer)
[17] Bir G L and Pikus G E 1974 Symmetry and Strain-Induced Effects in Semiconductors (Jerusalem: Keter)
[18] Sai-Halasz G A, Chang L L, Walter J M, Chang C A and Esaki L 1978 Solid State Commun. 27 935
[21] Tuttle G, Kroemer H and English J H 1990 J. Appl. Phys. 67 3032
[22] Chow D H, Miles R H and Hunter A T 1992 J. Vac. Sci. Technol. B 10 888
[23] Schulman J N 1986 MRS Symp. Proc. 56 279
[24] See, for example, Kane E O 1957 J. Phys. Chem. Solids 1 249
[25] Nelson J S, Kurtz S R, Dawson L R and Lott J A 1990 Appl. Phys. Lett. 57 578

APPENDIX B

Effects of interface stoichiometry on the structural and electronic properties of $Ga_{1-x}In_xSb/InAs$ superlattices

D. H. Chow, R. H. Miles, and A. T. Hunter

Hughes Research Laboratories, Malibu, California 90265

We report an investigation of the effects of interface layer composition on the structural and electronic properties of $Ga_{1-x}In_xSb/InAs$ superlattices, which are of interest for infrared detector applications. Shutter sequencing during growth of a series of $Ga_{0.75}In_{0.25}Sb$ (8 ML)/ InAs (13 ML) superlattices by molecular-beam epitaxy has been employed to select structures with GaInAs-like interfaces, InSb-like interfaces, and intermediate choices of interfacial composition. Comparison of x-ray diffraction scans from the superlattices confirms that a superlattice with GaInAs-like interfaces has a 1.6% smaller average interatomic spacing in the growth direction than a sample with InSb-like interfaces, in near agreement with expected interfacial bond length differences. Hall measurements of intrinsic carrier concentrations at high temperatures indicate an increase in superlattice energy gap when interfaces are switched from InSb-like to GaInAs-like, consistent with intuitive expectations. Low temperature Hall measurements suggest that both the type and the level of background doping in $Ga_{1-x}In_xSb/InAs$ superlattices may depend upon interfacial composition.

I. INTRODUCTION

Heterostructures containing combinations of arsenides and antimonides are of interest for a number of electronic and optoelectronic device applications, including field effect transistors,[1] 2–5 μm semiconductor lasers,[2] THz oscillators,[3] and superlattice infrared (IR) detectors.[4,5] In many of these structures, multiple possibilities exist for bond configurations at arsenide/antimonide heterointerfaces. Tuttle *et al.* demonstrated recently that the transport properties of InAs/AlSb quantum wells (QWs) can be profoundly affected by interfacial composition.[6] We anticipate that an understanding of the electronic effects of varying interfacial composition will be of vital importance in realizing many of the potential device applications of mixed arsenide/antimonide heterostructures.

We report here a study of the consequences of varying interfacial composition in $Ga_{1-x}In_xSb/InAs$ superlattices, which are potential candidates for IR detector applications in the 8–14 μm range and beyond.[4,5,7,8] Since the atoms residing on both group III and group V sublattices change across a $Ga_{1-x}In_xSb/InAs$ interface, it is possible to obtain two distinctly different interfacial bond configurations. If a $Ga_{1-x}In_xSb$ layer is terminated with a final monolayer of Sb, the adjoining InAs layer will commence with a monolayer of In (assuming that group III and group V atoms are restricted to their respective sublattices), leading to InSb bonds across the interface (an "InSb-like" interface). Conversely, if a $Ga_{1-x}In_xSb$ layer is terminated with a final monolayer of $Ga_{1-x}In_x$, the adjoining InAs layer will commence with a monolayer of As, resulting in $Ga_{1-x}In_xAs$ bonds across the interface (a "GaInAs-like" interface). It should be noted that intermediate interfacial compositions are also possible; an example is described in Sec. II. It is reasonable to expect that the choice of inter-

facial composition and growth conditions will play a key role in determining the nature and quantity of interfacial defects, which may have implications for detector performance.

II. MOLECULAR-BEAM EPITAXY GROWTH

The $Ga_{1-x}In_xSb/InAs$ superlattices studied here were grown by molecular-beam epitaxy (MBE) in a Perkin Elmer 430P system equipped with reflection high-energy electron diffraction (RHEED), and cracked arsenic and antimony sources. The superlattices were deposited on thick (0.5–1.0 μm) stress–relaxes GaSb buffer layers on lattice-mismatched, (100)-oriented, InP or GaAs substrates. The procedure we use for deposition of GaSb buffer layers has been described elsewhere.[9,10] All of the superlattices described here consist nominally of 8 ML (25 Å) of $Ga_{0.75}In_{0.25}Sb$ and 13 ML (39 Å) of InAs. Total superlattice thicknesses are 80 periods (0.5 μm). Superlattices with these parameters, in which growth was interrupted (no group III flux) in an Sb_2 flux for 5 s at each interface, have previously been shown to result in samples with energy gaps near 110 meV (11 μm).[5] The method used to reproducibly select substrate temperatures for these structures has been described elsewhere.[9]

Figure 1 depicts the shutter sequences we have used to produce superlattices with $Ga_{0.75}In_{0.25}As$-like and InSb-like interfaces. In the case of $Ga_{0.75}In_{0.25}As$-like interfaces, deposition of each 13 ML thick InAs layer is followed by a 5 s "soak" in As in an attempt to terminate the layer with As atoms. A 1×2 RHEED pattern is observed during both the InAs layer and As soak. Next, the As shutter is closed, and the Ga and In shutters are opened (without an accompanying group V flux) for the time required for deposition of 1 ML of $Ga_{0.75}In_{0.25}$. This step results in a transforma-
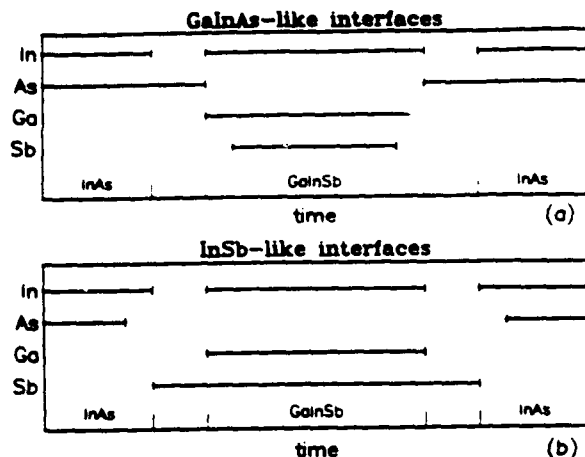
FIG. 1. Illustration of MBE shutter sequences (not to scale in time) used to produce Ga₁₋ₓInₓSb/InAs superlattices with (a) GaInAs-like interfaces, and (b) InSb-like interfaces. Solid bars indicate time periods in which shutters are open.

tion of the RHEED pattern to 4×4 (presumably a metal rich surface reconstruction). The Sb shutter is then opened for the time needed to deposit 6 ML of $Ga_{0.75}In_{0.25}Sb$ (nominally resulting in 6 ML of $Ga_{0.75}In_{0.25}$ separating 7 ML of Sb), and closed again for the time required for a single monolayer of $Ga_{0.75}In_{0.25}$. The characteristic 1×3 RHEED pattern observed during growth of the $Ga_{0.75}In_{0.25}Sb$ layer is transformed to a 4×1 pattern (again due to a metal rich reconstruction) when the Sb shutter is closed. The sample is then soaked for 5 s in an As flux, resulting in a 1×3 RHEED pattern, prior to the next 13 ML InAs deposition.

In the case of InSb-like interfaces, deposition of each 8 ML thick $Ga_{0.75}In_{0.25}Sb$ layer is followed by a 5 s soak in Sb. A transformation from 1×3 to 1×5 in surface reconstruction is observed during the Sb soak. Next, the Sb shutter is closed, and the In shutter is opened for the time needed to deposit a monolayer of In, resulting in a return to a 1×3 RHEED pattern. The As shutter is then opened for the time needed to deposit 11 ML of InAs (nominally resulting in 11 ML of In separating 12 ML of As) and closed again for the time required for a single monolayer of In. The 1×2 RHEED pattern observed during growth of the InAs layer is transformed to a 2×4 pattern when the As shutter is closed. The sample is then soaked for 5 s in an Sb flux, resulting in a 1×3 RHEED pattern, prior to the next 8 ML $Ga_{0.75}In_{0.25}Sb$ deposition.

In addition to $Ga_{1-x}In_xSb/InAs$ superlattices with all InSb-like interfaces and all GaInAs-like interfaces, we have grown one sample in which $Ga_{1-x}In_xSb$ on InAs interfaces are grown InSb-like and InAs on $Ga_{1-x}In_xSb$ interfaces are grown GaInAs-like, and one sample with the opposite interfacial configurations. We have also grown a superlattice with an intermediate interfacial composition by depositing interfacial monolayers consisting of In (0.5 ML)/$Ga_{0.75}In_{0.25}$ (0.5 ML) sandwiched between Sb-terminated $Ga_{0.75}In_{0.25}Sb$ and As-terminated InAs layers. We note that the total group III deposition times are the same

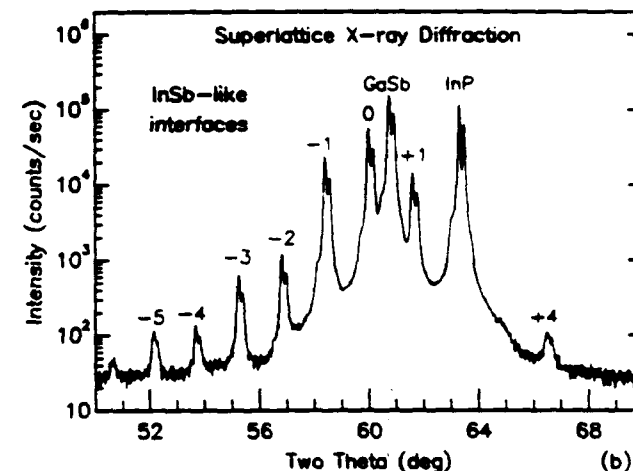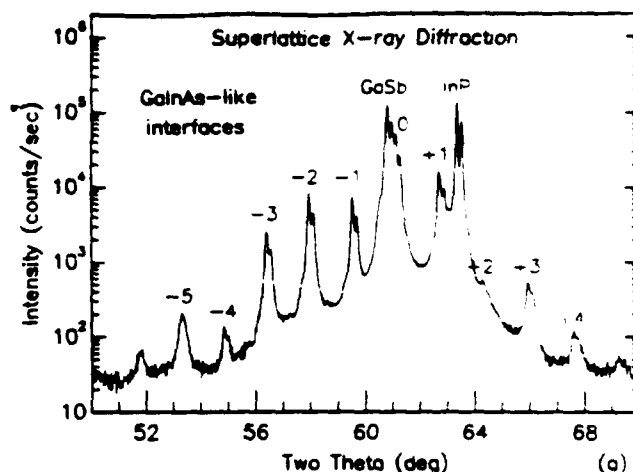FIG. 2. $\Theta/2\Theta$ x-ray diffraction scans from $Ga_{0.75}In_{0.25}Sb$ (8 ML)/InAs(13 ML) superlattices with (a) GaInAs-like interfaces and (b) InSb-like interfaces. The samples were irradiated with Cu $K\alpha$ x-rays. Each peak appears to be bimodal due to the $K\alpha$ doublet. The InP substrate peak, GaSb buffer peak, and superlattice satellite indices are labeled in each scan. A significant difference in average interatomic spacing (zeroth order x-ray satellite) is observed.

for all cases, ensuring that the number of monolayers in each superlattice period are unaffected by the choice of interfacial composition.

III. X-RAY DIFFRACTION

Structural analysis of the $Ga_{1-x}In_xSb/InAs$ superlattices discussed here has been performed via (400)-like $\Theta/2\Theta$ x-ray diffraction. The period and average interatomic spacing of each superlattice has been determined from the x-ray data by measuring the satellite spacings and zeroth order satellite position, respectively. Figures 2(a) and 2(b) show $\Theta/2\Theta$ x-ray diffraction data taken from $Ga_{1-x}In_xSb/InAs$ superlattices with all GaInAs-like and all InSb-like interfaces, respectively. A striking shift in zeroth order peak position is observed between the two diffraction scans (note that the zeroth order peaks in the two scans are on opposite sides of the GaSb buffer layer peak), indicating a significant difference in average interatomic spacing between the two superlattices. We believe that this
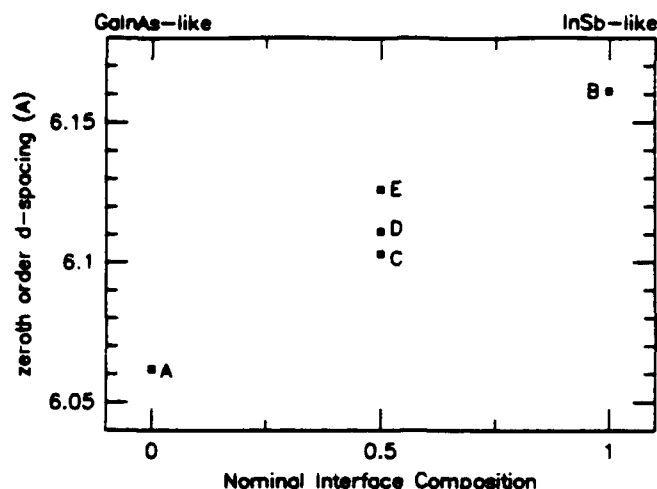
FIG. 3. Plot of zeroth order d-spacing vs nominal interfacial composition for five $Ga_{1-x}In_xSb/InAs$ superlattices. Sample A = all GaInAs-like interfaces; Sample B = all InSb-like interfaces; Sample C = GaInAs-like interfaces when growing InAs on GaInSb and InSb-like interfaces when growing GaInSb on InAs; Sample D = opposite of Sample C; Sample E = intermediate interfacial composition. The data show a clear correlation between average interatomic spacing and nominal interfacial composition.

shift results from the tremendous difference between the interfacial bond lengths of InSb and GaInAs.

Figure 3 is a plot of the measured zeroth order d-spacing versus nominal interfacial composition for each of the five superlattices studied here. In the plot, the superlattice with InSb-like interfaces is assigned a nominal interfacial composition of 1, while the superlattice with GaInAs-like interfaces is assigned a value of 0. The superlattices with half of each type of interface and the superlattice with intermediate interfacial configuration (described in Sec.

II) are assigned nominal compositions of 0.5. The plot shows a clear correlation between nominal interfacial composition and the resulting interatomic spacing. Ideally, a change from InSb-like interfaces to GaInAs-like interfaces would result in two $Ga_{0.75}In_{0.25}Sb$ bonds per superlattice period becoming $Ga_{0.75}In_{0.25}As$ bonds, and two InSb bonds per superlattice period becoming InAs bonds. Assuming that the interfacial layers are coherently strained, and that there are a total of 42 bonds per superlattice period, we would expect a difference in average interatomic spacing of 1.4% between the two cases. From Fig. 3, the measured average interatomic spacing of the sample with GaInAs-like interfaces is 1.6% smaller than that of the sample with InSb-like interfaces. Hence, the measured difference in average interatomic spacing is in good agreement with that expected from a complete change from InSb-like interfaces to GaInAs-like interfaces.

IV. HALL MEASUREMENTS

Due to the narrow energy gaps of $Ga_{1-x}In_xSb/InAs$ superlattices, samples which are not intentionally doped show intrinsic behavior at high temperature (> 250 K). Hall measurements at these temperatures are dominated by electron transport, as electron mobilities are greater than hole mobilities (due to the difference in effective mass). Neglecting the dependences of energy gap and effective density of states on temperature, the number of intrinsic carriers n_i is proportional to $\exp(-E_g/2kT)$, where E_g is the energy gap of the superlattice. Hence, high temperature Hall data can be used to estimate E_g. Figure 4 is a plot of the measured intrinsic carrier concentrations (plotted on a logarithmic scale) versus $1000/T$ for the $Ga_{1-x}In_xSb/InAs$ superlattices with InSb-like and GaInAs-like interfaces. The data reveal that the superlattice with InSb-like interfaces has a higher intrinsic carrier
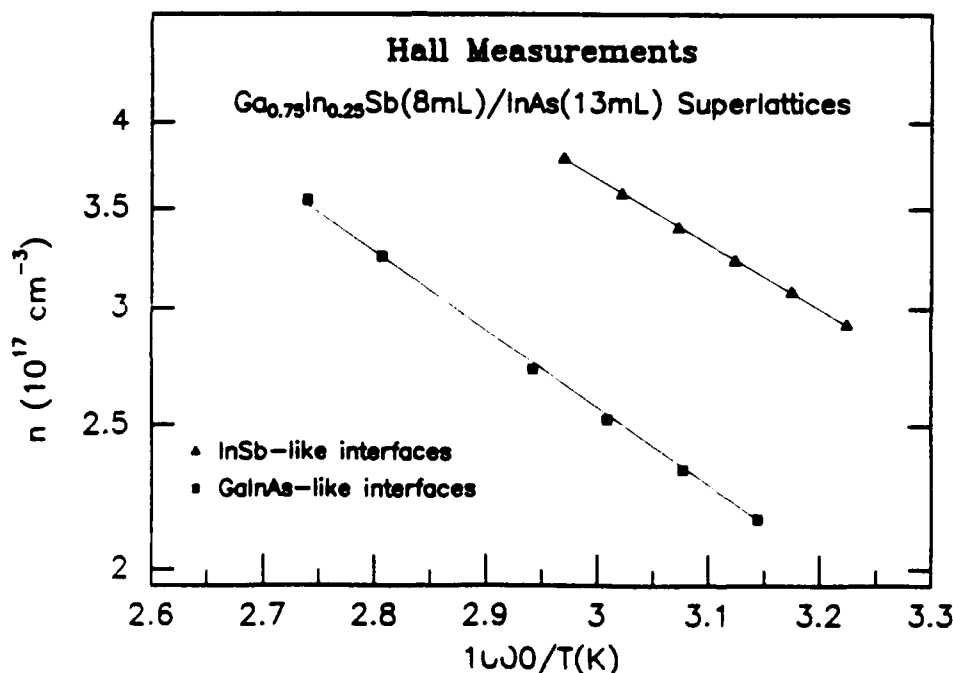

FIG. 4. Plot of intrinsic carrier concentrations (on a logarithmic scale) vs $1000/T(K)$ for superlattices with GaInAs-like interfaces (squares) and InSb-like interfaces (triangles). The data were obtained by Hall effect measurements.

concentration than the sample with GaInAs-like interfaces, consistent with a smaller energy gap. Furthermore, the slopes of the two sets of data differ by about 20%, consistent with a difference of 25 meV in energy gap. This observation is in accord with the intuitive expectation that the presence of 1 ML of relatively wide gap material in a superlattice with GaInAs-like interfaces will increase its energy gap relative to a superlattice with 1 ML of InSb, which is a narrow gap material.

Low temperature Hall measurements of our Ga$_{1-x}$In$_x$Sb/InAs superlattices generally reveal unintentional p-type background concentrations in the 10^{16} cm^{-3} range. However, the superlattice with GaInAs-like interfaces displays n-type carrier concentrations at low temperatures. Possible explanations for this observation include the formation of a surface inversion layer, or the creation of As antisite defects. The remaining four superlattices included this study all showed p-type behavior at low temperatures. There is evidence that antimonides tend to contain group III antisite defects, which result in high background acceptor levels.[11] Determination of the source and reduction of the level of unintentional background doping in Ga$_{1-x}$In$_x$Sb/InAs superlattices is the subject of ongoing investigations.

V. SUMMARY

Mixed antimonide/arsenide heterostructures are of interest for a number of potential device applications. In most, if not all, of these structures, atoms residing on both the group III and the group V sublattices change across the heterojunction interfaces. The result is a nonuniqueness in the configuration of interfacial bonds. It is possible that the control of electrically active interfacial defects may hinge upon control of these interfacial compositions; many potential device applications would likely benefit from such a capability. We have studied the specific case of Ga$_{1-x}$In$_x$As-like and InSb-like interfaces in

Ga$_{1-x}$In$_x$Sb/InAs superlattices, which are of interest for infrared detector applications. X-ray diffraction scans revealed a significant difference in average interatomic spacing between superlattices with nominally GaInAs-like and InSb-like interfaces, verifying that these interfacial compositions can be controlled via MBE shutter sequencing. Hall measurements of intrinsic carrier concentrations indicated that superlattices with GaInAs-like interfaces have slightly larger energy gaps than those with InSb-like interfaces, in agreement with intuitive expectations. Low temperature Hall measurements suggested that background doping levels may vary significantly with interfacial composition.

[1] L. F. Luo, R. Beresford, W. I. Wang, and H. Munekata, Appl. Phys. Lett. 55, 789 (1989).
[2] H. K. Choi and S. J. Eglash, Appl. Phys. Lett. 59, 1165 (1991).
[3] E. R. Brown, J. R. Söderstrom, C. D. Parker, L. J. Mahoney, K. M. Molvar, and T. C. McGill, Appl. Phys. Lett. 58, 2291 (1991).
[4] D. L. Smith and C. Maihiot, J. Appl. Phys. 62, 2545 (1987).
[5] R. H. Miles, D. H. Chow, J. N. Schulman, and T. C. McGill, Appl. Phys. Lett. 57, 801 (1990).
[6] G. Tuttle, H. Kroemer, and J. H. English, J. Appl. Phys. 67, 3032 (1990).
[7] D. H. Chow, R. H. Miles, J. R. Söderstrom, and T. C. McGill, Appl. Phys. Lett. 56, 1418, 1990.
[8] I. H. Campbell, I. Sela, B. K. Laurich, D. L. Smith, C. R. Bolognesi, L. A. Samoska, A. C. Gossard, and H. Kroemer, Appl. Phys. Lett. 59, 846 (1991).
[9] D. H. Chow, R. H. Miles, C. W. Nieh, and T. C. McGill, J. Cryst. Growth. 111, 683 (1991).
[10] D. H. Chow, R. H. Miles, J. R. Söderstrom, and T. C. McGill, J. Vac. Sci. Technol. B. 8, 710 (1990).
[11] K. F. Longenbach and W. I. Wang, Appl. Phys. Lett. 59, 1117 (1991).

APPENDIX C

High structural quality $Ga_{1-x}In_xSb$/InAs strained-layer superlattices grown on GaSb substrates

R. H. Miles and D. H. Chow
Hughes Research Laboratories, Malibu, California 90265

W. J. Hamilton
Santa Barbara Research Center, Goleta, California 93117

Strained $Ga_{1-x}In_xSb$/InAs superlattices exhibiting a high degree of structural perfection have been grown on GaSb substrates. The superlattices display ideal, defect-free structure, to within the resolution limits of transmission electron microscopy (TEM) and high-resolution x-ray diffraction. Cross-sectional micrographs reveal the layers to be highly planar, regular, and coherently strained to the GaSb substrates. No crystalline defects were observable by TEM, despite an internal lattice mismatch of almost 2%. Planarity of the layers is confirmed by the presence of Pendellösung fringes in high-resolution x-ray diffraction, while the observation of numerous sharp satellite peaks indicates little or no interdiffusion within the superlattices. Observed x-ray diffraction is closely fit by simulations based on a kinematical model which accounts properly for the highly strained interfaces and absence of strict translational symmetry in the superlattice growth direction. Based on this fit, an InSb-rich character is assigned to the interfaces, yielding superlattice layer thicknesses and compositions that are in quantitative agreement with those derived from independent growth rate calibrations.

I. INTRODUCTION

$Ga_{1-x}In_xSb$/InAs superlattices are of considerable technological interest as candidate long-wavelength infrared detector structures. Theoretical predictions[1,2] of 8–12-μm optical-absorption coefficients comparable to those of $Hg_{1-x}Cd_xTe$ have been confirmed,[3] and preliminary photoconductive[4,5] and photovoltaic[6] detectors have been demonstrated. Focal plane arrays fabricated from these superlattices have been projected to benefit both from well-established III-V processing techniques and from suppressed thermal and tunneling noise currents relative to HgCdTe.[1,2,7] It is also hoped that these structures might constitute viable intrinsic detectors at wavelengths beyond those attainable with HgCdTe.

Previous work into the growth by molecular-beam epitaxy (MBE) of $Ga_{1-x}In_xSb$/InAs superlattices has addressed both complications derived from mixing arsenides and antimonides within a single heterostructure and difficulties associated with the considerable lattice mismatch between InAs and $Ga_{1-x}In_xSb$ ($f = 2.2\%$ for an InSb fraction $x = 0.25$).[8,9] Abrupt compositional profiles have been demonstrated, and x-ray-diffraction data and transmission electron micrographs suggest that the superlattices are largely coherently strained to GaSb buffer layers and free of internal misfit dislocations. However, growth on GaAs or InP substrates results in threading dislocations originating at the base of GaSb or InAs buffer layers and propagating through the superlattices in densities of roughly 10^9 cm^{-2}. As there is a wealth of data to suggest that the performance of minority-carrier devices is greatly degraded by the presence of structural defects such as threading or misfit dislocations, elimination of these defects may be crucial to obtaining a competitive $Ga_{1-x}In_xSb$/InAs superlattice infrared detector.[10,11]

Unlike many strained layer superlattices, $Ga_{1-x}In_xSb$/InAs structures have been projected to benefit from lattice matching to a binary substrate. Grown to the in-plane lattice constant of GaSb, InAs is in tension with a lattice mismatch of 0.6%, whereas $Ga_{1-x}In_xSb$ is in compression, with a mismatch of 1.6% for $x = 0.25$. Consequently, appropriate choices of InAs and $Ga_{1-x}In_xSb$ layer thicknesses balance the alternating compressive and tensile elastic stresses within the superlattice, removing the driving force towards misfit dislocation formation at the base of the superlattice. In this paper we present data derived from $Ga_{1-x}In_xSb$/InAs superlattices grown on GaSb substrates. The high quality of these substrates and the excellent lattice match to our superlattices results in structures of unusually high quality, as evidenced by sharp x-ray rocking curve peaks displaying Pendellösung fringes in outstanding agreement with theory, and by the absence of dislocations in cross-sectional transmission electron microscopy (TEM).

II. EXPERIMENTAL

The samples used in this study were grown by MBE in a Perkin Elmer 430P system equipped with cracked arsenic and antimony sources. The superlattices were grown on circular, (100)-oriented GaSb substrates, 30 mm in diameter. The substrates were mounted in custom-designed molybdenum wafer holders during growth, to allow radiative heating. Use of this solderless substrate mounting was found to be necessary to prevent warping and/or cracking of the GaSb substrates under thermal stresses. The substrates were chemically cleaned prior to growth by a standard decreasing procedure, followed by a 10-min etch in

Br$_2$:HNO$_3$:HCl:CH$_3$COOH (0.35:2:36:460).[12] *In situ* cleaning consisted of outgassing at 250 °C in an ultrahigh-vacuum buffer chamber, followed by heating in an Sb flux to the oxide desorption temperature ($\approx$500 °C), in the growth chamber. The oxide desorption and subsequent growth of buffer and superlattice layers were monitored by reflection high-energy electron diffraction (RHEED).

Each of the samples consists of a 1000-Å GaSb buffer layer followed by a 40–80-period superlattice in which each period is nominally composed of 8 monolayers ($\approx$25 Å) of Ga$_{0.73}$In$_{0.27}$Sb and 13 monolayers ($\approx$39 Å) of InAs. Deposition of the group-III elements was interrupted for 5 s at each interface, effectively halting growth while the sample was exposed only to an Sb$_2$ flux. The surface morphology and overall structural quality of the superlattices were found to depend sensitively on the substrate temperature during growth. This temperature was reproducibly set at approximately 380 °C by referencing a transition from 1×3 to 1×5 in the RHEED pattern obtained from the Ga$_{0.73}$In$_{0.27}$Sb surface during a growth interrupt (in an Sb$_2$ flux) at this substrate temperature. This transition in surface reconstruction also occurs at $\approx$440 °C for a GaSb surface in an Sb$_2$ flux, and at $\approx$410 °C during growth of GaSb. Our observations suggest that the 1×3 to 1×5 transition in antimonide surface reconstruction is caused by an increase in Sb surface coverage at temperatures below the transition temperature.

The structural quality of our superlattices was determined by x-ray diffraction and transmission electron microscopy. X-ray rocking curves were obtained on high-resolution Blake and Phillips diffractometers equipped with Cu-anode x-ray sources. The CuKα_1 x-ray line was selected using a four-crystal monochromator employing a (220) Ge diffraction. This yielded an instrument linewidth of approximately 12 arcsec for each of the diffractometers. Cross-sectional transmission electron micrographs and diffraction patterns were obtained on a Phillips JEOL 2000FX operated at 200 kV. Samples were prepared by standard diamond turning, dimpling, and ion-milling techniques, and were lightly carbon coated to assure adequate conductivity.

III. RESULTS AND DISCUSSION

A cross-sectional transmission electron micrograph from one of our superlattices is shown in Fig. 1. The micrograph shows a two-beam bright-field image of our sample, with the beam direction tilted a few degrees from the [011] zone axis and a [200] diffraction vector operating. Also shown, as an inset in the figure, is a [011] zone axis electron-diffraction pattern from the specimen, exhibiting clear superlattice satellites around {200}, {111}, and {022} diffraction spots. Blemishes appearing as darker regions in the bright-field image are interpreted to be artifacts of the specimen preparation procedure, and are not intrinsic to the samples. We associate these with a tendency to form In islands during room-temperature ion milling of the sample. The highly planar and regular nature of the layers is apparent from the micrograph, as is the absence of threading or misfit dislocations. We were unable to image

FIG. 1. Cross-sectional transmission electron micrograph and electron diffraction from a Ga$_{1-x}$In$_x$Sb/InAs superlattice, illustrating the uniform and dislocation-free character of the epilayer.

any dislocations in our superlattice, despite scanning the sample in search of defects. In consideration of the 20-μm lineal distance thoroughly examined under several diffraction conditions, we place an upper bound on the dislocation density of 10^7 cm^{-2} for this superlattice (the sample was 0.5 μm thick). The actual dislocation density is likely much lower than this, but could not be determined through TEM. This result is in marked contrast to those derived from samples grown previously on InP or GaAs substrates, for which we have measured densities of $\approx$10^9 cm^{-2}.[8]

An x-ray rocking curve for one of the superlattices is shown in Fig. 2. An envelope of sharp (004)-like superlattice peaks is apparent, in addition to the (004) diffraction
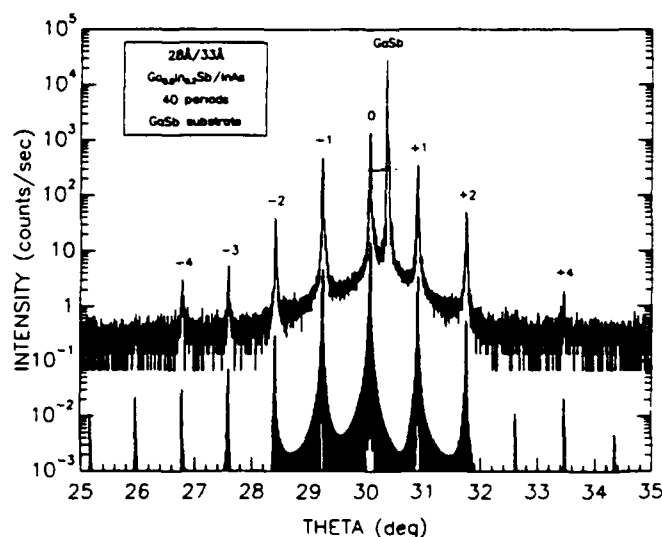

FIG. 2. Comparison of observed x-ray rocking curve with diffraction calculated from a kinematical model. The simulation is highly sensitive to the nature of the highly strained interfaces, which were assumed to be 78% InSb-like in this sample.
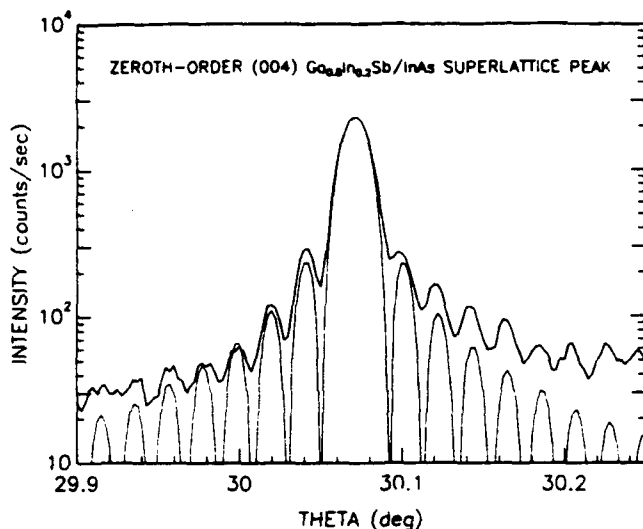
Miles, Chow, and Hamilton

C-2

FIG. 3. Measured and calculated Pendellösung fringes around the zeroth-order (004)-like superlattice diffraction peak.

peak arising from the GaSb substrate. The outstanding structural quality of the superlattice is evidenced by the considerable amplitude of higher-order superlattice peaks, and by the absence of appreciable broadening of the satellites; interdiffusion would lower the intensity of higher-order satellites, while dislocations could be expected to widen each of the observed peaks. An additional indication of high structural quality comes from the presence of Pendellösung fringes, illustrated in Fig. 3. These fringes are evident on the 0, ±1, and ±2 superlattice peaks. Those illustrated here are from the zeroth-order peak. Pendellösung fringes are observed only in exceptionally planar and regular heterostructures. This is, to our knowledge, the first observation of finite thickness fringes in a semiconductor heterostructure with this great a lattice mismatch between constituents (1.9%).

We have analyzed the x-ray diffraction from our superlattices and have used the results to simulate the dif-
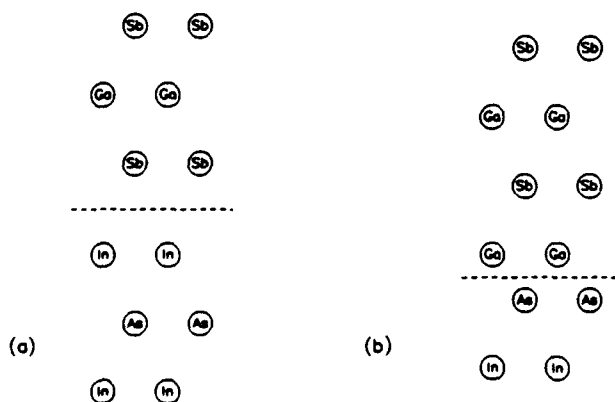

FIG. 4. Schematic of the highly strained InSb- and $Ga_{1-x}In_xAs$-like interfaces [(a) and (b), respectively] possible in a $Ga_{1-x}In_xSb/InAs$ superlattice (adapted from Ref. 13).

fraction using a kinematical model. Analysis of the diffraction was complicated substantially by the uncertain nature of the highly strained interfaces in $Ga_{1-x}In_xSb/InAs$ superlattices. As illustrated in Fig. 4, the interfaces range from $Ga_{1-x}In_xAs$-like to InSb-like, depending upon the group-V element terminating each layer. (Electrical characteristics of these classes of interfaces have been the subject of previous studies.[13]) Simulation of this diffraction is further complicated by the absence of strict translational symmetry in the growth direction in an MBE-grown superlattice, since layers are terminated upon deposition of a fixed amount of material, rather than upon deposition of a fixed integral number of monolayers. We employ a kinematical model in which diffraction is calculated by explicitly summing scattering amplitudes from each superlattice layer, allowing the changing form factors and interplanar spacings of interfacial layers to be accounted for correctly.

Experimental x-ray diffraction from the superlattices was analyzed to yield the period and average perpendicular lattice constant of the structure, derived from the separation of satellite peaks and the position of the zeroth-order superlattice diffraction peak, respectively. These data were then combined with known MBE shutter opening times, yielding the thicknesses and compositions of the layers comprising a superlattice period, assuming the InSb- or $Ga_{1-x}In_xAs$-like character of the interfaces to be known:

$$d^{sl} = t_{In}f_{In}a_\perp^{InAs} + t_{GaIn}(f_{Ga} + f_{In})a_\perp^{GaInSb}$$
$$+ [(1+y)/4](a_\perp^{InSb} - a_\perp^{InAs})$$
$$+ [(1-y)/4](a_\perp^{GaInAs} - a_\perp^{GaInSb}),$$

and

$$a_\perp^{sl} = d^{sl}/[t_{In}f_{In} + t_{GaIn}(f_{Ga} + f_{In})],$$

where t indicates the group-III deposition time for each layer; the character of the interface y varies from -1 ($Ga_{1-x}In_xAs$-like) to 1 (InSb-like); and d^{sl} and $a_\perp^{sl}$ represent the measured period and average perpendicular lattice constant of the superlattice, respectively. Expressing $a_\perp^{GaInSb}$ in terms of the group-III fluxes f and bulk GaSb and InSb elastic constants and lattice parameters yields two implicit equations for the unknowns f_{Ga} and f_{In}, from which we can derive layer thicknesses and compositions. Note that our relations assume equal In deposition rates during growth of the InAs and $Ga_{1-x}In_xSb$ layers (i.e., we are assuming, and solving for, only one value of f_{In}).

Superlattice parameters derived from this analysis were sensitive to the assumed character of the interfaces. Layer thicknesses and compositions were calculated as a function of the InSb or $Ga_{1-x}In_xAs$ nature of the interfaces, and these parameters were input in the kinematical model to simulate diffraction from the superlattices. Calculated diffraction was compared with experiment to obtain a best fit to the intensities of the observed superlattice peaks.

As shown in Figs. 2 and 3, the kinematical model provides an outstanding fit to the data. The calculated diffraction corresponds to a 28-Å/33-Å $Ga_{0.80}In_{0.20}Sb/InAs$ su-

Miles, Chow, and Hamilton

C-3

perlattice with a 78% InSb character to the interfaces. This fraction yielded the best fit to the data (the calculated diffraction was highly sensitive to the interfacial composition), and was consistent with layer thicknesses in good agreement with those anticipated from independent calibrations of the MBE growth rates. In addition, the InSb-rich nature of the interfaces is plausible as an Sb flux was maintained during the 5-s interrupt in group-III flux imposed at each of the interfaces. In our calculation, we have assumed the $Ga_{1-x}In_xSb$ layers to be terminated in a completely InSb-like interface, leaving the overall 78% InSb-like nature of the interfaces to be achieved by assuming a 56% InSb-, 44% $Ga_{1-x}In_xAs$-like termination of the InAs layers. Although we have no direct experimental evidence for this configuration (the x-ray diffraction was comparatively insensitive to this assumption), the considerable barrier against exchanging group-V surface atoms at a growth temperature as low as 380 °C argues for this distribution.

The agreement between theory and experiment is further illustrated by the comparison of calculated and observed diffraction in the vicinity of the zeroth-order superlattice peak, shown in Fig. 3. We believe the slight asymmetry in the experimental peak, which is not mimicked in the calculation, to be due to contributions from the nearby (004) GaSb substrate peak, which was not included in the simulation.

The analysis and simulation of our x-ray-diffraction data neglect the possibility of arsenic incorporation in our antimonide layers. While we have no direct evidence of this incorporation, consideration of the kinetics of group-V incorporation and evidence of roughly 0.5% As in GaSb layers grown at ≈ 500 °C suggest the possibility of As in our $Ga_{1-x}In_xSb$ layers, possibly at levels as high as 1%. Including such a level of incorporation in our analysis of the diffraction increases slightly the In fraction x in the $Ga_{1-x}In_xSb$ layers, while reducing the thickness of these layers. Assessing directly the extent of this As incorporation is the subject of ongoing work.

IV. CONCLUSIONS

We have established that $Ga_{1-x}In_xSb/InAs$ superlattices can be grown with a high degree of structural perfection, despite a layer-to-layer lattice mismatch of almost 2% and a substantially greater strain at internal InSb-like interfaces. The importance of controlling these interfaces for maintaining defect-free growth is the subject of ongoing work, as is the role of these interfaces in determining the electrical characteristics of our samples. The demonstration of essentially dislocation-free $Ga_{1-x}In_xSb/InAs$ superlattices is expected to be important to the application of these structures as infrared detectors.

ACKNOWLEDGMENTS

[1] D. L. Smith and C. Mailhiot, J. Appl. Phys. 62, 2545 (1987).
[2] C. Mailhiot and D. L. Smith, J. Vac. Sci. Technol. A 7, 445 (1989).
[3] R. H. Miles, D. H. Chow, J. N. Schulman, and T. C. McGill, Appl. Phys. Lett. 57, 801 (1990).
[4] R. H. Miles, D. H. Chow, J. R. Söderstrom, and T. C. McGill, Proc. SPIE 1285, 132 (1990).
[5] I. H. Campbell, I. Sela, B. K. Laurich, D. L. Smith, C. R. Bolognesi, L. A. Samoska, A. C. Gossard, and H. Kroemer, Appl. Phys. Lett. 59, 846 (1991).
[6] D. H. Chow, R. H. Miles, J. N. Schulman, D. A. Collins, and T. C. McGill, Semicond. Sci. Technol. (to be published).
[7] D. L. Smith (private communication).
[8] D. H. Chow, R. H. Miles, J. R. Söderstrom, and T. C. McGill, J. Vac. Sci. Technol. B 8, 710 (1990).
[9] D. H. Chow, R. H. Miles, and T. C. McGill, J. Cryst. Growth 111, 683 (1991).
[10] H. Kroemer, Tak-Yu Liu, and P. M. Petroff, J. Cryst. Growth 95, 96 (1989).
[11] P. M. Petroff, Semiconductors and Semimetals, Vol. 22, Part A (Academic, Orlando, 1985), Chap. 6, p. 379.
[12] S. J. Eglash (private communication).
[13] Gary Tuttle, H. Kroemer, and J. H. English, J. Appl. Phys. 67, 3032 (1990).

J. Appl. Phys., Vol. 71, No. 1, 1 January 1992

C-4

Miles, Chow, and Hamilton

Type II superlattices for infrared detectors and devices

D H Chow†, R H Miles†, J N Schulman†, D A Collins‡ and T C McGill‡

† Hughes Research Laboratories. Malibu. CA 90265. USA
‡ California Institute of Technology. Pasadena. CA 91125. USA

Abstract. Superlattices consisting of combinations of III–V semiconductors with type II band alignments are of interest for infrared applications because their energy gaps can be made smaller than those of any 'natural' III–V compounds. Specifically, it has been demonstrated that both $InSb/InAs_xSb_{1-x}$ superlattices and $Ga_{1-x}In_xSb/InAs$ superlattices can possess energy gaps in the 8–14 μm range. Our efforts have focused on the $Ga_{1-x}In_xSb/InAs$ system because of its extreme broken gap band alignment, which results in narrow energy gaps for very short superlattice periods. We have previously demonstrated that $Ga_{0.75}In_{0.25}Sb/InAs$ superlattices (with periods less than 75 Å) grown on thick, stress-relaxed GaSb buffer layers on GaAs or InP substrates possess photoconductive thresholds throughout the 8–14 μm range and beyond: these superlattices simultaneously display optical absorption coefficients comparable to those of bulk HgCdTe. We report here the use of in situ chemical doping of $Ga_{1-x}In_xSb/InAs$ superlattices to fabricate p–n photodiodes. These diodes display a clear photovoltaic response with a threshold near 12 μm. We have also attained outstanding structural quality in $Ga_{1-x}In_xSb/InAs$ superlattices grown on radiatively heated GaSb substrates. Cross-sectional transmission electron microscope images of these superlattices display no dislocations, while high resolution x-ray diffraction scans reveal sharp high-order superlattice satellites and strong Pendellösung fringes. We anticipate that this high level of structural quality will be of importance in determining material characteristics, such as carrier lifetimes, which are crucial for detector performance.

1. Introduction

It has been several years since the first proposal that superlattices could be used as alternative materials for infrared detection [1, 2]. It is anticipated that this class of materials will have several advantages over bulk $Hg_{1-x}Cd_xTe$ (the current industry standard) for this application:

(i) a higher degree of uniformity, which is of importance for detector arrays:

(ii) smaller leakage currents due to the suppression of tunnelling (larger effective masses) available in superlattices:

(iii) lower Auger recombination rates (in some superlattices) due to substantial splitting of the light- and heavy-hole bands and increased electron effective masses (D L Smith. private communication): and

(iv) well understood device fabrication and materials processing techniques.

Unfortunately. early attempts to realize superlattices with properties suitable for infrared detection were un-

successful. largely because of the difficulties associated with epitaxial deposition of HgTe/CdTe superlattices. More recently. significant interest has been shown in doped multi-quantum well (MQW) approaches to infrared detection. most notably $GaAs/Al_xGa_{1-x}As$ MQWs [3, 4]. However, these detectors are extrinsic in nature. and have been predicted to be limited to performance inferior to that of intrinsic detectors. including both bulk HgCdTe and superlattices with infrared energy gaps [5].

Superlattices composed of III–V semiconductors with type II band alignments are of interest for infrared applications because they provide the possibility of realizing materials with energy gaps smaller than those of any 'natural' III–V semiconductors. Both $Ga_{1-x}In_xSb/InAs$ and $InSb/InAs_xSb_{1-x}$ superlattices have recently been demonstrated to possess energy gaps in the 8–14 μm range [6-9]. Both types of superlattice rely upon an intrinsic valence to conduction band absorption process. Our efforts have focused on the $Ga_{1-x}In_xSb/InAs$ materials system because of its extreme broken gap band alignment which allows the realization of 8-14 μm energy gaps with very thin super-

lattice layers (< 40 Å) [6, 10]. The GaSb valence band edge lies approximately 100 meV above the InAs conduction band edge at low temperature. This band alignment becomes more extreme with increasing In content in the $Ga_{1-x}In_xSb$ layers due to strain [10]. In contrast, $InSb/InAs_xSb_{1-x}$ superlattices require fairly thick layers (75 Å) for long-wavelength infrared response. Furthermore, a lattice-matched substrate, GaSb, exists for $Ga_{1-x}In_xSb/InAs$ superlattices (for specific choices of composition and layer thickness), while $InSb/InAs_xSb_{1-x}$ superlattices must be grown on relaxed buffer layers on InSb substrates.

We have previously demonstrated that $Ga_{1-x}In_xSb/InAs$ superlattices grown on stress-relaxed GaSb buffer layers on GaAs or InP substrates possess energy gaps and absorption coefficients suitable for infrared detection in the 8–14 μm range. Figure 1 displays photoconductive spectra from five $Ga_{1-x}In_xSb/InAs$ superlattices with varying $Ga_{1-x}In_xSb$ compositions and layer thicknesses. The spectra demonstrate that an increase in cut-off wavelength is observed when either the In content of the $Ga_{1-x}In_xSb$ layers or the InAs layer thickness is increased. Figure 2 contains a plot of the absorption coefficient measured from a 25 Å/41 Å $Ga_{0.75}In_{0.25}Sb/InAs$ superlattice as a function of wavelength. The measured absorption is in excellent agreement with a calculated absorption coefficient which is also plotted. The calculation was performed via a two-band tight-binding model which includes the effects of strain.
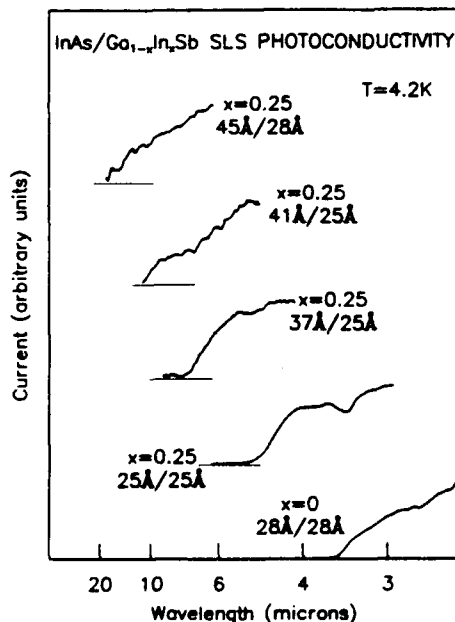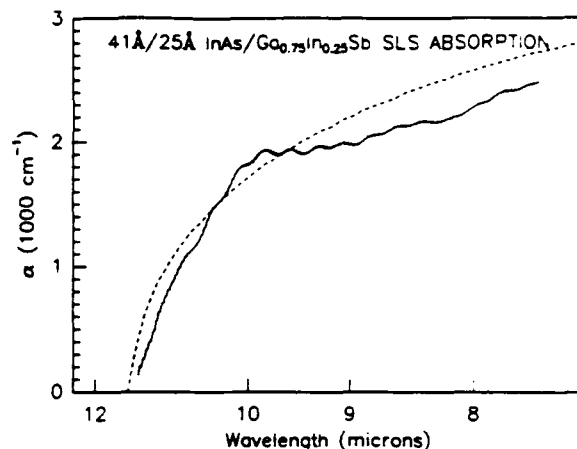

Figure 2. Measured (full curves) and calculated (broken curves) absorption coefficients for a 25 Å/41 Å $Ga_{0.75}In_{0.25}Sb/InAs$ superlattice at 5 K. The observed absorption is comparable in magnitude to that of bulk $Hg_{1-x}Cd_xTe$ (with the same energy gap).

We report here the results of two more recent experiments: growth and structural characterization of $Ga_{1-x}In_xSb/InAs$ superlattices grown on GaSb substrates, and fabrication of p–n junctions in $Ga_{1-x}In_xSb/InAs$ superlattices via in situ chemical doping during growth by molecular beam epitaxy (MBE). Section 2 of the paper describes the experimental procedure used to grow the samples for this study. Section 3 contains structural characterizaton of superlattices grown on GaSb substrates by high-resolution x-ray diffraction (HRXRD). Section 4 discusses some considerations for doping $Ga_{1-x}In_xSb/InAs$ superlatices to fabricate p–n junctions. Photovoltaic characterization of a junction is presented. Finally, section 5 contains a summary of the results presented in the paper.

2. Growth of $Ga_{1-x}In_xSb/InAs$ superlattices

All of the samples for this study were grown by MBE in a Perkin Elmer 430P system equipped with cracked arsenic and antimony sources. $Ga_{1-x}In_xSb/InAs$ superlattices were deposited on three different types of substrate: GaAs, InP and GaSb. In the cases of lattice-mismatched GaAs and InP substrates, thick (0.5–1.0 μm) stress-relaxed GaSb buffer layers were deposited prior to growth of the superlattices. The procedure used for deposition of these buffer layers has been described elsewhere [11, 12]. Superlattices grown in this manner yield excellent surface morphology and sharp $\Theta/2\Theta$ x-ray diffraction satellites. However, cross sectional transmission electron microscope (TEM) images reveal dislocation densities as high as $10^9 \, cm^{-2}$ [12] in these samples: high-resolution x-ray diffraction satellites from these samples are characteristically broad and weak. The observed threading dislocations appear to result solely from relaxation of the GaSb buffer layers, with no evidence of relaxation observed in the individual superlattice layers nor be-

Figure 1. Photoconductivity spectra from five $Ga_{1-x}In_xSb/InAs$ superlattices at 5 K. Nominal layer thicknesses and compositions are shown. The cut-off wavelength is observed to increase with increasing In content of the $Ga_{1-x}In_xSb$ layers and increasing InAs layer thickness.

tween the superlattices and buffer layers. For growth of $Ga_{1-x}In_xSb/InAs$ superlattices on GaSb substrates, round (30 mm diameter), (100)-oriented wafers were used. These substrates were radiatively heated (In-free) for MBE growth via custom-designed molybdenum wafer holders. The use of solderless substrate mounting was found to be of importance in preventing warping and/or cracking of the substrate due to thermal stress. The substrates were chemically cleaned prior to growth by a standard degrease and 10 min etch in $Br_2:HNO_3:HCl:CH_3COOH$ (0.35 : 2 : 36 : 460) (S J Eglash, private communication). *In situ* cleaning consisted of outgassing at 250 °C in an ultrahigh vacuum buffer chamber, followed by heating in an Sb flux to the oxide desorption temperature (≈ 500 °C) in the growth chamber. Reflection high-energy electron diffraction (RHEED) was used to monitor the oxide desorption process.

Typical superlattice layer thicknesses and compositions are eight monolayers (25 Å) of $Ga_{0.73}In_{0.27}Sb$ and thirteen monolayers (39 Å) of InAs. These parameters have previously been shown to result in a superlattice with an energy gap near 100 meV (12 μm) [6]. Total superlattice thicknesses range from 40 to 80 periods (0.25 to 0.5 μm). At each interface of the superlattice, growth was interrupted (no group III flux) in an Sb_2 flux for 5 s.

During growth of the $Ga_{1-x}In_xSb$ layers, a 1 × 3 RHEED pattern is observed, while InAs layers display a 1 × 2 pattern. As the substrate temperature is varied, a transition from 1 × 3 to 1 × 5 in the RHEED pattern from the $Ga_{0.73}In_{0.27}Sb$ surface during a growth interruption (in an Sb_2 flux) is observed. The transition point is approximately 380 °C. The superlattices studied here were grown at substrate temperatures just below this point. A similar transition in surface reconstruction also occurs at ≈ 440 °C for a GaSb surface in an Sb_2 flux, and at ≈ 410 °C during growth of GaSb. These observations suggest that the 1 × 3 to 1 × 5 transition in antimonide surface reconstruction is caused by an increase in Sb surface coverage at temperatures below the transition temperature. This explanation is supported by the fact that incorporation of As in antimonide layers has been observed to increase with substrate temperature [11], and is nearly eliminated in antimonide layers grown below the transition temperature.

3. Structural characterization

We anticipate that the structural quality of $Ga_{1-x}In_xSb/InAs$ superlattices will have profound effects upon material properties, such as carrier lifetimes and mobilities, which are crucial for detector performance. Although some workers have reported success in reducing dislocation densities in relaxed buffer layers [13], high structural quality is commonly obtained only on lattice-matched substrates.

Figure 3(a) displays high-resolution x-ray diffraction scans (rocking curves) from $Ga_{1-x}In_xSb/InAs$ superlattices grown on InP (broken curve) and GaSb (full curve)
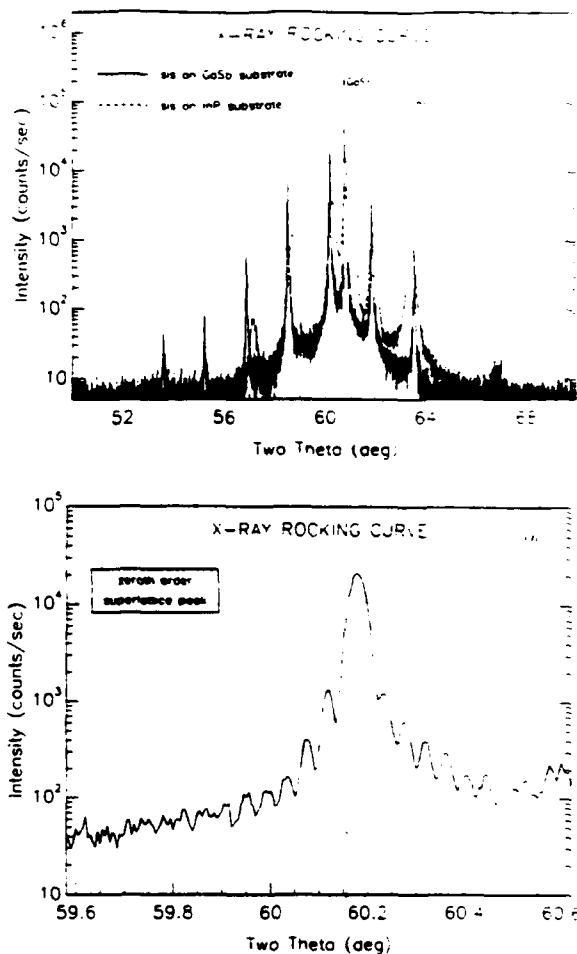

Figure 3. (a) High-resolution x-ray diffraction from $Ga_{1-x}In_xSb/InAs$ superlattices (sls) grown on InP (broken curve) and GaSb (full curve) substrates. The superlattices were grown with similar layer thicknesses and composition, under the growth conditions described in section 2. A peak due to the GaSb buffer layer grown on the InP substrate prior to deposition of the superlattice is also visible in the broken curve.
(b) Rocking-curve data from the superlattice grown on GaSb over a small angular range. Clear Pendellosung fringes are observed.

substrates. The diffraction data were taken with a Cu $K\alpha$ source passed through a four-crystal Ge monochromator. Long counting times (15 s) were used to improve signal-to-noise ratio in the scans. The two superlattices were both grown with a nominal In content of $x = 0.27$ in the $Ga_{1-x}In_xSb$ layers, with growth conditions as described in section 2. The period of the superlattice grown on GaSb is slightly shorter (61 Å) than that of the superlattice grown on InP (64 Å), as evidenced by its slightly greater x-ray satellite spacing. Examination of figure 3(a) reveals that x-ray diffraction satellites from the sample grown on GaSb are sharper, persistent to higher order, and more intense than those from the sample grown on InP. All of these features are indications of dramatic differences in structural quality between the two samples. It should be noted that we have

attempted several different growth schemes to reduce threading dislocation densities in GaSb buffer layers grown on GaAs and InP substrates, including additional strained-layer superlattices, annealing and encapsulated annealing. None of these approaches resulted in high-resolution x-ray diffraction significantly better than that shown in the broken curve of Figure 3(a).

Figure 3(b) displays a plot of the diffraction data from the sample grown on GaSb over a small angular range, revealing clear Pendellösung fringes around the zeroth-order superlattice satellite. Theoretical simulations confirm that the width of this peak is determined by the thickness of the superlattice (0.25 μm), as opposed to irregularities in superlattice period or lattice spacing. Consistent with this finding, we were unable to detect the presence of any dislocations in cross sectional TEM images of a superlattice grown on a GaSb substrate. The ability to grow $Ga_{1-x}In_xSb/InAs$ superlattices which are dislocation free may be anticipated to have positive effects upon material properties which are crucial for infrared detectors. For example, carrier diffusion lengths may be limited by scattering from threading dislocations. Hence, the availability of a lattice-matched substrate represents a significant advantage for detectors based on $Ga_{1-x}In_xSb/InAs$ superlattices relative to materials which must be grown on relaxed buffer layers.

4. p–n junctions

The ability to dope an infrared material both p type and n type is necessary for the realization of photovoltaic detectors. One significant advantage which III–V semiconductors hold over II–VI compounds is the greater availability of well-behaved substitutional impurity dopants. For III–V MBE growth, silicon and beryllium are by far the most popular dopants. It has recently been demonstrated that silicon is a well-behaved p-type dopant for GaSb [14], while it is an n-type dopant for InAs. Beryllium is known to be an acceptor for all of the conventional III–V compounds. Hence, it should be possible to dope $Ga_{1-x}In_xSb/InAs$ superlattices p type by co-deposition of Be during growth of either or both constituent layers, or by co-deposition of Si during growth of $Ga_{1-x}In_xSb$ layers only (assuming that the diffusion of Si atoms is limited). Conversely, co-deposition of Si during growth of InAs layers should result in an n-type superlattice: we have observed well-behaved n-type doping of $Ga_{1-x}In_xSb/InAs$ superlattices via this *in situ* technique up to levels of 1×10^{18} cm^{-3}. Higher levels of n-type doping have not yet been attempted, and are probably unnecessary for photovoltaic detectors.

Although intentional doping in $Ga_{1-x}In_xSb/InAs$ superlattices is fairly straightforward, achieving low background (unintentional) carrier concentrations may be more difficult. To date, we have consistently observed background p-type doping in $Ga_{1-x}In_xSb/InAs$ superlattices, with carrier concentrations of approximately 5×10^{16} cm^{-3} at low temperatures. It is highly desirable to decrease this background concentration as Auger
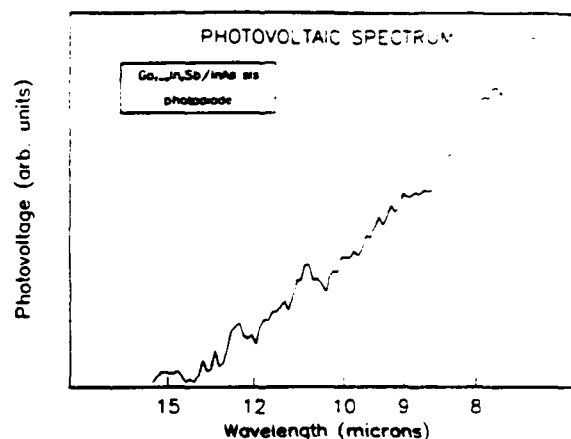

Figure 4. Photovoltaic spectrum from a 24 Å/40 Å $Ga_{0.75}In_{0.25}Sb/InAs$ photodiode at 5 K. The spectrum displays a threshold near 12 μm.

lifetimes and depletion lengths are strongly dependent upon carrier densities. Recent efforts directed towards determining the source of the background acceptors will be reported elsewhere [15].

Figure 4 displays a photovoltaic spectrum taken from a 24 Å/40 Å $Ga_{0.75}In_{0.25}Sb/InAs$ superlattice photodiode The p-n junction was formed by growing 0.25 μm of nominally undoped superlattice material on top of 0.25 μm of intentionally n-doped material. The two sides of the junction had the same superlattice layer thicknesses and composition. Photodiodes were fabricated by chemically etching mesas [6] to isolate the junction and by depositing Al contact metal on both the tops of the mesas and the etched surface. This chip was then mounted on a header with a hole in its base for backside illumination, and wire bonds were connected to the two terminal devices. The spectrum in figure 4 was taken by using one of the photodiodes as a detector in a BOMEM Fourier transform infrared spectrometer. A clear photovoltaic response is observed from the photodiode, with a threshold near 12 μm, consistent with the energy gap expected from this superlattice. This demonstration of photovoltaic response verifies that photovoltaic detectors can be straightforwardly realized in the $Ga_{1-x}In_xSb/InAs$ materials system.

5. Summary

Infrared detectors based on III–V compounds are highly desirable as an alternative to $Hg_{1-x}Cd_xTe$, because of their materials processing and uniformity advantages Type II superlattices offer the possibility of creating III–V materials with cut-off wavelengths in the 8–14 μm range which simultaneously possess the high detectivities and operating temperatures of an intrinsic detector. Of the two material systems which have been demonstrated to have long-wavelength infrared response, $Ga_{1-x}In_xSb/InAs$ has two significant advantages over $InSb/InAs_xSb_{1-x}$: energy gaps in the 8–14 μm range are

compatible with both reasonable interlayer strains and strong absorption coefficients, and $Ga_{1-x}In_xSb/InAs$ superlattices can be grown lattice-matched to GaSb substrates. We have demonstrated experimentally that large absorption coefficients are compatible with long-wavelength response in $Ga_{1-x}In_xSb/InAs$ superlattices, and that nearly ideal structural quality can be obtained for $Ga_{1-x}In_xSb/InAs$ superlattices grown on radiatively heated GaSb substrates. In addition, we have recently demonstrated photovoltaic response at 12 μm from an as-grown p-n junction. These results are promising for the eventual realization of material properties suitable for high-performance detectors.

Acknowledgments

References

[1] Schulman J N and McGill T C 1979 *Appl. Phys. Lett.* **34** 663

[2] Smith D L, McGill T C and Schulman J N 1983 *Appl. Phys. Lett.* **43** 180

[3] Levine B F, Bethea C G, Hasnain G, Shen V O, Pelve E, Abbott R R and Hsieh S J 1990 *Appl. Phys. Lett.* **56** 851

[4] Levine B F, Gunapala S D and Kopf R F 1991 *Appl. Phys. Lett.* **58** 1551

[5] Kinch M A and Yariv A 1989 *Appl. Phys. Lett.* **55** 2093

[6] Miles R H, Chow D H, Schulman J N and McGill T C 1990 *Appl. Phys. Lett.* **57** 801

[7] Campbell I H, Sela I, Laurich B K, Smith D L, Bolognesi C R, Samoska L A, Gossard A C and Kroemer H 1991 *Appl. Phys. Lett.* **59** 84

[8] Kurtz S R, Biefeld R M, Dawson L R, Fritz I J and Zipperian T E 1988 *Appl. Phys. Lett.* **53** 1961

[9] Kurtz S R, Dawson L R, Biefeld R M, Fritz I J and Zipperian T E 1989 *IEEE Electron Device Lett.* **10** 150

[10] Smith D L and Maihiot C 1987 *J. Appl. Phys.* **62** 2545

[11] Chow D H, Miles R H, Söderström J R and McGill T C 1990 *J. Vac. Sci. Technol.* B **8** 710

[12] Chow D H, Miles R H, Nieh C W and McGill T C 1991 *J. Cryst. Growth* **111** 68

[13] Yamaguchi M 1991 *J. Mater. Res.* **6** 376

[14] Rossi T M, Collins D A, Chow D H and McGill T C 1990 *Appl. Phys. Lett.* **57** 2256

[15] Chow D H and Miles R H unpublished

APPENDIX E

Growth of InAs/Ga$_{1-x}$In$_x$Sb infrared superlattices

D.H. Chow *, R.H. Miles, C.W. Nieh

Hughes Research Laboratories, Malibu, California 90265, USA

and

T.C. McGill

T.J. Watson, Sr., Laboratory of Applied Physics, California Institute of Technology, Pasadena, California 91125, USA

A set of InAs/Ga$_{1-x}$In$_x$Sb superlattices has been grown by molecular beam epitaxy. The superlattices are deposited on thick, stress-relaxed buffer layers of GaSb on (100)-oriented GaAs substrates. A short-period, heavily strained superlattice has been inserted at the GaAs/GaSb interface. Transmission electron microscope (TEM) images reveal that a dense network of dislocations forms at this interface, with the vast majority of threading dislocations propagating no further than the first 1000 Å of the GaSb buffer layer. Planar superlattice layers are observed, with no evidence of stress relaxation between the layers or between the InAs/Ga$_{1-x}$In$_x$Sb superlattice and GaSb buffer. Analysis of X-ray diffraction satellites reveals that cross-incorporation of As in GaSb and Ga$_{1-x}$In$_x$Sb layers is virtually eliminated at low growth temperatures. Photoconductivity spectra from the superlattices display sharp photocurrent threshold energies, in agreement with previously published energy gaps derived from calculations and photoluminescence data. Thresholds in the 8–14 μm range are obtained from superlattices with very thin layers (≈ 40 Å), which are necessary for strong optical absorption in a type II superlattice. Finally, an absorption coefficient of ≈ 2000 cm^{-1} is measured at 10 μm from a superlattice with an energy gap of 11.4 μm. This value is comparable to that of bulk Hg$_{1-x}$Cd$_x$Te, the current industry standard for infrared detectors in the 8–14 μm range.

1. Introduction

InAs/Ga$_{1-x}$In$_x$Sb superlattices show promise as materials for infrared detection in the 8–14 μm range [1–4]. In comparison to Hg$_{1-x}$Cd$_x$Te, the current industry standard, InAs/Ga$_{1-x}$In$_x$Sb superlattices are expected to hold several advantages: (i) a higher degree of uniformity, which is crucial for the fabrication of large infrared detector arrays, (ii) smaller leakage currents, due to the tunable increase in effective mass available in a superlattice, (iii) reduced Auger recombination rates, due to the substantial splitting of the light and heavy hole bands and the increase in electron effective mass [5], (iv) better understood device processing techniques, and (v) compatibil-

ity with GaAs-based readout electronics. Furthermore, the performance of infrared detectors based on InAs/Ga$_{1-x}$In$_x$Sb superlattices should not be limited by the high thermal generation rates which preclude large D^*'s in multiquantum well infrared detectors (such as GaAs/AlGaAs multiquantum wells, for example) [6].

The conceptual basis for achieving far-infrared energy gaps in InAs/Ga$_{1-x}$In$_x$Sb superlattices has been discussed previously [1–4]. Briefly, the broken-gap band alignment between the two constituent materials yields a small energy gap for the superlattice once quantum confinement effects are considered (assuming reasonably thin layers). The presence of coherent strain between the InAs and Ga$_{1-x}$In$_x$Sb layers shifts the band edges such that the superlattice energy gap is reduced. This shift is advantageous because narrower energy gaps (longer cutoff wavelengths) can be obtained with

* Formerly at California Institute of Technology, Pasadena, California, USA.

reduced layer thicknesses, leading to enhanced optical absorption and carrier transport properties.

In this paper, we present structural and optical characterization of a set of InAs/Ga$_{1-x}$In$_x$Sb superlattices grown by molecular beam epitaxy (MBE). Layer thicknesses and compositions have been varied, resulting in samples with energy gaps ranging from 80 to 340 meV (3.5 to 15 μm). Structural characterization of the superlattices consisted of reflection high energy electron diffraction (RHEED), X-ray diffraction, and (in some cases) transmission electron microscopy (TEM). Spectrally resolved photoconductivity and optical transmission experiments have also been performed. Absorption coefficients comparable to those of bulk Hg$_{1-x}$Cd$_x$Te have been observed.

2. Growth and structural characterization

All of the samples discussed here have been grown by MBE on (100)-oriented GaAs substrates in a Perkin-Elmer 430 system equipped with both arsenic and antimony crackers. Measurements of the substrate temperature were obtained through a thermocouple, which was either in contact with a molybdenum block (in the case of indium-soldered substrates), or a heat diffuser (in the case of indium-free substrate mounts). In both cases, the thermocouple readings were calibrated to optical pyrometer readings above 500°C. At lower substrate temperatures, a transition in the GaSb surface reconstruction under an Sb$_2$ flux from 1 × 3 to 1 × 5 was used as a point of calibration for thermocouple readings. Nominal growth rates were calibrated via bulk film thickness measurements and RHEED oscillations measured during homoepitaxial growth of GaAs and InAs. A "nude" ion gauge was used to monitor the Sb$_2$ and As$_2$ fluxes.

Growth of each of the superlattices studied here commenced with 3000 Å of GaAs, grown at a substrate temperature of 600°C. Following the GaAs layer, a ten period, 1 monolayer/1 monolayer, GaSb/GaAs superlattice was deposited at 520°C. Spotty RHEED patterns, indicative of a three-dimensional growth mode, were observed al-most immediately upon commencement of the short period superlattice. However, streaky RHEED patterns were recovered within the first 100 Å of a 5000 Å GaSb buffer layer, grown at 420–450°C on top of the short period superlattice. A 1 × 3 RHEED pattern was observed throughout the deposition of the GaSb buffer layer, which is stress relaxed (free standing) as determined by X-ray diffraction. Growth was completed by deposition of an InAs/Ga$_{1-x}$In$_x$Sb superlattice on top of the buffer layer. The choice of GaSb as a buffer layer material for the strained-layer InAs/Ga$_{1-x}$In$_x$Sb superlattices was made because of the intermediate value of the lattice constant of GaSb with respect to the two constituent materials of the superlattice. Substrate temperatures ranging from 350 to 400°C were selected for the InAs/Ga$_{1-x}$In$_x$Sb superlattices studied here. Ga$_{1-x}$In$_x$Sb and InAs displayed 1 × 3 and 1 × 2 surface reconstructions, respectively, as observed via RHEED patterns during growth of the superlattices. For substrate temperatures below 370°C (approximately), a transition to a 1 × 5 RHEED pattern was observed during growth interrupts (in an Sb flux) on Ga$_{1-x}$In$_x$Sb surfaces.

A cross-sectional TEM photograph of an InAs/Ga$_{1-x}$In$_x$Sb superlattice grown by the method described above is shown in fig. 1. The figure reveals a dense network of dislocations at the GaSb/GaAs interface, the vast majority of which do not propagate past the first 1000 Å of buffer layer growth. The remaining threading dislocations persist through the entire structure, with a density of approximately 10^9 cm^{-2}. There is no evidence of plastic stress relaxation in any of the superlattice layers, nor between the superlattice and buffer layer. In spite of the high threading dislocation densities, TEM images reveal smooth, planar, InAs/Ga$_{1-x}$In$_x$Sb superlattice layers over most of the sample area. It is likely that substantial improvements in structural quality can be achieved by growing InAs/Ga$_{1-x}$In$_x$Sb superlattices on GaSb substrates. However, GaAs substrates are substantially less expensive and provide the possibility of monolithic integration with readout circuitry.

Fig. 2 displays (400)-like, $\theta/2\theta$ X-ray diffraction data from an 80 period, 41 Å/25 Å, InAs/

Fig. 1. Cross-sectional TEM image of an InAs/Ga$_{1-x}$In$_x$Sb superlattice grown on a GaAs substrate by the method described in the text. A dense network of dislocations is observed at the GaAs/GaSb interface: most of these dislocations do not propagate past the first 1000 Å of the GaSb buffer layer.

Ga$_{0.75}$In$_{0.25}$Sb superlattice, grown by the method described previously. The period and average interatomic spacing of the superlattice has been determined from the X-ray data by measuring the satellite spacings and zeroth order satellite posi-
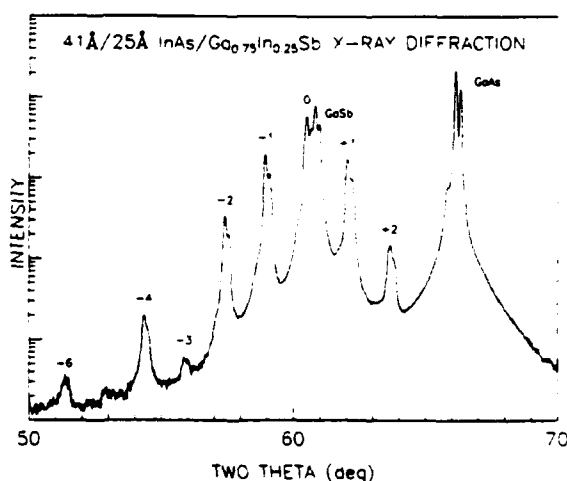
Fig. 2. $\theta/2\theta$ X-ray diffraction data for an 80 period, 41 Å/25 Å. InAs/Ga$_{0.75}$In$_{0.25}$Sb superlattice, showing (400)-like diffraction peaks. The sample was irradiated with Cu Kα X-rays. Each peak in the figure is bimodal due to the Kα doublet. The GaSb buffer and GaAs substrate peaks are labeled.

tion, respectively. This information is sufficient to compute the In and Ga fluxes used during growth (two measured quantities, two determined variables), assuming the structure is in a known strain state. Hence, the layer thicknesses and Ga$_{1-x}$In$_x$Sb composition, x, of the superlattice can be determined from the X-ray data without relying on nominal growth rates. The intensities of the superlattice satellite peaks shown in fig. 2 are in excellent agreement with those predicted by kinematical theory. The widths of the peaks are limited by the resolution of the X-ray diffractometer used here. The intensity and narrowness of the satellite peaks is indicative of highly regular superlattice growth with limited interdiffusion between layers [7].

The position of the GaSb buffer layer peak in fig. 2 indicates that there is virtually no cross-incorporation of As into the layer (< 0.1%). We have previously reported that growth of GaSb (with a cracked Sb source), in an As background produced by a hot, shuttered, As cracker, yields substantial cross-incorporation (7–30%) of As over the substrate temperature range 450–530°C; in that study, lower substrate temperatures were found to yield lesser degrees of As-incorporation [8]. A substrate temperature of approximately

425°C was chosen for growth of the GaSb buffer layer in the sample used to produce fig. 2. resulting in the virtual elimination of As from the layer. These results suggest that: (i) increased coverage of Sb on the GaSb surface occurs as the substrate temperature is lowered, and (ii) the As-sticking coefficient is more strongly dependent on surface composition (Sb-coverage) than substrate temperature over the temperature range studied here. The effects of increased Sb-surface coverage would be enhanced if As$_4$ molecules dominate the As-background pressure when the As shutter is closed, since adjacent lattice sites are required for incorporation of As$_4$ into GaAs [9,10]. We have, furthermore, estimated the cross-incorporation of arsenic in the Ga$_{1-x}$In$_x$Sb layers of the superlattice used to produce fig. 2 to be no greater than 1%. This estimate was made by assuming that the nominal GaSb growth rate was accurate to ±20%, and applying the X-ray analysis described in the previous paragraph to determine the In flux and the degree of As-incorporation.

3. Optical characterization

Photoconductive devices have been fabricated for this study by chemically etching mesa structures into the InAs/Ga$_{1-x}$In$_x$Sb superlattices. Evaporated aluminum contacts were then placed on the tops of the mesas and etched surfaces, forming sets of diodes. Fig. 3 displays spectrally resolved photocurrent data from five InAs/ Ga$_{1-x}$In$_x$Sb superlattices. The spectra were obtained under backside illumination at different applied biases. All of the data presented in fig. 3 were obtained at 5 K; to date, temperature dependence has been studied in only the 25 Å/25 Å InAs/Ga$_{0.75}$In$_{0.25}$Sb superlattice, revealing no appreciable changes in photoconductive response up to 100 K. As can be seen from the figure, photoconductive thresholds shift to lower energies as the InSb fraction and/or InAs layer thickness are increased. The photoconductive thresholds displayed in fig. 3 are in excellent agreement with previously published energy gaps derived from calculations and photoluminescence spectra [4]. It should be noted that operation in the 8–14 μm
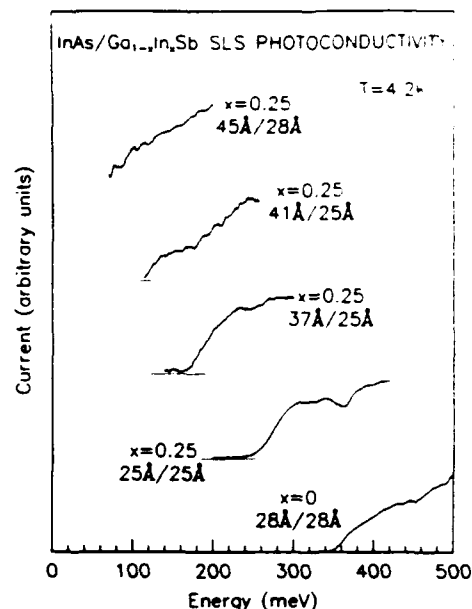
Fig. 3. Photoconductivity spectra from five in InAs/ Ga$_{1-x}$In$_x$Sb superlattices.

range is obtained for reasonably thin layers (≈ 40 Å), which are necessary for strong optical absorption.

Fig. 4 contains an experimental absorption spectrum, taken from the 41 Å/25 Å InAs/
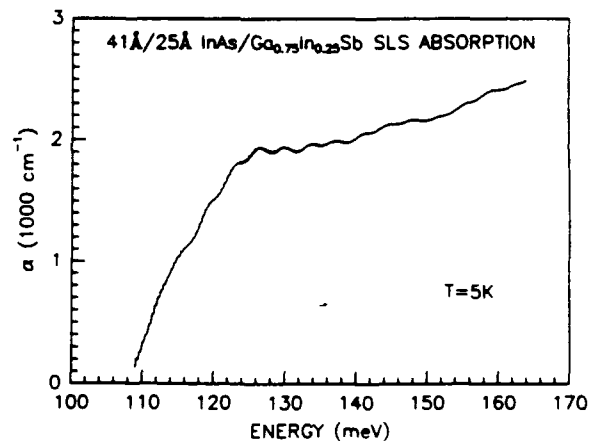
Fig. 4. Measured absorption coefficient for a 41 Å/25 Å InAs/Ga$_{0.75}$In$_{0.25}$Sb superlattice. Absorption at 10 μm is comparable to that of bulk Hg$_{1-x}$Cd$_x$Te with the same energy gap. The small amplitude oscillations observed in the figure are interference fringes resulting from a difference in thickness between the sample and a reference piece of a GaAs substrate.

E-4

$Ga_{0.7}In_{0.3}Sb$ superlattice for which X-ray and photocurrent data are displayed in figs. 2 and 3, respectively. The superlattice absorption edge is abrupt (the absorption increases by one order of magnitude within 10 meV of the threshold energy), attaining a value of approximately 2000 cm^{-1} at 10 μm. This value is comparable to that of bulk $Hg_{1-x}Cd_xTe$ with the same energy gap. The observation of large absorption coefficients from a type II superlattice is consistent with the prediction of large electron effective masses in these structures, which may reduce leakage currents and Auger recombination rates. Comparison of figs. 3 and 4 reveals that the absorption edge of the superlattice is coincident with its photoconductive threshold, as expected.

4. Conclusions

In summary, we have grown a set of InAs/ $Ga_{1-x}In_xSb$ strained-layer superlattices by molecular beam epitaxy. The superlattices were deposited on thick, stress relaxed GaSb buffers layers on GaAs substrates. A two-dimensional growth mode is recovered within the first 100 Å of the buffer layer when a short period, heavily strained superlattice is inserted at the GaAs/GaSb interface. TEM images reveal planar superlattice layers, with residual threading dislocation densities of approximately 10^9 cm^{-2}. However, no evidence of stress relaxation in the superlattice layers has been observed. X-ray diffraction data from the super-lattices show intense, sharp satellite peaks, which have been used to determine the layer thicknesses and compositions of our samples. Further analysis of the X-ray data is consistent with the virtual elimination of cross-incorporated As in the GaSb buffer and $Ga_{1-x}In_xSb$ superlattice layers at low growth temperatures. The InAs/$Ga_{1-x}In_xSb$ superlattices studied here display sharp photocon-

ductive thresholds at energies which agree well with calculated energy gaps. Finally, an absorption coefficient of 2000 cm^{-1} at 10 μm has been measured from a superlattice with an 11 μm energy gap. As this value is comparable to that of bulk $Hg_{1-x}Cd_xTe$, we feel it is a promising result for detectors based on InAs/$Ga_{1-x}In_xSb$ super-lattices.

References

[1] D.L. Smith and C. Mailhiot, J. Appl. Phys. 62 (1987) 2545.
[2] Mailhiot and D.L. Smith, J. Vacuum Sci. Technol. A7 (1989) 445.
[3] D.H. Chow, R.H. Miles, J.R. Söderström and T.C. McGill, Appl. Phys. Letters 56 (1990) 1418.
[4] R.H. Miles, D.H. Chow, J.N. Schulman and T.C. McGill, Appl. Phys. Letters 57 (1990) 801.
[5] D.L. Smith, private communication.
[6] M.A. Kinch and A. Yariv, Appl. Phys. Letters 55 (1989) 2093.
[7] B.M. Clemens and J.G. Gay, Phys. Rev. B35 (1987) 9337.
[8] D.H. Chow, R.H. Miles, J.R. Söderström and T.C. McGill, J. Vacuum Sci. Technol. B8 (1990) 710.
[9] C.T. Foxon and B.A. Joyce, Surface Sci. 50 (1975) 434.
[10] C.T. F   , and B.A. Joyce, Surface Sci. 64 (1977) 293.

Infrared optical characterization of InAs/Ga$_{1-x}$In$_x$Sb superlattices

R. H. Miles
Hughes Research Laboratories, Malibu, California 90265

D. H. Chow
T. J. Watson, Sr., Laboratory of Applied Physics, California Institute of Technology, Pasadena, California 91125

J. N. Schulman
Hughes Research Laboratories, Malibu, California 90265

T. C. McGill
T. J. Watson, Sr., Laboratory of Applied Physics, California Institute of Technology, Pasadena, California 91125

InAs/Ga$_{1-x}$In$_x$Sb superlattices have been examined by photoluminescence, photoconductivity, and infrared optical transmission. Samples display clear photoconductive thresholds at energies in agreement with band gaps derived from photoluminescence. Far-infrared energy gaps (8–14 μm and beyond) are obtained for InAs/Ga$_{0.75}$In$_{0.25}$Sb superlattices with periods <75 Å, in good agreement with gaps calculated from a simple two-band model. An absorption coefficient of ~2000 cm^{-1} at 10 μm is measured in a superlattice with an energy gap of 11.4 μm. The magnitude and shape of this absorption edge is comparable to that of bulk Hg$_{1-x}$Cd$_x$Te, suggesting that infrared detectors based on InAs/Ga$_{1-x}$In$_x$Sb superlattices may be competitive in the 8–14 μm range and beyond.

InAs/Ga$_{1-x}$In$_x$Sb superlattices have been proposed for infrared detector applications in the 8–14 μm range.[1,2] It has been suggested that these superlattices might enjoy a number of advantages over bulk Hg$_{1-x}$Cd$_x$Te (the current industry standard), including lower leakage currents, greater uniformity, and a more readily processed material system. Far-infrared response in these structures arises from the broken gap band alignment between InAs and Ga$_{1-x}$In$_x$Sb, depicted in Fig. 1. The band alignment is presumed to result in a zero gap superlattice in the absence of quantum confinement effects; in the case of InAs/GaSb, the transition to a semimetallic superlattice band structure has been observed to occur at layer thicknesses of ~100 Å.[3] However, as the type-II band alignment localizes electrons and holes in different layers of the superlattice, electron-hole overlap is small in narrow-gap InAs/GaSb structures, yielding small optical absorption coefficients.[4] Smith and Mailhiot[1,2] suggested adding indium to the antimonide layers to reduce the layer thicknesses necessary for long wavelength response, thereby increasing the electron-hole overlap. Absorption coefficients comparable to those of Hg$_{1-x}$Cd$_x$Te were calculated for these structures.[1]

In this letter we present experimental evidence that energy band gaps spanning the far infrared may be obtained in thin layer InAs/Ga$_{1-x}$In$_x$Sb superlattices, and that absorption in these structures is comparable to that of Hg$_{1-x}$Cd$_x$Te. We have estimated superlattice energy gaps from photoluminescence, and have correlated these with photoconductive thresholds. Experimental band gaps are compared with theoretical values derived from a simple

two-band model. An optical absorption spectrum is presented for a superlattice with an 11.4 μm gap.

InAs/Ga$_{1-x}$In$_x$Sb superlattices with layer thicknesses of 25–45 Å and InSb fractions x of 0 and 0.25 were grown on (100) GaAs substrates by molecular beam epitaxy (MBE). Details of the growth have been presented elsewhere.[5,6] X-ray diffraction[5] and transmission electron microscopy[7] were used to examine the structural quality of the superlattices. Threading dislocation densities of 10^9 cm^{-2} are apparent through transmission electron microscopy, originating at the initial interfaces between the GaAs substrates and InAs or GaSb buffer layers. Despite these dislocation densities, the superlattice layers appear highly planar, regular, and uniform across a 2 in. wafer. X-ray diffraction yields numerous sharp superlattice satellite peaks, in excellent agreement with diffraction calculated from a kinematical model. We find no evidence of plastic
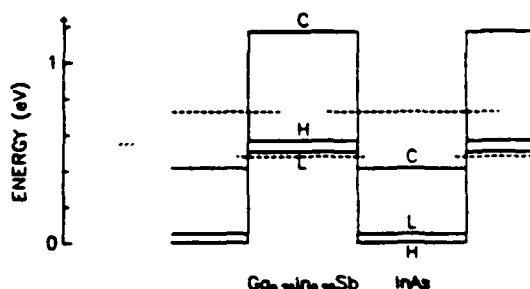

FIG. 1. Band alignments for the InAs/Ga$_{1-x}$In$_x$Sb superlattice. Bulk heavy-hole, light-hole, and conduction-band edges are indicated by H, L, and C, respectively. Localization of electrons in the InAs layers and holes in the Ga$_{1-x}$In$_x$Sb is indicated by the dashed line superlattice energy levels.
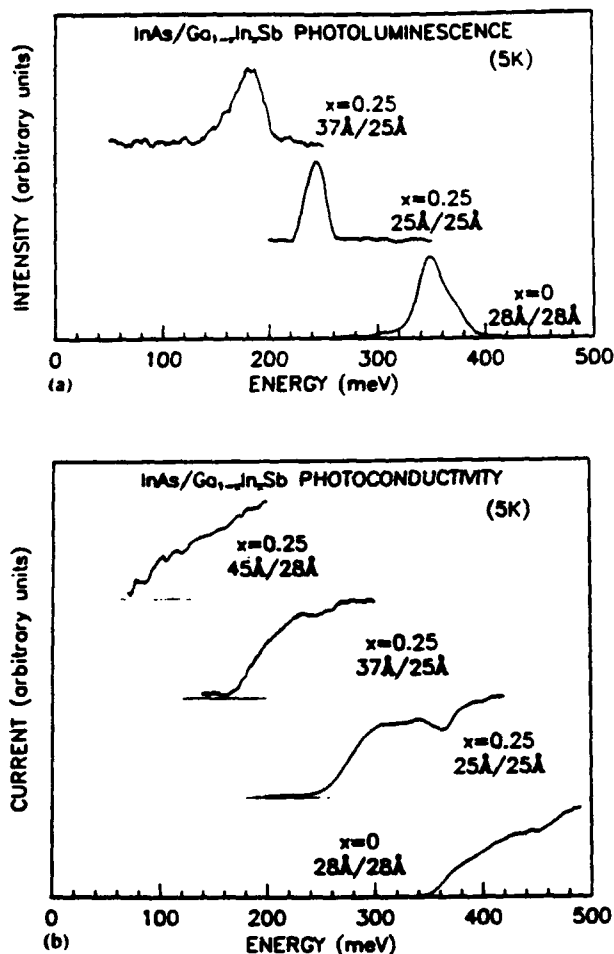
FIG. 2. (a) Photoluminescence spectra from three InAs/Ga₁₋ₓInₓSb superlattices (28 Å/28 Å InAs/GaSb, 25 Å/25 Å InAs/Ga₀.₇₅In₀.₂₅Sb, and 37 Å/25 Å InAs/Ga₀.₇₅In₀.₂₅Sb). (b) Photoconductivity spectra from the same samples and an additional 45 Å/28 Å InAs/Ga₀.₇₅In₀.₂₅Sb superlattice. All data were taken at 5 K.

TABLE I. Comparison of energy band gaps derived from photoluminescence, photoconductivity, and theory for the InAs/Ga₁₋ₓInₓSb superlattices examined here.

Layer Thickness (Å)					Energy gap (meV)		
InAs	Ga₁₋ₓInₓSb	As$_y$	x	y	PL	PC	Theory
28	28		0	0.07	330 ± 10	350 ± 10	320
25	25		0.25	0.08	240 ± 10	250 ± 10	280
37	25		0.25	0.05	150 ± 10	170 ± 10	180
41	25		0.25	0		110 ± 10	110
45	28		0.25	0		80 ± 10	100

stress relaxation in any of the individual superlattice layers, nor between the superlattices and buffer layers.

Photoluminescence from three superlattices is shown in Fig. 2. As with all of the optical results presented here, these spectra were obtained on a Bomem Fourier transform infrared (FTIR) spectrometer. Photoluminescence was obtained at 5 K using an Ar⁺ laser or AlGaAs laser diode pump modulated at 40 kHz, and was detected by an InSb or a HgCdTe detector cooled to 77 K, or by a Si:As detector at 4.2 K. Phase-sensitive detection of a modulated luminescence signal was necessary to discriminate weak luminescence from the substantial 300 K blackbody background.[8]

We associate luminescence peaks from each of the samples with fundamental conduction to heavy hole valence band transitions. In the cases of the 28 Å/28 Å InAs/GaSb and 37 Å/25 Å InAs/Ga₀.₇₅In₀.₂₅Sb superlattices, luminescence was detected only for average pump powers greater than 350 mW into approximately 0.1 mm². The intensity of these optical pumps likely contributed to the observed broadenings, leading us to associate the energy gaps with the low-energy luminescence edges. How-

ever, in the case of the 25 Å/25 Å InAs/Ga₀.₇₅In₀.₂₅Sb superlattice, luminescence was obtained with a 70 mW AlGaAs laser diode pump. The approximately Gaussian shape of the luminescence peak from this sample suggests a random variation in superlattice parameters, leading us to associate the band gap with the luminescence peak energy in this sample. Consistent with this interpretation, the 30 meV width of the luminescence peak coincides with the change in superlattice energy gap expected from a single monolayer fluctuation in InAs well thickness (the gap is less sensitive to changes in Ga₁₋ₓInₓSb layer thickness). Although we have demonstrated sample-to-sample growth to be reproducible to better than 1 Å in superlattice period, discrete interfacial fluctuations of one monolayer can be expected in samples grown by MBE in a standard two-dimensional growth mode.[9]

Also shown in Fig. 2 are spectrally resolved photoconductive responses of the three superlattices for which photoluminescence spectra are shown, and of a narrow gap superlattice which did not yield distinguishable luminescence. Photoconductive devices were fabricated by contacting mesa structures etched into the superlattices. Photocurrent was measured under backside illumination at different applied biases. All spectra shown in Fig. 2 were obtained at 5 K; to date, temperature dependence has been studied in only the 25 Å/25 Å InAs/Ga₀.₇₅In₀.₂₅Sb superlattice, revealing no appreciable changes in photoconductive response up to 100 K. As can be seen from the figure, photoconductive thresholds are in good agreement with energy gaps derived from photoluminescence. In addition, a photoconductive threshold beyond 15 μm is observed from the 45 Å/28 Å InAs/Ga₀.₇₅In₀.₂₅Sb superlattice.

Figure 2 clearly illustrates the drop in superlattice energy gap as the InSb fraction x is increased from 0 to 0.25, and shows the systematic decrease in energy gap with increasing InAs layer thickness. These dependences are enumerated in Table I, which also compares experimental band gaps with those derived from a two-band model. Calculated gaps are based on a tight-binding model[10] modified to include effects due to strain. This model yielded gaps in good agreement with those of Smith and Mailhiot.[1,2] A column has been added in Table I to identify the extent of arsenic incorporation in our antimonide layers, which initially posed a problem in the growth of these samples.[5] In our calculations, As incorporation is assumed to increase the energy band gaps of the InAs/Ga₁₋ₓInₓSb superlattices by linearly reducing the valence-band offset between
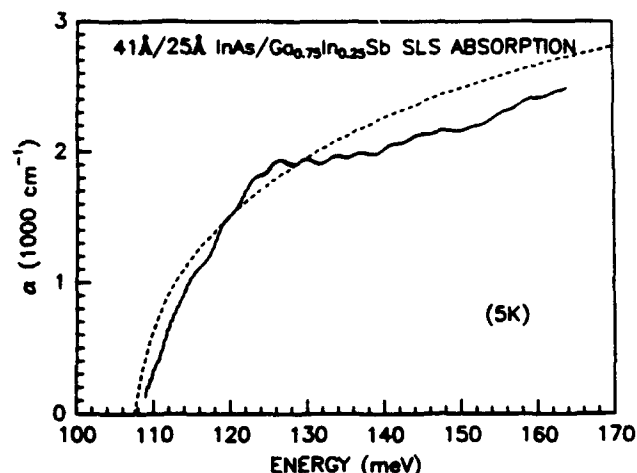
F-2

FIG. 3. Experimental and theoretical absorption coefficients (solid and broken lines, respectively) for a 41 Å/25 Å InAs/$Ga_{0.75}In_{0.25}Sb$ superlattice. Absorption at 10 μm is comparable to that of bulk $Hg_{1-x}Cd_xTe$ with the same energy gap.

arsenide and antimonide layers. The 7% incorporation in our InAs/GaSb superlattice explains the small discrepancy between our energy gap and that expected from the data previously reported for this system.[11] Agreement between the measured and calculated energy gaps in Table I is excellent, given the uncertainties in input parameters associated with calculating the energy gaps.

Experimental and theoretical absorption spectra for a 41 Å/25 Å InAs/$Ga_{0.75}In_{0.25}Sb$ superlattice are shown in Fig. 3. The calculated spectrum was derived from the same two-band tight-binding model used to calculate the superlattice energy gaps. As is apparent from the figure, both the observed energy gap of 108 meV and the measured absorption coefficient are in excellent agreement with theory. The superlattice absorption edge is abrupt, attaining a value of approximately 2000 cm^{-1} at 10 μm. As this value is comparable to that of bulk $Hg_{1-x}Cd_xTe$ with the same gap, we feel it is a promising result for detectors based on InAs/$Ga_{1-x}In_xSb$ superlattices. In addition, the magnitude of this absorption is consistent with the prediction that the perpendicular electron effective mass in the superlattice is greater than that of $Hg_{1-x}Cd_xTe$. Although the oscillator strengths in these type-II superlattices are expected to be smaller than those of $Hg_{1-x}Cd_xTe$, comparable absorption

coefficients were predicted due to the higher density of states associated with larger effective masses in the superlattices.[1] These larger effective masses present potential for improved performance over $Hg_{1-x}Cd_xTe$, as they could suppress tunneling responsible for leakage currents in present detectors.

Our results show promise for long wavelength infrared detectors based on InAs/$Ga_{1-x}In_xSb$ strained-layer superlattices. In particular, we have demonstrated an absorption coefficient comparable to that of bulk $Hg_{1-x}Cd_xTe$ at 10 μm, and have obtained infrared response spanning the 8–14 μm range and beyond in other thin-layer superlattices. Energy gaps derived from photoconductivity and photoluminescence are in excellent agreement with each other and with gaps calculated from a simple two-band model. Quantifying the observed photoconductive response is the subject of ongoing work, as is the issue of doping associated with fabrication of a photovoltaic device.

[1] D. L. Smith and C. Mailhiot, J. Appl. Phys. 62, 2545 (1987).
[2] C. Mailhiot and D. L. Smith, J. Vac. Sci. Technol. A 7, 445 (1989).
[3] L. L. Chang, N. J. Kawai, G. A. Sai-Halasz, R. Ludeke, and L. Esaki, Appl. Phys. Lett. 35, 939 (1979).
[4] D. K. Arch, G. Wicks, T. Tonaue, and J.-L. Staudenmann, J. Appl. Phys. 58, 3933 (1985).
[5] D. H. Chow, R. H. Miles, J. R. Söderström, and T. C. McGill, J. Vac. Sci. Technol. B (to be published).
[6] D. H. Chow, R. H. Miles, J. R. Söderström, and T. C. McGill, Appl. Phys. Lett. 56, 1418 (1990).
[7] C. W. Nieh (unpublished).
[8] J. P. Baukus, A. T. Hunter, O. J. Marsh, C. E. Jones, G. Y. Wu, S. R. Hetzler, T. C. McGill, and J.-P. Faurie, J. Vac. Sci. Technol. A 4, 2110 (1986).
[9] P. M. Petroff, J. Cibert, A. C. Gossard, G. J. Dolan, and C. W. Tu, J. Vac. Sci. Technol. B 5, 1204 (1987).
[10] J. J. Song, Y. S. Yoon, A. Fedotowsky, Y. B. Kim, J. N. Schulman, C. W. Tu, D. Huang, and H. Morkcc, Phys. Rev. B 34, 8958 (1986).
[11] P. Voisin, G. Bastard, C. E. T. Goncalves da Silva, M. Voos, L. L. Chang, and L. Esaki, Solid State Commun. 39, 79 (1981).

F-3

Reprinted from

Growth of Semiconductor Structures and High-Tc Thin Films on Semiconductors

20–21 March 1990
San Diego, California

P

Volume 1285

InAs/Ga$_{1-x}$In$_x$Sb Superlattices for Infrared Applications

R. H. Miles

Hughes Research Laboratories
Malibu, CA 90265

D. H. Chow and T. C. McGill

California Institute of Technology
Pasadena, California 91125

ABSTRACT

We report the successful growth of InAs/Ga$_{1-x}$In$_x$Sb strained-layer superlattices, which have been proposed for far-infrared applications. Samples were grown by molecular beam epitaxy and characterized by reflection high energy electron diffraction, transmission electron microscopy, x-ray diffraction, photoluminescence, and photoconductivity. Excellent structural quality is achieved for superlattices grown on thick, strain relaxed GaSb buffer layers on GaAs substrates at fairly low substrate temperatures ($< 400\,°C$). Photoluminescence and photoconductivity measurements indicate that the energy gaps of the strained-layer superlattices are smaller than those of InAs/GaSb superlattices with the same layer thicknesses, in agreement with the theoretical predictions of Smith and Mailhiot.[1,2] In the case of a 45 Å/28 Å InAs/Ga$_{0.75}$In$_{0.25}$Sb superlattice, an energy gap of 80meV ($> 15\,\mu$m) is measured. These results suggest that far-infrared cutoff wavelengths are compatible with the thin superlattice layers required for strong optical absorption in type-II superlattices.

1. INTRODUCTION

We present results of the first experimental study of InAs/Ga$_{1-x}$In$_x$Sb superlattices, which have been proposed for application as infrared detectors. InAs/Ga$_{1-x}$In$_x$Sb superlattices with $x = 0$ and 0.25 grown by molecular beam epitaxy (MBE) have been characterized structurally by reflection high energy electron diffraction (RHEED), x-ray diffraction, and transmission electron microscopy. Infrared photoluminescence and photoconductive responses have been obtained for the superlattices, yielding experimental energy band gaps. These results have been compared with theoretical gaps derived from a two-band $k \cdot p$ model in reasonable agreement with more sophisticated calculations.

Several superlattices have received attention as alternatives to Hg$_{1-x}$Cd$_x$Te for infrared detection, especially in the $8 - 12\,\mu$m region.[1-5] Difficulties in controlling and reproducing Hg$_{1-x}$Cd$_x$Te alloy band gaps originally stimulated interest in HgTe/CdTe superlattices.[3,4] As pointed out by Smith et al,[4] compositional fluctuations create difficulties in controlling alloy band gaps which can be circumvented by growing superlattice structures consisting of thin, repeated layers of pure HgTe and CdTe. It has been demonstrated that the gap of such a superlattice can be more easily controlled for growth by MBE,[6] as it depends on control of layer thicknesses, rather than composition. In addition to allowing finer control of the small band gaps necessary for long wavelength detection, these superlattices should allow

electronic transport properties to be tailored independently of band gap. In particular, as electrons and holes are confined primarily in the small gap HgTe layers, the superlattice band gap is determined largely by the HgTe layer thicknesses, while transport of electrons normal to the layers is dictated primarily by the thickness of interleaved CdTe barriers. By adding an extra degree of freedom to the structure, it is hoped that electron effective masses can be raised above the bulk $Hg_{0.8}Cd_{0.2}Te$ value of $0.0088m_e$, thereby reducing leakage currents arising from electron tunneling under an applied bias. $HgTe/Hg_{1-x}Cd_xTe$ superlattices are the subject of ongoing research.[7]

Superlattices of $InAs_{1-x}Sb_x$ have also attracted attention as long wavelength detectors,[5,8,9] without the materials problems inherent to $Hg_{1-x}Cd_xTe$. Although the III-V's offer no narrow gap analogue of HgTe ($InAs_{0.39}Sb_{0.61}$ has the smallest bulk alloy gap, $E_g(77K) \simeq 140\,meV$), it was suggested that far infrared energy gaps could be obtained in a strained-layer $InAs_{1-x}Sb_x$ superlattice.[5] Energy gaps in the $8 - 12\,\mu m$ region have been demonstrated for these structures, and infrared detection obtained with photoconductive and photovoltaic devices.[8,9] However, these long wavelength cutoffs have only been achieved for relatively thick layers ($> 75\,Å$). As the $InAs_{1-x}Sb_x/InAs_{1-y}Sb_y$ superlattice confines electrons and holes in different layers, these thick layers result in small electron-hole overlap, which has translated into small absorption coefficients.

We report here a study of $InAs/Ga_{1-x}In_xSb$ strained-layer superlattices, which promise advantages of the $HgTe/Hg_{1-x}Cd_xTe$ and $InAs_{1-x}Sb_x/InAs_{1-y}Sb_y$ superlattices while avoiding some of their pitfalls.[1,2] Like the $InAs_{1-x}Sb_x/InAs_{1-y}Sb_y$ system, far-infrared response in $InAs/Ga_{1-x}In_xSb$ superlattices comes from a type-II band alignment. However, unlike $InAs_{1-x}Sb_x$, effects due to strain are combined with a substantial valence band offset ($\Delta E_v \simeq 510\,meV$). As can be seen in Fig. 1, the unstrained conduction band edge of InAs lies below the unstrained valence band edges of InSb or GaSb. Semimetallic behavior has been reported in the lightly strained InAs/GaSb superlattice,[11] which has been studied extensively.[12-16] However, this is only achieved for InAs layer thicknesses greater than approximately $100\,Å$, resulting in comparatively poor absorption due to the effective localization of electrons and holes in opposite layers of the superlattice. Smith and Mailhiot suggested substituting a $Ga_{1-x}In_xSb$ alloy for GaSb, thereby lowering the gap of the antimonide layer and further misaligning the band edges through strain effects.[1,2] Thus, the bands are sufficiently misaligned that the quantum confinement effects resulting from ultrathin layers are essential for a nonzero band gap. Narrowing the layers to achieve this infrared band gap also increases the electron-hole overlap, improving long-wavelength absorption; absorption coefficients comparable to those of $Hg_{1-x}Cd_xTe$ and greatly exceeding those of $InAs_{1-x}Sb_x$ have been projected for this system. Calculations also yield an electron effective mass $m_e^* \simeq 0.03m_e$ for this superlattice, a value large enough to suppress electron tunneling currents but small enough to permit effective carrier transport after excitation of an electron-hole pair.

2. EXPERIMENTAL

$InAs/Ga_{1-x}In_xSb$ superlattice growth conditions summarized here have been described in detail elsewhere.[17,18] Superlattices were grown by MBE on strain-relaxed GaSb or InAs buffer layers atop (100) GaAs substrates. Growth commenced with deposition of $3000\,Å$ of
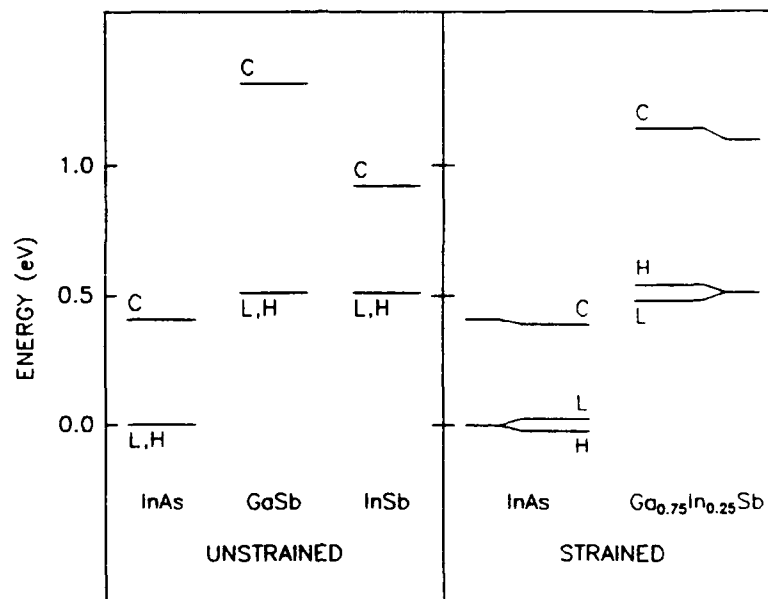
Fig. 1. Alignment of the conduction and valence band edges of bulk and strained InAs, GaSb, and InSb. The generally accepted InAs/GaSb valence band offset of 510meV places the InAs conduction band edge below the GaSb valence band edge,[10] yielding a semimetallic (zero energy gap) band lineup in the absence of quantum confinement. Strain effects further misalign the energy bands, allowing thin layer InAs/$Ga_{1-x}In_xSb$ superlattices to have band gaps tunable throughout the infrared. (After Ref. 1.)

GaAs atop the substrate, followed by growth of a thin, highly strained, short period superlattice (5 periods of an $In_{0.7}Ga_{0.3}As$/GaAs 2 monolayer / 2 monolayer superlattice for subsequent growth of an InAs buffer layer, or 10 periods of a 1 monolayer / 1 monolayer GaSb/GaAs superlattice for an overlying GaSb buffer layer). $0.5 - 1.0\,\mu m$ buffer layers of InAs or GaSb were then grown, at substrate temperatures of $450 - 520\,°C$ or $430 - 520\,°C$, respectively. Previous studies have demonstrated that these preliminary short period superlattices can improve the quality of subsequent overlayers.[19,20] Utilizing this scheme, we achieved threading dislocation densities of roughly $10^9 cm^{-2}$ in the InAs or GaSb buffer layers.[21] Misfit accommodating dislocations necessary to relieve stresses in these structures were confined strictly within these initial short period superlattices.

Several InAs/$Ga_{1-x}In_xSb$ superlattices were grown, with layer thicknesses of $25 - 45$ Å and InSb fractions $x = 0$ and 0.25. Incorporation of background As was found to be a problem in the antimonide layers, but was reduced by lowering the substrate temperature and reducing the As flux. The temperature of the As evaporator was lowered to the point where RHEED patterns indicated a transition from an As- to an In-stabilized surface at a
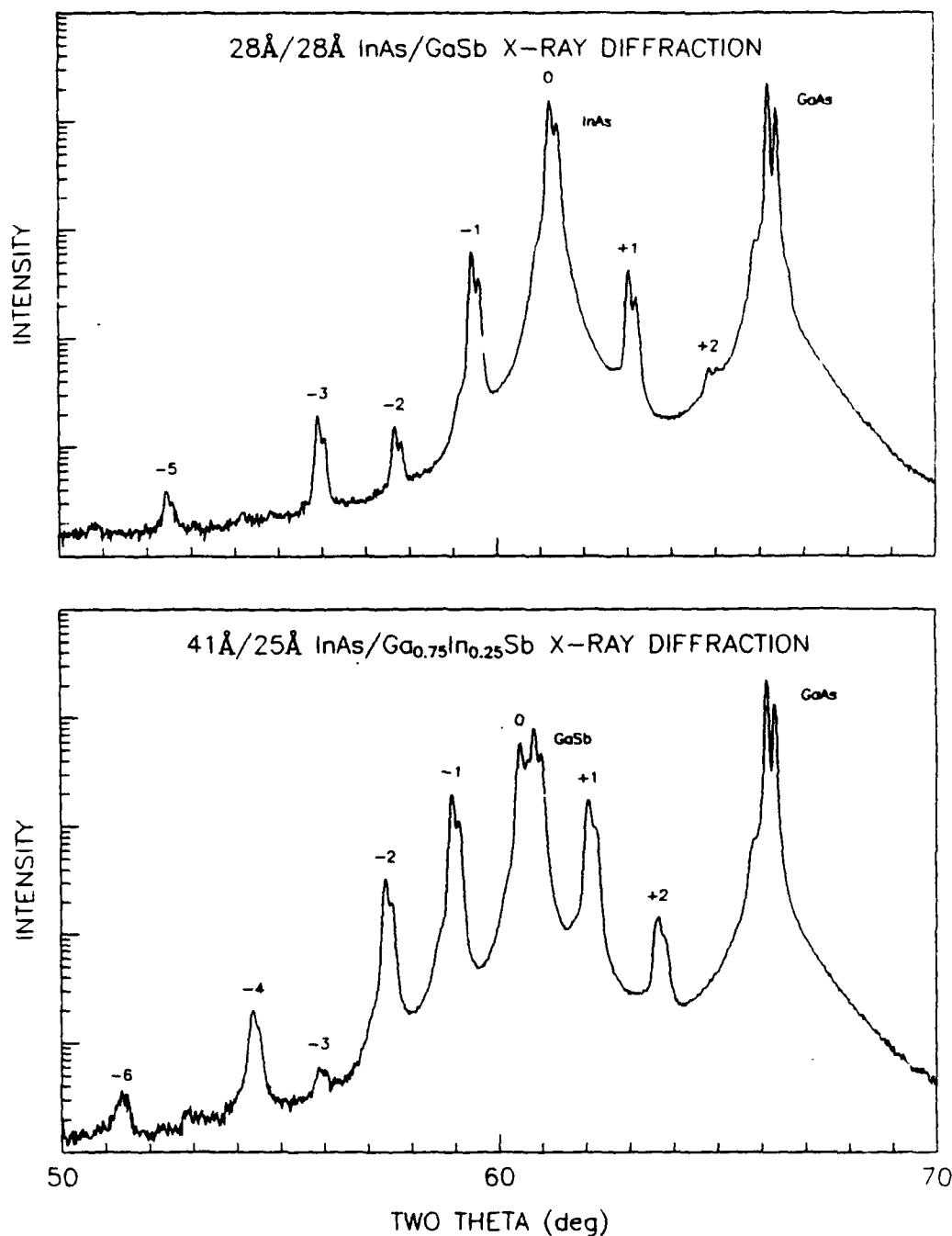
Fig. 2. X-ray diffraction from InAs/GaSb and InAs/Ga$_{0.75}$In$_{0.25}$Sb superlattices. The narrow, regularly spaced superlattice satellite peaks are in good agreement with theory and indicate high structural quality. Doublets are due to separation of the Cu $K\alpha_1$ and $K\alpha_2$ x-ray lines (peak widths are limited by instrumental resolution). Proximity of the zeroth-order superlattice peaks to the buffer layer peaks illustrates the small net strains in these superlattices.

fixed InAs growth rate of 0.2 monolayer/sec. Despite efforts to reduce As incorporation, our Sb layers show residual As fractions of up to 7%.[17] The nature of this incorporation and its possible correlation with background levels of As trimers and tetramers is the subject of ongoing work. High quality $x = 0.25$ superlattices exhibiting x-ray diffraction such as that shown in Fig. 2 could only be achieved for growth temperatures below 400 °C. Bulk InAs and $Ga_{1-x}In_xSb$ and InAs/GaSb superlattices could be grown at substantially higher temperatures, but growth of the InAs/$Ga_{0.75}In_{0.25}Sb$ superlattices at 400 °C or above resulted in poor surface morphology and weak, broad x-ray diffraction peaks. The reason for this disparity between bulk and superlattice growth temperatures is not yet clear, although the lattice mismatch between InAs and $Ga_{0.75}In_{0.25}Sb$ can drive formation of structural defects through a number of thermally activated processes.[22,23]

X-ray diffraction from two of the superlattices is shown in Fig. 2. The scans were taken on a Phillips $\Theta/2\Theta$ diffractometer using a Cu x-ray source. Doublets apparent in the diffraction scans are intrinsic not to the samples but to the Cu x-ray source, due to closely spaced $K\alpha_1$ and $K\alpha_2$ lines; contributions from $K\beta$ were removed with a graphite monochromator and Ni filter. The appearance of numerous sharp, regularly spaced, x-ray satellites is an indication of high structural quality with little interdiffusion.[24] The x=0.25 superlattice was grown on a GaSb buffer layer so as to distribute the strain between both sets of layers in the superlattice. While the individual superlattice layers each lie substantially below predicted elastic limits,[25] it has been demonstrated that strained superlattices can break away as a whole from underlying buffer layers to which they are poorly matched.[26,27] However, our x-ray diffraction data show no evidence of strain relaxation, consistent with the absence of interfacial misfit dislocations in preliminary TEM studies.[21]

Superlattice band gaps have been inferred from low temperature photoluminescence spectra accumulated on a Bomem Fourier Transform Infrared Spectrometer (FTIR). Optical excitation was achieved with a cooled AlGaAs laser diode gated at 40kHz, or with an Ar^+ ion laser gated at the same frequency by an acousto-optic modulator. Luminescence was detected by InSb and HgCdTe detectors cooled to 77K, or by a Si:As detector at 4.2K. Signals were amplified, filtered, and demodulated with a lockin amplifier before passing through the Fourier transform electronics, enabling weak luminescence to be detected against 300K background radiation.

Photoluminescence (PL) spectra from three of the samples are shown in Fig. 3. Luminescence from a 28 Å/28 Å InAs/GaSb superlattice is in excellent agreement with previously reported data.[12] The narrowest peak, from the 25 Å/25 Å InAs/$Ga_{0.75}In_{0.25}Sb$ superlattice, is approximately Gaussian in shape, with a half width of 30meV. This energy spread coincides with the change in superlattice band gap under a single monolayer fluctuation in InAs well thickness (the gap is less sensitive to changes in $Ga_{1-x}In_xSb$ layer thickness). While the reproducibility and uniformity of growth was substantially better than one monolayer, this value clearly represents a lower limit for interfacial fluctuations in a ledge growth mode.[28] Analysis of the luminescence line shapes was not possible for the other superlattices, as luminescence was observed only under high (degenerate) excitation.

We associate the InAs/$Ga_{1-x}In_xSb$ superlattice band gaps with the low energy luminescence cutoffs, assigning the luminescence to a conduction to valence band transition. This
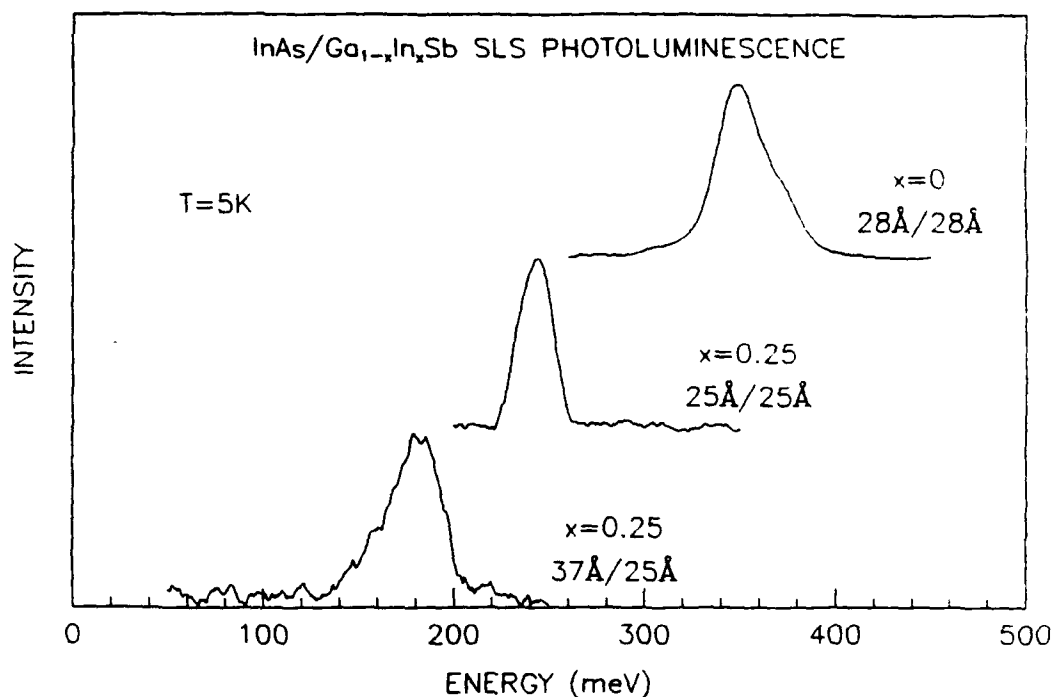
Fig. 3. Photoluminescence at 5K from three InAs/Ga$_{1-x}$In$_x$Sb superlattices, illustrating the shift to longer wavelength (lower energy) with increasing InSb content x or increasing layer thickness.

assignment is consistent with the previous work on InAs/GaSb, and is likely an excellent assumption for the narrower gap superlattices, since binding energies diminish as the band gap narrows. As is apparent from Fig. 3, the addition of In to the antimonide layers clearly has the effect of lowering the energy gap, despite the slightly *greater* thickness of the layers in the InAs/GaSb superlattice examined here. As discussed by Smith and Mailhiot,[1,2] this reduction stems both from strain effects in the superlattice, and from the lowering of the antimonide layer band gap. Maintaining fixed compositions but increasing the InAs layer thickness to 37 Å reduces the gap further, to a value of about 140 meV, or about 9 μm.

Photoconductive responses have been examined in these and other superlattices. Photolithography was used to fabricate mesa structures, with an etch stopping within the superlattice, near the buffer layer interface. Al contacts were evaporated on the top and base of the mesas, and photocurrent measured under backside illumination for different applied biases. As shown in Fig. 4, sharp photoconductive turn-ons have been observed at thresholds in excellent agreement with energy gaps derived from PL. This technique has also been used to estimate energy gaps in superlattices not showing clear luminescence. As expected, we find a systematic decrease in energy gap with increasing InAs layer thickness at a fixed InSb fraction $x = 0.25$. A photoconductive cutoff beyond 15 μm has been observed in a 45 Å/28 Å

InAs/Ga$_{1-x}$In$_x$Sb SLS PHOTOCONDUCTIVITY

(T=4.2K)

x=0.25
45Å/28Å

x=0.25
37Å/25Å

x=0.25
25Å/25Å

x=0
28Å/28Å

CURRENT (arbitrary units)

0   100   200   300   400   500

ENERGY (meV)
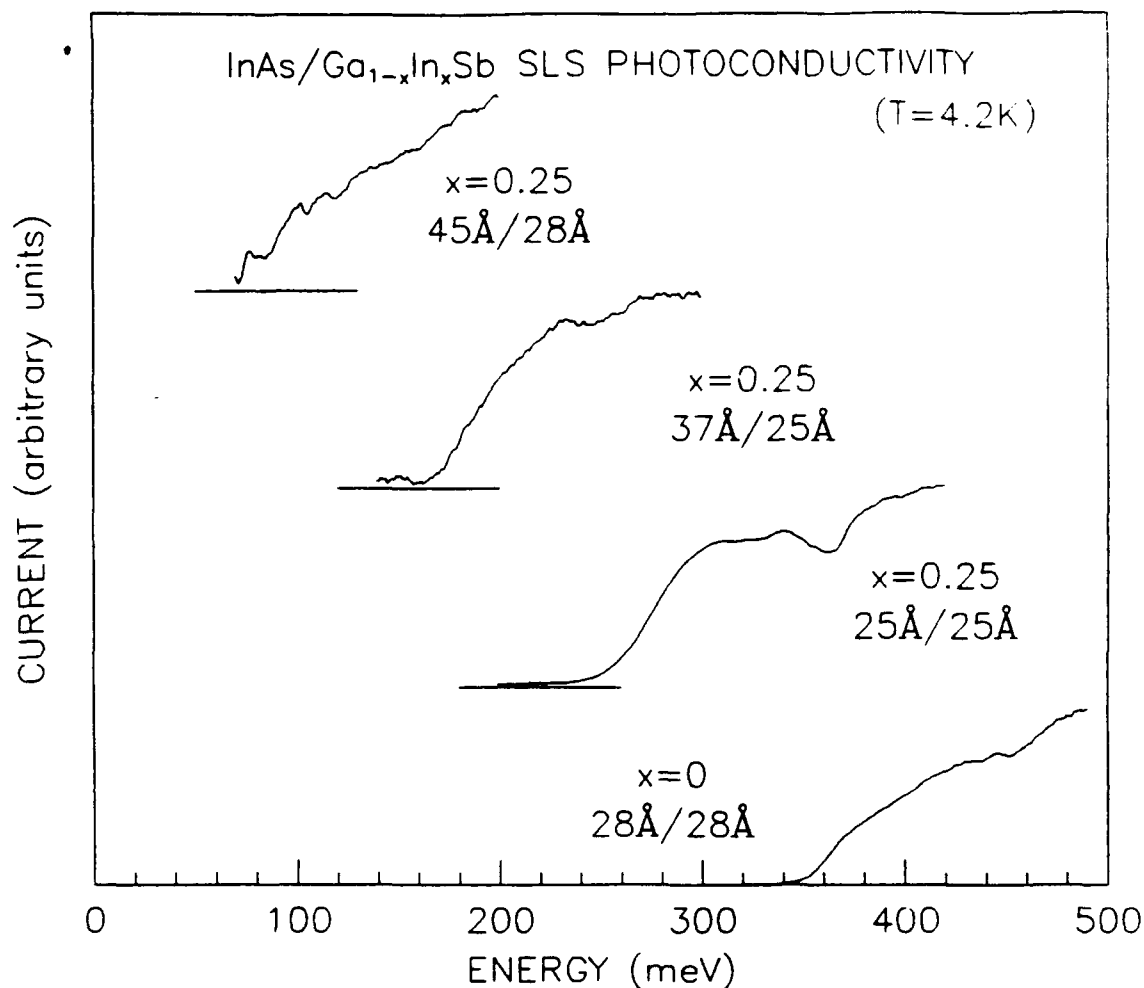
Fig. 4. Low temperature photoconductive response from InAs/Ga$_{1-x}$In$_x$Sb superlattices. Cutoffs are consistent with energy gaps derived from photoluminescence. Infrared response to 15 μm has been demonstrated.

InAs/Ga$_{0.75}$In$_{0.25}$Sb superlattice. Longer wavelengths could clearly be obtained either by further increasing layer thicknesses, or by increasing x, the In content within the antimonide layers. The demonstration of these long wavelength energy gaps in superlattices of layer thicknesses of 45 Å and less is important as it shows that far infrared response is compatible with thin layers in this material system. As explained previously, the type-II band alignment localizes electrons and holes in dissimilar layers, with the consequence that large absorption coefficients are only predicted for thin layer structures, in which the electron-hole overlap remains high.

As shown in Table 1, superlattice energy gaps derived from photoluminescence are in excellent agreement with those inferred from photoconductivity measurements, and in fair

LAYER THICKNESS (Å)			ENERGY GAP (meV)		
InAs	$Ga_{1-x}In_xSb$	x	PL	PC	Theory
28	28	0	330±20	350±10	310
25	25	0.25	230±20	250±10	250
37	25	0.25	150±20	170±10	160
41	25	0.25	*	120±10	140
45	28	0.25	*	80±10	110

Table 1. Comparison of theoretical and experimental energy gaps for five InAs/$Ga_{1-x}In_xSb$ superlattices. Asterisks in the PL column indicate samples in which no luminescence was detected.

agreement with gaps calculated from a two band $k \cdot p$ model. This two band model yielded energy gaps slightly greater than those from the more sophisticated calculations of Smith and Mailhiot.[1,2] The 7% As incorporation in our $Ga_{1-x}In_xSb$ layers was assumed to reduce the Sb/As valence band offset by 7%. This assumption clearly represents an additional source of uncertainty in our calculations. Nevertheless, reasonable agreement between our experimental results and the calculated gaps appears to validate the assumption of a small InSb/GaSb valence band offset.

3. CONCLUSION

We have grown InAs/$Ga_{1-x}In_xSb$ strained-layer superlattices by MBE on GaAs substrates. Substrate temperatures below 400 °C have been shown to yield excellent x-ray diffraction and surface morphology for InAs/$Ga_{0.75}In_{0.25}Sb$ superlattices, whereas raising the temperature yields rough surfaces and weak, broad diffraction peaks. X-ray diffraction shows the superlattices grown at low temperature to be coherently strained, with little interdiffusion. Threading dislocation densities of $10^9 cm^{-2}$ are obtained for a buffer layer scheme utilizing a thin, strained-layer superlattice at the initial GaAs/GaSb or GaAs/InAs buffer interface. Energy gaps derived from photoluminescence and photoconductivity are in excellent agreement with theory, and show that far infrared response can be obtained with these superlattices. A 15 μm energy gap has been obtained in a structure with a 73 Å period, suggesting that large absorption coefficients (obtained only with thin layers in a type-II superlattice) are compatible with long wavelength infrared response in this system.

4. ACKNOWLEDGMENTS

REFERENCES

1. D. L. Smith and C. Mailhiot, "Proposal for strained type II superlattice infrared detectors," *J. Appl. Phys.* **62**, pp. 2545-2548 (1987).

2. C. Mailhiot and D. L. Smith, "Long-wavelength infrared detectors based on strained type-II superlattices," *J. Vac. Sci. Technol. A* **7**, pp. 445-449 (1989).

3. J. N. Schulman and T. C. McGill, "The CdTe/HgTe superlattice: Proposal for a new infrared material," *Appl. Phys. Lett.* **34**, pp. 663-665 (1979).

4. D. L. Smith, T. C. McGill, and J. N. Schulman, "Advantages of the HgTe-CdTe superlattices as an infrared detector material," *Appl. Phys. Lett.* **43**, pp. 180-182 (1983).

5. G. C. Osbourn, "InAsSb strained-layer superlattices for long wavelength detector applications," *J. Vac. Sci. Technol. B* **2**, pp. 176-179 (1984).

6. J. Reno and J.-P. Faurie, "Experimental relation between cut-off wavelength and HgTe layer thickness for HgTe-CdTe superlattices," *Appl. Phys. Lett.* **49**, pp. 409-410 (1986).

7. O. K. Wu, F. A. Shirland, J. P. Baukus, J. N. Schulman, G. S. Kamath, "MBE growth and characterization of Hg-based superlattices," *J. Cryst. Growth* **95**, pp. 594-598 (1989).

8. S. R. Kurtz, G. C. Osbourn, R. M. Biefeld, L. R. Dawson, and H. J. Stein, "Extended infrared response of InAsSb strained-layer superlattices," *Appl. Phys. Lett.* **52**, pp. 831-833 (1988).

9. S. R. Kurtz, L. R. Dawson, R. M. Biefeld, I. J. Fritz, and T. E. Zipperian, "Long-wavelength InAsSb strained-layer superlattice photovoltaic infrared detectors," *IEEE Electron Dev. Lett.* **10**, pp. 150-152 (1989).

10. G. J. Gualtieri, G. P. Schwartz, R. G. Nuzzo, R. J. Malik, and J. F. Walker, "Determination of the (100) InAs/GaSb heterojunction valence-band discontinuity by x-ray photoemission core level spectroscopy," *J. Appl. Phys.* **61**, pp. 5337-5341 (1987).

11. G. A. Sai–Halasz, L. L. Chang, J.-M. Welter, C.-A. Chang, and L. Esaki, "Optical absorption of $In_{1-x}Ga_xAs$-$GaSb_{1-y}As_y$ superlattices," *Solid State Commun.* **27**, pp. 935-937 (1978).

12. L. L. Chang, N. J. Kawai, G. A. Sai-Halasz, R. Ludeke, and L. Esaki, "Observation of semiconductor-semimetal transition in InAs-GaSb superlattices," *Appl. Phys. Lett.* **35**, pp. 939-942 (1979).

13. P. Voisin, G. Bastard, C. E. T. Goncalves da Silva, M. Voos, L. L. Chang, and L. Esaki, "Luminescence from InAs-GaSb superlattices," *Solid State Commun.* **39**, pp. 79-82 (1981).

14. D. K. Arch, G. Wicks, T. Tonaue, J.-L. Staudenmann, "Optical absorption and x-ray diffraction in narrow-band-gap InAs/GaSb superlattices," *J. Appl. Phys.* **58**, pp. 3933-3935 (1985).

15. W. K. Chu, F. W. Saris, C.-A. Chang, R. Ludeke, and L. Esaki, "Ion-beam crystallography of InAs-GaSb superlattices," *Phys. Rev. B* **26**, pp. 1999-2010 (1982).

16. L. L. Chang and L. Esaki, "Electronic properties of InAs-GaSb superlattices," *Surf. Sci.* **98**, pp. 70-89 (1980).

17. D. H. Chow, R. H. Miles, J. R. Söderström, and T. C. McGill, "InAs/$Ga_{1-x}In_xSb$ strained-layer superlattices grown by molecular beam epitaxy," *J. Vac. Sci. Technol. B*, to be published.

18. D. H. Chow, R. H. Miles, J. R. Söderström, and T. C. McGill, "Growth and characterization of InAs/$Ga_{1-x}In_xSb$ strained layer superlattices," *Appl. Phys. Lett.*, to be published.

19. S. Kalem, J. I. Chyi, H. Morkoc, R. Bean, and K. Zanio, "Growth and transport properties of InAs epilayers on GaAs," *Appl. Phys. Lett.* **53** pp. 1647-1649 (1988).

20. J. R. Söderström, D. H. Chow, and T. C. McGill, "MBE-growth of InAs and GaSb epitaxial layers on GaAs substrates," *Mat. Res. Soc. Symp. Proc.* **145**, pp. 409-414 (1989).

21. C. W. Nieh, unpublished.

22. R. H. Miles, T. C. McGill, P. P. Chow, D. Johnson, R. J. Hauenstein, O. J. Marsh, C. W. Nieh, and M. D. Strathman, "Dependence of critical thickness on growth temperature in Ge_xSi_{1-x}/Si superlattices," *Appl. Phys. Lett.* **52**, pp. 916-918 (1989).

23. R. Hull and J. C. Bean, "Thermal stability of Si/Ge_xSi_{1-x}/Si heterostructures," *Appl. Phys. Lett.* **55**, pp. 1900-1902 (1989).

24. B. M. Clemens and J. G. Gay, "Effect of layer-thickness fluctuations on superlattice diffraction," *Phys. Rev. B* **35**, pp. 9337-9340 (1987).

25. J. W. Matthews and A. E. Blakeslee, "Defects in epitaxial materials. III. Preparation of almost perfect multilayers," *J. Cryst. Growth* **32**, pp. 265-273 (1976).

26. R. Hull, J. C. Bean, F. Cerdiera, A. T. Fiory, and J. M. Gibson, "Stability of semiconductor strained-layer superlattices," *Appl. Phys. Lett.* **48**, pp. 56-58 (1986).

27. R. H. Miles, G. Y. Wu, M. B. Johnson, T. C. McGill, J.-P. Faurie, and S. Sivananthan, "Photoluminescence studies of ZnTe-CdTe strained-layer superlattices," *Appl. Phys. Lett.* **48**, pp. 1383-1385 (1986).

28. P. M. Petroff, J. Cibert, A. C. Gossard, G. J. Dolan, and C. W. Tu, "Interface structure and optical properties of quantum wells and quantum boxes," *J. Vac. Sci. Technol. B* **5**, pp. 1204-1208 (1987).

APPENDIX H

INFRARED PHOTOCONDUCTIVITY AND PHOTOLUMINESCENCE FROM InAs/Ga₁₋ₓInₓSb STRAINED-LAYER SUPERLATTICES

R. H. MILES,[*] D. H. CHOW,[**] AND T. C. MCGILL[**]

[*]Hughes Research Laboratories. 3011 Malibu Canyon Road. Malibu. CA 90265

[**]T. J. Watson, Sr., Laboratory of Applied Physics. California Institute of Technology
Pasadena, CA 91125

ABSTRACT

We have examined spectrally resolved photoconductivity and photoluminescence from InAs/Ga₁₋ₓInₓSb strained-layer superlattices. which have been proposed as infrared detectors in the 8-14 μm region. Our measurements indicate that the energy gaps of the strained-layer superlattices are substantially smaller than those of InAs/GaSb superlattices with similar layer thicknesses, in agreement with previous theoretical predictions. Measurements on InAs/Ga₁₋ₓInₓSb superlattices with $x=0$ and 0.25 and layer thicknesses of 25 – 45 Å indicate superlattice band gaps of 3 – 15 μm, in excellent agreement with gaps calculated by a two band $k \cdot p$ model. Our results demonstrate that far-infrared energy gaps are compatible with the thin layers necessary for strong optical absorption in type-II superlattices, and suggest that InAs/Ga₁₋ₓInₓSb superlattices are promising candidates for far-infrared detection.

INTRODUCTION

We present the first optical study of InAs/Ga₁₋ₓInₓSb strained-layer superlattices. Interest in these structures stems from their potential as infrared detectors. especially in the 8 – 14 μm region.[1,2] It has been suggested that InAs/Ga₁₋ₓInₓSb superlattices might enjoy a number of advantages over bulk Hg₁₋ₓCdₓTe (the current industry standard), including lower leakage currents, greater uniformity, and a more readily processed material system.

While InAs and Ga₁₋ₓInₓSb have energy band gaps too large to allow intrinsic bulk absorption in the 8 – 14 μm range, the broken-gap band alignment[3] yields theoretical superlattice gaps at these wavelengths and beyond, tailored by the choices of layer thicknesses and Ga₁₋ₓInₓSb composition.[1,2] Band gaps spanning the 8 – 14 μm range have been demonstrated previously for InAs/GaSb superlattices, but only for comparatively thick constituent layers (> 60 Å).[4-6] As the band alignment in this system localizes electrons and holes in different layers of the superlattice, layers this thick greatly diminish electron-hole overlap, yielding poor absorption coefficients.[6] The addition of In to the GaSb layers was suggested to allay this problem.[1,2] Band edge energies for an InAs/Ga₀.₇₅In₀.₂₅Sb superlattice are indicated in Fig. 1. For fixed layer thicknesses, alloying the antimonide layers was predicted to reduce the superlattice band gap, both by lowering the energy gap of the antimonide layer, and by further misaligning the energy bands through strain effects. As a result, thin layers are essential for raising the InAs/Ga₁₋ₓInₓSb superlattice energy gap out of a semimetallic ("negative" gap) regime to the infrared regions of interest. Reducing the layer thicknesses associated with a particular band gap should, in turn, have the effect of increasing the absorption coefficient; unlike other type-II superlattices, absorption comparable to that in narrow gap Hg₁₋ₓCdₓTe has been calculated for InAs/Ga₁₋ₓInₓSb.

EXPERIMENTAL

MBE growth conditions for our InAs/Ga₁₋ₓInₓSb superlattices are described in detail elsewhere.[7,8] The superlattices have been shown to be of high structural quality, as judged by transmission electron microscopy and x-ray diffraction.[7] Initial optical characterization consisted of low temperature photoluminescence and photoconductivity measurements.
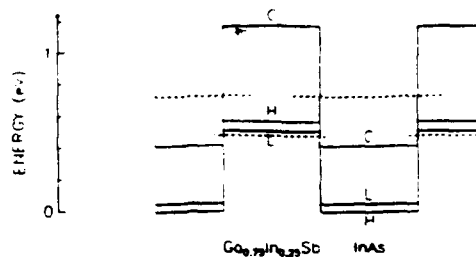
Fig. 1. Energy band edges in a InAs/Ga$_{1-x}$In$_x$Sb superlattice. illustrating the magnitude of the band misalignment and the localization of electrons and holes in the InAs and Ga$_{0.75}$In$_{0.25}$Sb layers of the superlattice, respectively. Bulk heavy-hole. light-hole, and conduction band edges are indicated by solid lines labeled H. L. and C. respectively. Dashed lines indicate the energies of superlattice states weakly localized in different layers.

Photoluminescence spectra were taken on a Bomem Fourier Transform Infrared Spectrometer (FTIR). Samples were mounted on a cold finger with care taken to effectively heat sink the samples to the cold copper block. At high pump powers, possible heating was monitored by analyzing the position and intensity of luminescence from a reference InAs sample. Spectra shown here were obtained at a nominal temperature of 5 K, with a maximum error of approximately +20 K. Optical excitation was achieved with an AlGaAs laser diode cooled to 77 K or, when pump powers greater than 70 mW were required, with an Ar$^+$ ion laser. Luminescence was detected by an InSb or a HgCdTe detector cooled to 77 K, or by a Si:As detector at 4.2 K.

A double modulation technique was necessary to discriminate weak PL signals against a substantial blackbody background.[9] As the FTIR technique derives spectra by modulating input light at comparatively low frequencies (up to ~ 5 kHz in our experiment), we chose to modulate the optical pumps at 40 kHz and monitor mixed sum and difference frequency signals. This modulation was achieved with an acousto-optic cell, in the case of the 514 nm Ar$^+$ pump, or by directly gating the electrical input to the AlGaAs diode. After preamplification, 10 – 20 kHz high-pass filters were used to reduce the (singly modulated) blackbody background relative to the mixed luminescence signal. This filtered signal was then demodulated with a lockin amplifier before returning to the FTIR electronics for analog-to-digital conversion, numerical filtering, and a Fourier transform of the resulting interferogram.

Photoluminescence spectra from three samples are shown in Fig. 2. Consistent with previous work,[10] we associate the broad luminescence from the 28 Å/28 Å InAs/GaSb superlattice with the fundamental conduction to heavy hole valence band transition. Luminescence due to the superlattice was detected only for pump powers greater than 350 mW into approximately 0.1 mm^2; the intensity of this optical pump likely contributed to the observed broadening. Based on the peak assignment, we associate the energy gap with the low energy luminescence edge, $E_g = 330 \pm 10$ meV. This value exceeds those expected from previous studies of InAs/GaSb,[4,6,10] due presumably to arsenic incorporation at levels up to 7% in our antimonide layers. While the effect of this incorporation on the GaSb$_{1-x}$As$_x$ gap is probably small, it might be expected to increase the superlattice band gap by lowering the valence band offset between the InAs and GaSb layers.

Figure 2 illustrates the pronounced shift to lower energy of photoluminescence from an
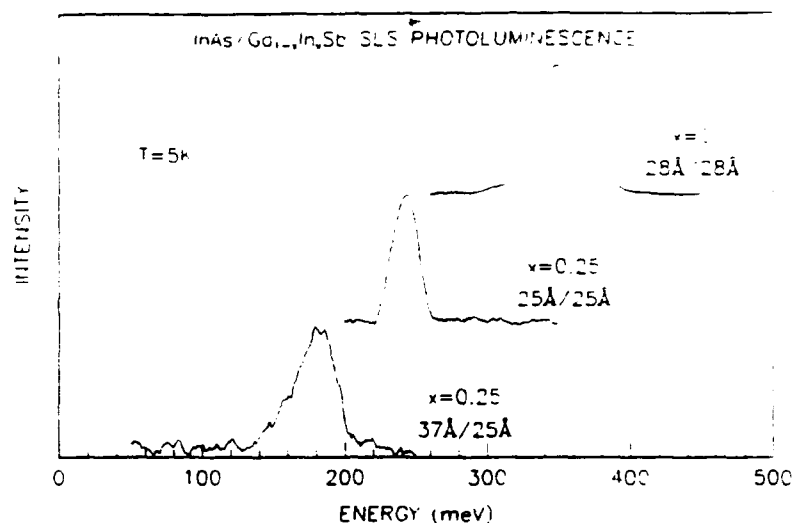
InAs/Ga$_{1-x}$In$_x$Sb SLS PHOTOLUMINESCENCE

T = 5K

x = 0.25
28Å/28Å

x = 0.25
25Å/25Å

x = 0.25
37Å/25Å

INTENSITY

ENERGY (meV)

Fig. 2. Photoluminescence at 5K from three InAs/Ga$_{1-x}$In$_x$Sb superlattices. illustrating the shift to longer wavelength (lower energy) with increasing InSb content x or increasing InAs layer thickness.

InAs/Ga$_{0.75}$In$_{0.25}$Sb superlattice similar in layer thicknesses to the InAs/GaSb structure. The spectrum shown was obtained with a 70 mW AlGaAs laser diode pump, focused to an area of approximately 0.1 mm^2. The luminescence peak is approximately Gaussian in shape, with a half width of 30 meV. This width coincides with the change in superlattice energy gap due to a single monolayer fluctuation in InAs well thickness (the gap is less sensitive to changes in Ga$_{1-x}$In$_x$Sb layer thickness). While the sample-to-sample reproducibility and uniformity of growth was substantially better than one monolayer (x-ray diffraction demonstrated reproducibility of better than 0.1 Å in superlattice period), this value clearly represents a lower limit for interfacial fluctuations in a two-dimensional ledge growth mode.[11] Based on this interpretation, we associate the luminescence peak with the average energy gap, yielding a value $E_g = 240 \pm 10$ meV.

Analysis of the luminescence from the 37 Å/25 Å InAs/Ga$_{0.75}$In$_{0.25}$Sb superlattice was similar to that for the InAs/GaSb structure. As luminescence was apparent only under intense excitation. we assign the gap to the low energy edge, $E_g = 150 \pm 10$ meV. The sample demonstrates the clear shift in band gap to lower energies as InAs layer thickness is increased.

We have spectrally resolved photoconductive response in these and other superlattices. Mesa structures were patterned using photolithography, with an etch stopping within the superlattice. near the buffer layer interface. Aluminum contacts were evaporated on the top and base of the mesas. and photocurrent measured under backside illumination for different applied biases. Figure 3 illustrates the clear photoconductive thresholds observed in four of the samples. This technique yields energy gaps in good agreement with those derived from photoluminescence. and has also been used to estimate gaps in superlattices not showing clear luminescence. As expected, for a fixed InSb fraction $x = 0.25$ we find a systematic decrease in energy gap with increasing InAs layer thickness. As shown
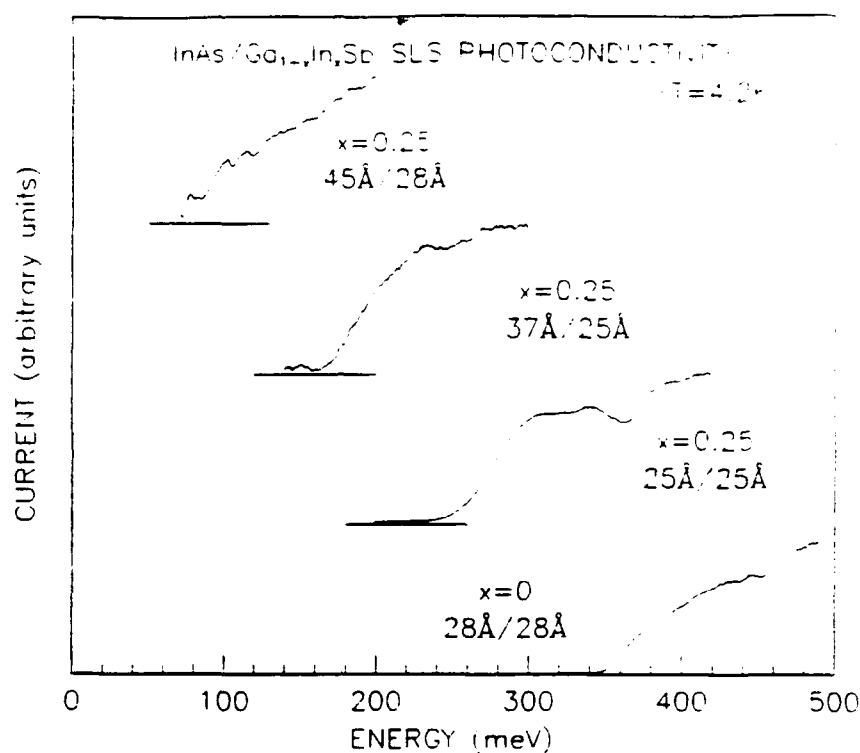
Fig. 3. Low temperature photoconductive response from $InAs/Ga_{1-x}In_xSb$ super-lattices. Cutoffs are consistent with energy gaps derived from photoluminescence. Infrared response to 15 μm has been demonstrated.

in the figure, we have observed a photoconductive cutoff beyond 15 μm in a 45 Å/28 Å $InAs/Ga_{0.75}In_{0.25}Sb$ superlattice. Longer wavelengths could clearly be obtained either by further increasing layer thicknesses, or by increasing x, the In content within the antimonide layers. The experimental confirmation of these long wavelength energy gaps in superlattices of layer thicknesses of 45 Å and less is important as it shows that far infrared response is compatible with thin layers in this material system. As explained previously, the type-II band alignment localizes electrons and holes in dissimilar layers, with tne consequence that large absorption coefficients are only predicted for thin layer structures, in which the electron-hole overlap remains high.

As shown in Table 1, superlattice energy gaps derived from photoluminescence are in excellent agreement with those inferred from photoconductivity measurements, and in reasonable agreement with gaps calculated from a two band $k \cdot p$ model. This two band model yielded energy gaps slightly greater than those from the more sophisticated calculations of Smith and Mailhiot.[1,2] The 7% As incorporation in our $Ga_{1-x}In_xSb$ layers was assumed to reduce the Sb/As valence band offset by 7%. While this assumption clearly represents a source of uncertainty in our calculations, reasonable agreement between our experimental results and the calculated gaps appears to validate the assumption of a small

H-4

LAYER THICKNESS (Å)			ENERGY GAP (meV)		
InAs	$Ga_{1-x}In_xSb$	x	PL	PC	Theory
28	28	0	330±10	350±10	310
25	25	0.25	240±10	250±10	250
37	25	0.25	150±10	170±10	160
41	25	0.25	*	110±10	140
45	28	0.25	*	80±10	110

Table 1. Comparison of theoretical and experimental energy gaps for five InAs/$Ga_{1-x}In_xSb$ superlattices. (Energies can be converted to wavelengths through $E_g(eV) \simeq 1.24/\lambda_g(\mu m)$.) Asterisks in the PL column indicate samples in which no luminescence was detected.

InSb/GaSb valence band offset.

CONCLUSION

Our results show promise for long wavelength infrared detectors based on InAs/$Ga_{1-x}In_xSb$ strained-layer superlattices. Energy gaps derived from photoluminescence and photoconductivity are in excellent agreement with theory, and demonstrate that infrared response spanning the 8 – 14 μm range and beyond can be obtained for thin layer superlattices. In particular, a 15 μm energy gap has been obtained in a structure with a 73 Å period. These results suggest that long wavelength infrared response is compatible with large absorption coefficients (obtained only with thin layers in a type-II superlattice) in this system. Preliminary results suggest that the absorption coefficients in these structures are indeed comparable to those of bulk $Hg_{1-x}Cd_xTe$.[12] This is the subject of ongoing work, as is the issue of doping associated with fabrication of a photovoltaic device.

ACKNOWLEDGMENTS

REFERENCES

1. D. L. Smith and C. Mailhiot. J. Appl. Phys. 62, 2545 (1987).

2. C. Mailhiot and D. L. Smith. J. Vac. Sci. Technol. A 7, 445 (1989)

3. G. J. Gualtieri, G. P. Schwartz, R. G. Nuzzo, R. J. Malik, and J. F. Walker, J. Appl. Phys. 61, 5337 (1987).

4. G. A. Sai-Halasz, L. L. Chang, J.-M. Welter, C.-A. Chang, and L. Esaki. Solid State Commun. 27, 935 (1978).

5. L. L. Chang, N. J. Kawai. G. A. Sai-Halasz, R. Ludeke, and L. Esaki. Appl Phys Lett. 35, 939 (1979).

6. D. K. Arch, G. Wicks, T. Touaue, J.-L. Staudenmann, *J. Appl. Phys.* **58**, 3933 (1985).

7. D. H. Chow, R. H. Miles, J. R. Söderström, and T. C. McGill, *J. Vac. Sci. Technol. B*, to be published.

8. D. H. Chow, R. H. Miles, J. R. Söderström, and T. C. McGill, *Appl. Phys. Lett.* **56**, 1418 (1990).

9. J. P. Baukus, A. T. Hunter, O. J. Marsh, C. E. Jones, G. Y. Wu, S. R. Hetzler, T. C. McGill, and J.-P. Faurie, *J. Vac. Sci. Technol. A* **4**, 2110 (1986).

10. P. Voisin, G. Bastard, C. E. T. Goncalves da Silva, M. Voos, L. L. Chang, and L. Esaki, *Solid State Commun.* **39**, 79 (1981).

11. P. M. Petroff, J. Cibert, A. C. Gossard, G. J. Dolan, and C. W. Tu, *J. Vac. Sci. Technol. B* **5**, 1204 (1987).

12. R. H. Miles, D. H. Chow, J. N. Schulman, and T. C. McGill, submitted to *Appl. Phys. Lett.*

H-6

InAs/Ga$_{1-x}$In$_x$Sb strained-layer superlattices grown by molecular-beam epitaxy

D. H. Chow

T. J. Watson Sr. Laboratory of Applied Physics, California Institute of Technology, Pasadena, California 91125

R. H. Miles

Hughes Research Laboratories, Malibu, California 90265

J. R. Söderström[a] and T. C. McGill

T. J. Watson Sr. Laboratory of Applied Physics, California Institute of Technology, Pasadena, California 91125

We report the successful growth of InAs/Ga$_{1-x}$In$_x$Sb strained-layer superlattices by molecular-beam epitaxy. The superlattices are grown on thick, strain-relaxed InAs or GaSb buffer layers on (100)-oriented GaAs substrates. A short-period, heavily strained superlattice at the GaAs interface is found to improve the structural quality of the buffer layer. Arsenic incorporation in nominally pure GaSb layers is found to depend strongly on substrate temperature and As-background pressure. Best strained-layer superlattice structural quality is achieved for samples grown at fairly low substrate temperatures (< 400 °C). Photoluminescence measurements indicate that the energy gaps of the strained-layer superlattices are smaller than those of InAs/GaSb superlattices with the same layer thicknesses, in agreement with the theoretical predictions of Smith and Mailhiot [J. Appl. Phys. 62, 2545 (1987)]. Far-infrared photoluminescence is observed from a 37/25 Å, InAs/Ga$_{0.75}$In$_{0.25}$Sb superlattice, demonstrating that far-infrared cutoff wavelengths are compatible with short superlattice periods in this material system.

I. INTRODUCTION

The concept of superlattice infrared detectors was first suggested over ten years ago for the case of HgTe/CdTe superlattices as alternatives to Hg$_{1-x}$Cd$_x$Te alloys.[1,2] The advantages of superlattices over bulk materials derive mainly from the fact that layer thicknesses determine superlattice energy gaps, while compositional control is used to select energy gaps in bulk alloys. Epitaxial growth techniques, such as molecular-beam epitaxy (MBE), have made precise layer thickness control possible (to one monolayer in many cases). Hence, superlattices offer improved cutoff wavelength control and uniformity. Furthermore, effective masses can be selected to reduce leakage currents in a superlattice without altering its energy gap. In addition to HgTe/CdTe superlattices, InSb/InAs$_x$Sb$_{1-x}$ strained-layer superlattices have been proposed[3] and studied[4,5] as candidates for infrared detection applications. These (type II) superlattices would allow the extension of III–V growth and processing technology to wavelength ranges unavailable in bulk III–V materials. However, all experimental reports to date of far-infrared cutoff wavelengths in InSb/InAs$_x$Sb$_{1-x}$ superlattices have involved relatively thick layers (> 75 Å).[4,5] These thick layers degrade optical absorption significantly, as they increase the spatial separation between electrons and holes in the superlattice.

Recently, it has been proposed that InAs/Ga$_{1-x}$In$_x$Sb strained-layer superlattices have favorable properties for far-infrared (8–14 μm) detection.[6,7] This material system has type II (staggered) band alignments similar to the heavily studied InAs/GaSb system,[8–14] which is nearly lattice matched. In both cases, the InAs conduction band edge is presumed to be lower in energy than the Ga$_{1-x}$In$_x$Sb (or GaSb) valence band edge, with a positive superlattice energy gap resulting from quantum confinement of the electrons and holes (when the layers are sufficiently thin). The presence of coherent strain between the InAs and Ga$_{1-x}$In$_x$Sb layers shifts the band edges such that the superlattice energy gap is reduced. This shift is advantageous because far-infrared cutoff wavelengths can be obtained with reduced layer thicknesses (< 35 Å), leading to enhanced absorption and transport properties.[6,7] Thus, the InAs/Ga$_{1-x}$In$_x$Sb superlattice is a promising III–V alternative for far-infrared detection.

In this paper, we report the successful growth of far-infrared InAs/Ga$_{1-x}$In$_x$Sb strained-layer superlattices. The samples have been grown by MBE on (100)-oriented GaAs substrates. Structural characterization of the superlattices has been performed by reflection high-energy electron diffraction (RHEED), x-ray diffraction, and transmission electron microscopy (TEM). Far-infrared photoluminescence has been observed, yielding direct measurements of the superlattice energy gaps. Recent measurements of photoconductive response from the samples yield cutoff wavelengths in good agreement with the energy gaps determined by photoluminescence. In addition to exploring potential device applications for InAs/Ga$_{1-x}$In$_x$Sb superlattices, we have studied more fundamental materials issues which may be of consequence for other semiconductor heterostructures. Techniques for depositing high quality InAs and GaSb buffer layers on GaAs substrates have been explored, in an at-

tempt to provide a nearly lattice matched template for growth of the superlattice. We have also studied the degree to which background As is incorporated into GaSb films at different substrate temperatures. Sb fluxes, and As background pressures.

II. GROWTH

All of our samples have been grown by molecular-beam epitaxy (MBE) on (100)-oriented GaAs substrates in a Perkin Elmer 430 system equipped with both arsenic and antimony crackers. Measurements of the substrate temperature were obtained through a thermocouple in contact with a molybdenum block, to which the substrate was bonded with indium. The thermocouple readings were calibrated to optical pyrometer readings above 500 °C, the As-stabilized to In-stabilized transition during InAs growth, and to the GaAs oxide desorption point. Nominal growth rates were calibrated via bulk film thickness measurements and RHEED oscillations measured during homoepitaxial growth of GaAs and InAs. Bulk GaSb (InSb) growth rates were computed by multiplying the GaAs (InAs) rate by the ratio of the lattice constants of the two materials. A "nude" ion gauge was used to monitor the Sb$_2$ and As$_2$ fluxes. Estimates of the absolute As$_2$ flux were made through residual gas analyzer peak heights calibrated to transitions between the As-stabilized and Ga-stabilized RHEED patterns during growth of GaAs.

III. STRUCTURAL CHARACTERIZATION

A. Buffer layers

Techniques for depositing strain–relaxed InAs and GaSb buffer layers on (100)-oriented GaAs substrates have been explored in an attempt to provide a nearly lattice matched template for growth of the superlattice. For each of the two materials. methods employing severely lattice-mismatched superlattices at the GaAs interface have been tested. Similar schemes have been reported to improve epitaxial layer quality (as determined by surface morphology and electron mobility) in some studies.[15,16] Figure 1 illustrates the layer sequences used for the two types of buffers. For InAs layers. growth commenced with 3000 Å of GaAs at a substrate temperature of 600 °C. followed by a five period, 2 monolayer/2 monolayer. In$_0$$_7Ga_0$$_3$As/GaAs "superlattice" at 520 °C. and a 5000-Å thick InAs layer grown at 450–520 °C. GaSb buffer layers consisted of 3000 Å of GaAs grown at 600 °C. followed by a ten period. i monolayer/1 monolayer. GaSb-/GaAs superlattice at 520 °C. and a 5000-Å thick GaSb layer grown at 430–520 °C. Several InAs/Ga$_{1-x}$In$_x$Sb superlattices have been grown on each of the two types of buffer layers. However, we have generally employed GaSb buffer layers for more heavily strained superlattices ($x \simeq 0.25$) because of the intermediate value of the GaSb lattice constant with respect to the two constituent materials.

RHEED patterns observed during growth of the buffer layers became spotty immediately after commencement of the heavily strained superlattices. and regained a streaky appearance after 2 mins (about 300 Å) of growth of the InAs or GaSb bulk layers. The As-stabilized. 2 × 4 surface recon-
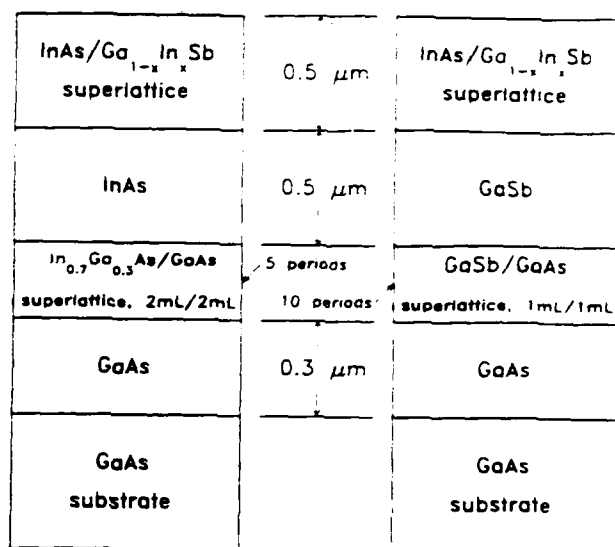

InAs/Ga$_{1-x}$In$_x$Sb superlattice	0.5 μm	InAs/Ga$_{1-x}$In$_x$Sb superlattice
InAs	0.5 μm	GaSb
In$_0$$_7Ga_0$$_3$As/GaAs superlattice. 2mL/2mL	5 perioas 10 perioas	GaSb/GaAs superlattice. 1mL/1mL
GaAs	0.3 μm	GaAs
GaAs substrate		GaAs substrate

FIG. 1. Schematic layer diagram. illustrating the two buffer layering schemes used to grow InAs/Ga$_{1-x}$In$_x$Sb superlattices on (100)-oriented GaAs substrates. The left (right) diagram depicts the method used to grow InAs (GaSb) buffer layers.

struction was observed throughout the InAs layers. while GaSb layers exhibited a characteristic 1 × 3 RHEED pattern. Cross-sectional TEM has been used to examine threading dislocations in the buffer layers and superlattices. The TEM images reveal dense dislocation networks localized at the GaAs/buffer layer interfaces, with the vast majority of dislocations vanishing within 1000 Å of buffer layer growth. The remaining threading dislocations persist through the buffer layer and superlattice with an approximate density of 10^9 cm^{-2}. In spite of these relatively high dislocation densities, the TEM images reveal smooth. planar InAs/Ga$_{1-x}$In$_x$Sb superlattice layers over most of the sample area.

B. Incorporation of background As in GaSb

X-ray diffraction from InAs/GaSb superlattices grown early in our study suggested that significant quantities of As were incorporated into GaSb layers (i.e., GaSb$_{1-x}$As$_x$ layers resulted even with the As-shutter closed). Conversely. Sb was not detectable in InAs layers. due largely to the high sticking coefficient of Sb to the closed shutter. In an attempt to minimize the incorporation of As in nominally pure antimonide layers. we grew a series of 2500 Å GaSb films on InAs buffer layers (which were deposited on GaAs substrates by the technique described in the previous section). X-ray diffraction was then used to measure the lattice constant of the resulting layer. resulting in a determination of x. The effects of substrate temperature. background As pressure (varied by changing the As evaporator temperature with the As-shutter closed). and Sb flux were studied.

Figures 2(a) and 2(b) display $\Theta/2\Theta$ x-ray diffraction data from the (400) planes of two GaSb. As layers grown under different conditions. These two layers represent the maximum and minimum degree of As incorporation

observed in our study (excluding samples grown with the As evaporator turned off). Diffraction peaks from the GaAs substrate and InAs buffer layer are also evident in each figure. The GaSb$_{1-y}$As$_y$ layer which provided the data shown in Fig. 2(a) was grown at a substrate temperature of 520 °C. A high As-background pressure was created by closing the As shutter, and setting the As evaporator to the temperature needed to maintain an As-stabilized InAs surface at a growth rate of 1 monolayer/s (roughly As$_2$/In $\approx$ 10). As-peak heights (As$^+$) on the residual gas analyzer in the MBE chamber are approximately five times higher with the As shutter open than with it closed. The data shown in Fig. 2(b)

were obtained from a GaSb$_{1-y}$As$_y$ layer grown at 450 °C. The As-background pressure was lowered by reducing the As-evaporator temperature to that needed to maintain an As-stabilized InAs surface at a growth rate of 0.2 monolayer/s. For both samples, a GaSb$_{1-y}$As$_y$ growth rate of 0.5 monolayer/s was used. The Sb$_2$ flux was estimated to be a factor of 4 greater than the Ga flux. In fact, our experiments revealed that the magnitude of the Sb$_2$ flux has no effect on As incorporation as long as it is sufficient to maintain an Sb-stabilized surface. The GaSb$_{1-y}$As$_y$ diffraction peak shown in Fig. 2(a) is in between the InAs and GaAs peaks, indicating a 30% incorporation of As in the film ($y \approx 0.3$). In contrast, Fig. 2(b) shows a GaSb$_{1-y}$As$_y$ diffraction peak at approximately the same angle as the peak from the InAs buffer layer, indicating that $y \approx 0.07$. It should be noted that samples grown at substrate temperatures and/or As-background pressures intermediate to those of the two samples discussed here yielded intermediate values of y, with monotonic behavior. These results suggest that As atoms compete strongly with Sb atoms for lattice sites in GaSb$_{1-y}$As$_y$, and that increasing substrate temperature favors increased As incorporation. Considerably different results have been reported for similar experiments on InSb$_{1-y}$As$_y$ films.[17,18] It is possible that the cracked arsenic and antimony sources used here yield significantly different sticking coefficients for the two materials than those obtained from tetrameric sources. However, the degree to which As$_2$ escapes past the closed shutter (during GaSb growth) has not been studied here.

C. Substrate temperature

Several different substrate temperatures have been used for deposition of the InAs/Ga$_{1-x}$In$_x$Sb superlattice layers, spanning the range 370–450 °C. The superlattices exhibited shiny, smooth surfaces for substrate temperatures < 400 °C, while higher substrate temperatures resulted in hazy, rough surfaces. X-ray diffraction peaks were sharpest and most intense for superlattices grown at 390 °C. It should be noted that we have successfully grown InAs and Ga$_{1-x}$In$_x$Sb bulk films with good surface morphology at temperatures as high as 525 and 450 °C, respectively. The need for lower growth temperatures in the case of the superlattice may be a result of interdiffusion and/or strain. RHEED patterns observed during growth of the superlattice indicated a 1 × 3 surface reconstruction for Ga$_{1-x}$In$_x$Sb, and an unusual 2 × 1 reconstruction for InAs.

Figures 3(a) and 3(b) display $\Theta/2\Theta$ x-ray diffraction data for two 100 period InAs/Ga$_{0.75}$In$_{0.25}$Sb superlattices grown at 390 and 450 °C, respectively. Both structures were grown on GaSb buffer layers, deposited by the method described previously. The intensities of the superlattice satellite peaks shown in Fig. 3(a) are in excellent agreement with those predicted by kinematical theory. The widths of the peaks are limited by the resolution of the x-ray diffractometer used here. The intensity and narrowness of the satellite peaks is indicative of highly regular superlattice growth with limited interdiffusion between layers.[19] In contrast, Fig. 3(b) displays broad peaks (note that the $K\alpha$ doublet is not resolved), and lower superlattice satellite intensities.
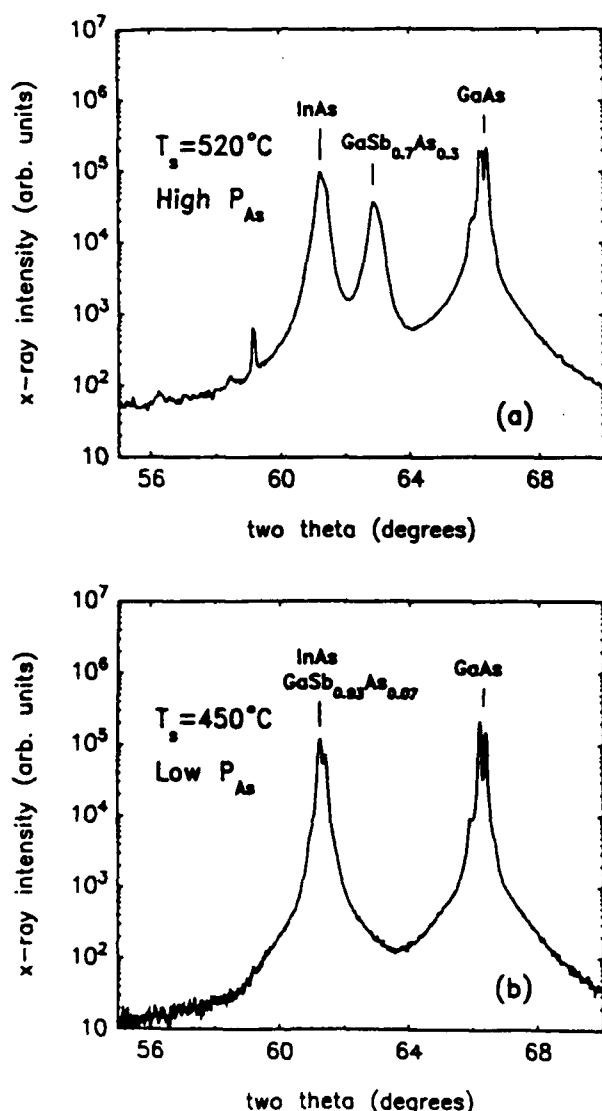

FIG. 2(a) and (b). $\Theta/2\Theta$ x-ray diffraction data from the (400) planes of two nominally pure (As-shutter closed), 2500-Å thick, GaSb films grown on InAs buffer layers. The samples were irradiated with Cu $K\alpha$ x-rays. In both figures, the InAs buffer layer and GaAs substrate diffraction peaks are labeled. The data displayed in (a) were taken from a sample grown at 520 °C under high As-background conditions. Figure (b) shows data taken from a sample grown at 450 °C under low As-background conditions. The measured lattice constants indicate As mole fractions of 0.3 and 0.07 in (a) and (b), respectively.
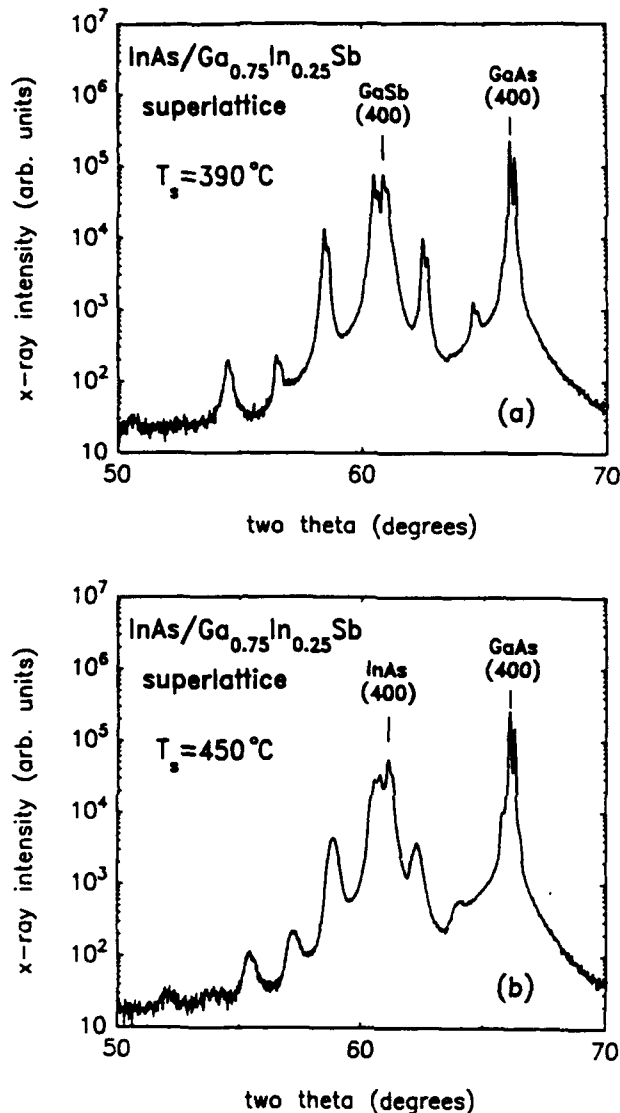
FIG. 3(a) and 3(b). $\Theta/2\Theta$ x-ray diffraction data for two 100 period InAs/Ga$_{0.75}$In$_{0.25}$Sb superlattices grown at 390 and 450 °C, respectively, showing (400)-like diffraction peaks. The samples were irradiated with Cu $K\alpha$ x rays. Each peak in figure (a) appears to be bimodal due to the $K\alpha$ doublet, while the peaks in figure (b) are too broad to resolve the doublet. The substrate (GaAs) and buffer layer (GaSb or InAs) peaks are labeled.

IV. OPTICAL CHARACTERIZATION

Photoluminescence spectra from the strained-layer superlattices have been obtained through a Bomem Fourier transform infrared spectrometer (FTIR). Optical excitation was provided by a cooled AlGaAs laser diode or by an Ar ion laser gated by an acousto-optic modulator. The pump sources were chopped at 40 kHz and the detected signal demodulated with a lock-in amplifier prior to passing through the Fourier transform electronics, enabling weak photoluminescence to be separated from background (blackbody) radiation. Luminescence was detected with an InSb detector cooled to 77 K or with a Si:As detector at 4.2 K.

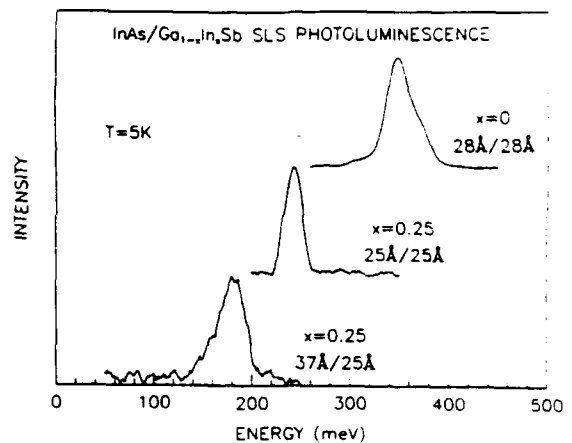Figure 4 displays photoluminescence spectra from three

FIG. 4. Photoluminescence spectra from a three InAs/Ga$_{1-x}$In$_x$Sb superlattices (SL). The top spectrum is from a 28/28 Å SL with $x = 0$, grown on an InAs buffer layer; the middle spectrum is from a 25/25 Å SL with $x = 0.25$, grown on a GaSb buffer layer; and the bottom spectrum is from a 37/25 Å SL with $x = 0.25$, grown on a GaSb buffer layer. All data were taken at 5 K.

InAs/Ga$_{1-x}$In$_x$Sb superlattices with different layer thicknesses and values of x. Comparison of the top two spectra in the figure demonstrates that the energy gap of an InAs/Ga$_{0.75}$In$_{0.25}$Sb superlattice is significantly lower than that of an InAs/GaSb superlattice with slightly greater layer thicknesses. It should be noted that the measured luminescence in the top spectrum is in excellent agreement with previously reported optical measurements from InAs/GaSb superlattices with similar layer thicknesses.[8,9] Furthermore, all of the photoluminescence spectra are in good agreement with the energy gap calculations of Mailhiot and Smith.[6,7] The shift of the strained-layer superlattice energy gap to longer wavelengths is important because good infrared detection requires thin superlattice layers for strong optical absorption (in a type II superlattice) and good transport properties. It is likely that the shift is due to strain-induced movement of the band edges and/or a favorable valence band offset between InSb and GaSb. In either case, increasing the value of x should further reduce the InAs/Ga$_{1-x}$In$_x$Sb superlattice cutoff wavelength. The bottom photoluminescence spectrum in Fig. 4 displays a low energy edge at 140 meV, or approximately 9 μm. This result demonstrates that cutoff wavelengths in or approaching the far-infrared range are obtainable for InAs/Ga$_{1-x}$In$_x$Sb superlattices with thin layers (< 40 Å). Furthermore, we have recently measured the photocurrent generated in the superlattices under an external bias as a function of incident photon energy. The spectra are characterized by sharp photocurrent turn ons at threshold energies which are in good agreement with the photoluminescence spectra in Fig. 4. Additional samples which do not give measureable luminescence have shown photoconductive response as far out as 15 μm.

V. CONCLUSIONS

In conclusion, we have successfully grown InAs/Ga$_{1-x}$In$_x$Sb strained-layer superlattices on GaAs sub-

I-4

strates. Techniques for depositing strain–relaxed InAs and GaSb buffer layers have been explored in an attempt to provide nearly lattice matched templates for growth of the superlattices. Good results have been obtained with a method which employs a short period, heavily strained superlattice at the GaAs/buffer layer interface. Incorporation of As in nominally pure GaSb layers has been found to depend strongly on substrate temperature and As-background pressure. Excellent surface morphology and x-ray diffraction data were obtained for strained-layer superlattices grown on GaSb buffer layers at relatively low substrate temperatures ($< 400\,°C$). Samples grown at higher substrate temperatures exhibited rough surfaces and weak x-ray diffraction. Photoluminescence spectra from strained-layer InAs/$Ga_{0.75}In_{0.25}Sb$ superlattices reveal energy gaps which are significantly lower than those of InAs/GaSb superlattices with similar layer thicknesses, in good agreement with the theoretical predictions of Mailhiot and Smith.[6,7] Furthermore, we have observed far-infrared luminescence from InAs/$Ga_{1-x}In_xSb$ superlattices with short periods (<65 Å). Recent photoconductivity spectra show photocurrent threshold energies (cutoff wavelengths) out to $15\,\mu m$ from superlattices with periods less than 75 Å. These results suggest that large optical absorption coefficients, which are theoretically obtainable only for thin layers in a type II superlattice, are compatible with far-infrared cutoff wavelengths in this material system.

ACKNOWLEDGMENTS

[a] Present address: Chalmers University of Technology, Department of Physics, S-41296, Göteborg, Sweden.

[1] J. N. Schulman and T. C. McGill, Appl. Phys. Lett. **34**, 663 (1979).

[2] D. L. Smith, T. C. McGill, and J. N. Schulman, Appl. Phys. Lett. **43**, 160 (1983).

[3] G. C. Osbourn, J. Vac. Sci. Technol. B **2**, 176 (1984).

[4] S. R. Kurtz, G. C. Osbourn, R. M. Biefeld, L. R. Dawson, and H. J. Stein, Appl. Phys. Lett. **52**, 831 (1988).

[5] S. R. Kurtz, L. R. Dawson, R. M. Biefeld, I. J. Fritz, and T. E. Zipperian, IEEE Electron Device Lett. **10**, 150 (1989).

[6] D. L. Smith and C. Mailhiot, J. Appl. Phys. **62**, 2545 (1987).

[7] C. Mailhiot and D. L. Smith, J. Vac. Sci. Technol. A **7**, 445 (1989).

[8] G. A. Sai-Halasz, L. L. Chang, J.-M. Welter, C.-A. Chang, and L. Esaki, Solid State Commun. **27**, 935 (1978).

[9] P. Voisin, G. Bastard, C. E. T. Goncalves da Silva, M. Voos, L. L. Chang, and L. Esaki, Solid State Commun. **39**, 79 (1981).

[10] D. K. Arch, G. Wicks, T. Tonaue, J.-L. Staudenmann, J. Appl. Phys. **58**, 3933 (1985).

[11] W. K. Chu, F. W. Saris, C.-A. Chang, R. Ludeke, and L. Esaki, Phys. Rev. B **26**, 1999 (1982).

[12] L. L. Chang and L. Esaki, Surf. Sci. **98**, 70 (1980).

[13] B. C. DeCooman, C. B. Carter, G. W. Wicks, T. Tanoue, and L. F. Eastman, Thin Solid Films **170**, 49 (1989).

[14] J. Bleuse, P. Voisin, M. Voos, H. Munekata, L. L. Chang, and L. Esaki, Appl. Phys. Lett. **52**, 462 (1988).

[15] S. Kalem, J. I. Chyi, H. Morkoç, R. Bean, and K. Zanio, Appl. Phys. Lett. **53**, 1648 (1988).

[16] J. R. Söderstrom, D. H. Chow, and T. C. McGill, Mat. Res. Soc. Symp. Proc. **145**, 409 (1989).

[17] M. Y. Yen, B. F. Levine, C. G. Bethea, K. K. Choi, and A. Y. Cho, Appl. Phys. Lett. **50**, 927 (1987).

[18] L. R. Dawson (private communication).

[19] B. M. Clemens and J. G. Gay, Phys. Rev. B **35**, 9337 (1987).

I-5

J. Vac. Sci. Technol. B, Vol. 8, No. 4, Jul/Aug 1990

Growth and characterization of InAs/Ga₁₋ₓInₓSb strained-layer superlattices

D. H. Chow

T. J. Watson Sr. Laboratory of Applied Physics, California Institute of Technology, Pasadena, California 91125

R. H. Miles

Hughes Research Laboratories, Malibu, California 90265

J. R. Söderström[a] and T. C. McGill

T. J. Watson Sr. Laboratory of Applied Physics, California Institute of Technology, Pasadena, California 91125

We report the successful growth of InAs/Ga₁₋ₓInₓSb strained-layer superlattices, which have been proposed for far-infrared applications. The samples were grown by molecular beam epitaxy, and characterized by reflection high-energy electron diffraction, x-ray diffraction, and photoluminescence. Best structural quality is achieved for superlattices grown on thick, strain-relaxed, GaSb buffer layers on GaAs substrates at fairly low substrate temperatures (< 400 °C). Photoluminescence measurements indicate that the energy gaps of the strained-layer superlattices are smaller than those of InAs/GaSb superlattices with the same layer thicknesses, in agreement with the theoretical predictions of Smith and Mailhiot [J. Appl. Phys. 62, 2545 (1987)]. In the case of a 37 Å/25 Å, InAs/Ga₀.₇₅In₀.₂₅Sb superlattice, an energy gap of 140 ± 40 meV ($\approx 9\ \mu m$) is measured. This result demonstrates that far-infrared cutoff wavelengths are compatible with short superlattice periods in this material system.

Superlattices show promise for solving some of the inherent problems associated with far-infrared detector materials. The concept of superlattice infrared detectors was first suggested for the case of HgTe/CdTe superlattices as alternatives to Hg₁₋ₓCdₓTe alloys.[1,2] Two major advantages of superlattices over bulk Hg₁₋ₓCdₓTe are (i) energy gaps are controlled by layer thicknesses rather than by compositions, resulting in enhanced uniformity across a wafer and (ii) leakage currents due to tunneling can be greatly reduced in superlattices without significant increases in energy gaps. It has also been proposed that InSb/InAsₓSb₁₋ₓ superlattices could have far-infrared cutoff wavelengths.[3] This proposal has the advantage of making III-V growth and processing technology available for applications to wavelength ranges which are unobtainable in bulk III-V's. However, all experimental reports to date of far-infrared cutoff wavelengths in InSb/InAsₓSb₁₋ₓ superlattices have involved relatively thick layers (>75 Å).[4,5] These thick layers degrade optical absorption significantly, as they increase the spatial separation between electrons and holes in the superlattice.

Recently, Mailhiot and Smith have proposed that InAs/Ga₁₋ₓInₓSb strained-layer superlattices are candidates for far-infrared applications.[6,7] This material system has type II (staggered) band alignments similar to the heavily studied InAs/GaSb material system,[8-14] which is nearly lattice matched. In both cases, the InAs conduction-band edge is presumed to be *lower* in energy than the InAs/Ga₁₋ₓInₓSb (or GaSb) valence-band edge, with a positive superlattice energy gap resulting from quantum confinement of the electrons and holes (when the layers are sufficiently thin). The presence of coherent strain between the InAs and Ga₁₋ₓInₓSb layers shifts the band edges such that the superlattice energy gap is reduced. This shift is advantageous because far-infrared cutoff wavelengths can be obtained with reduced layer thicknesses, leading to enhanced absorption and transport properties.[6,7] Hence, the InAs/Ga₁₋ₓInₓSb superlattice combines the advantages of the HgTe/CdTe and InSb/InAsₓSb₁₋ₓ superlattices without suffering the disadvantages of either. In this letter, we report the growth of high quality InAs/Ga₁₋ₓInₓSb strained-layer superlattices. The samples have been characterized by reflection high-energy electron diffraction (RHEED), x-ray diffraction, and photoluminescence.

All of our samples have been grown by molecular beam epitaxy (MBE) in a Perkin–Elmer 430 system equipped with both arsenic and antimony crackers. A total of 18 InAs/Ga₁₋ₓInₓSb superlattices have been grown to date, all on (100)-oriented GaAs substrates. Two different buffer layering schemes have been employed in an attempt to provide a nearly lattice-matched template for growth of the superlattice. Both methods employ severely lattice-mismatched superlattices, which have been found to improve buffer layer quality in some studies.[15,16] Figure 1 illustrates the layer sequences used for the two types of buffers. In the first scheme, growth commences with 3000 Å of GaAs at a substrate temperature of 600 °C, followed by a five-period, 2 monolayer/2 monolayer, In₀.₇Ga₀.₃As/GaAs "superlattice" at 520 °C, and a 5000-Å-thick InAs layer grown at 450–520 °C. The second type of buffer layer begins with 3000 Å of GaAs grown at 600 °C, followed by a ten-period, 1 monolayer/1 monolayer, GaSb/GaAs "superlattice" at 520 °C, and a 5000-Å-thick GaSb layer grown at 430–520 °C. RHEED patterns observed during growth of the buffer layers became spotty upon initiation of the heavily strained su-

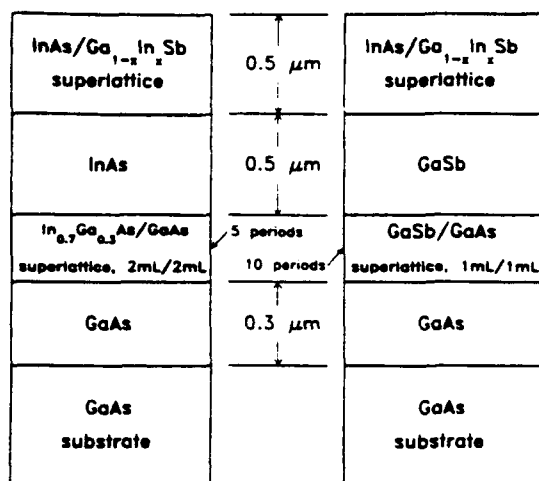[a] Present address: Chalmers University of Technology, Department of Physics, S-41296, Goteborg, Sweden.

FIG. 1. Schematic layer diagram, illustrating the two buffer layering schemes used to grow InAs/Ga$_{1-x}$In$_x$Sb superlattices on (100) GaAs substrates. The left (right) diagram depicts the method used to grow InAs (GaSb) buffer layers.

FIG. 2. $\Theta/2\Theta$ x-ray diffraction data for (a) a 100-period, 25 Å/25 Å InAs/Ga$_{0.75}$In$_{0.25}$Sb superlattice and (b) an 80-period, 37 Å/25 Å. InAs/Ga$_{0.75}$In$_{0.25}$Sb superlattice, showing (400)-like diffraction peaks. The samples were irradiated with Cu $K\alpha$ x rays. Each peak appears to be bimodal due to the $K\alpha$ doublet. The substrate (GaAs) and buffer layer (GaSb) peaks are labeled.

perlattices, and regained a streaky appearance after 2 min (about 300 Å) of growth of the InAs or GaSb bulk layers. The superlattices which yielded the best x-ray diffraction data were grown on GaSb buffer layers, which may be a result of the intermediate value of the GaSb lattice constant with respect to the two constituent materials in the superlattice.

Several different substrate temperatures have been used for deposition of the InAs/Ga$_{1-x}$In$_x$Sb superlattice layers, spanning the range 370–450 °C. Measurements of the substrate temperature were obtained through a thermocouple in contact with a molybdenum block, to which the substrate was bonded with indium. The thermocouple readings were calibrated to the As-stabilized to In-stabilized transition during InAs growth, and to the GaAs oxide desorption point. The superlattices exhibited shiny, smooth surfaces for substrate temperatures <400 °C, while higher substrate temperatures resulted in hazy, rough surfaces. X-ray diffraction peaks were sharpest and most intense for superlattices grown at 390 °C. It should be noted that we have successfully grown InAs and Ga$_{1-x}$In$_x$Sb bulk films with good surface morphology at temperatures as high as 525 and 450 °C, respectively. The need for lower growth temperatures in the case of the superlattice may be a result of interdiffusion and/or strain. RHEED patterns observed during growth of the superlattice indicated a 1×3 surface reconstruction for Ga$_{1-x}$In$_x$Sb, and an unusual 2×1 reconstruction for InAs.

Figures 2(a) and 2(b) display $\Theta/2\Theta$ x-ray diffraction data for a 100-period, 25 Å/25 Å, InAs/Ga$_{0.75}$In$_{0.25}$Sb superlattice (sample B in Table I), and an 80-period, 37 Å/25 Å. InAs/Ga$_{0.75}$In$_{0.25}$Sb superlattice (sample C in Table I), respectively. Both structures were grown on GaSb buffers at 390 °C. The intensities of the superlattice satellite peaks shown in Figs. 2(a) and 2(b) are in excellent agreement with those predicted by kinematical theory. The widths of the peaks are limited by the resolution of the x-ray diffractometer used here. The intensity and narrowness of the satellite peaks is indicative of highly regular superlattice growth
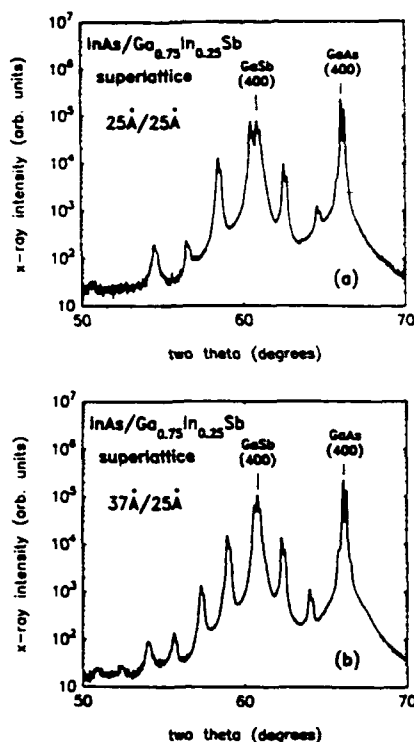
with limited interdiffusion between layers.[17] For both superlattices, the period projected from calibrated MBE growth rates agrees to within 2 Å of the actual period determined from the spacings of the x-ray satellites.

Photoluminescence spectra from the strained-layer superlattices were obtained through a Bomem Fourier transform infrared spectrometer (FTIR). Optical excitation was provided by a cooled AlGaAs laser diode or by an Ar ion laser gated by an acousto-optic modulator. The pump sources were chopped at 40 kHz and the detected signal demodulated with a lock-in amplifier prior to passing through the Fourier transform electronics, enabling weak photolu-
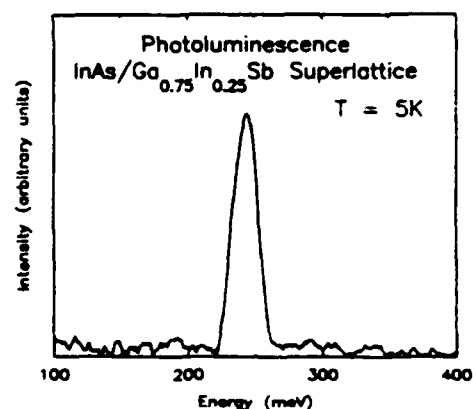

FIG. 3. Photoluminescence spectrum from a 100-period, 25 Å/25 Å. InAs/Ga$_{0.75}$In$_{0.25}$Sb superlattice. The spectrum was taken at 5 K.

Appl. Phys. Lett., Vol. 56, No. 15, 9 April 1990

J-2

Chow et al.

TABLE I. Structural parameters and energy gaps for three $InAs/Ga_{1-x}In_xSb$ superlattices. Layer thicknesses and composition x were estimated from calibrated MBE growth rates. Theoretical energy gaps were calculated through a two-band $k \cdot p$ model which yielded results in close agreement with those of Mailhiot and Smith.[a,b] Measured energy gaps were determined from photoluminescence data.

Sample	Periods	x	$Ga_{1-x}In_xSb$ layer thickness (Å)	InAs layer thickness (Å)	Energy gap (meV)	
					Theory	Measured
A	100	0	28	28	350	330 ± 20
B	100	0.25	25	25	250	220 ± 20
C	80	0.25	25	37	160	140 ± 40

[a] Reference 6.
[b] Reference 7.

minescence to be separated from background (blackbody) radiation. Luminescence was detected with an InSb detector cooled to 77 K or with a Si:As detector at 4.2 K.

Figure 3 is the photoluminescence spectrum obtained from sample B. The spectrum displays a peak centered at 240 meV. The full width at half maximum of the photoluminescence peak is 25 meV, which is comparable to the energy gap variation expected for layer thickness fluctuations of one monolayer.[6,7] The narrowness of the peak suggests that the luminescence is due to radiative conduction-to-valence band recombination, which is consistent with the analysis of Ref. 9. In keeping with this assignment, we associate the superlattice energy gap with the low-energy edge of the luminescence peak.

Table I lists the energy gaps of samples A, B, and C, determined through photoluminescence. The estimated uncertainties listed in the table were obtained from the widths of the photoluminescence peaks. Comparison of the table entries for samples A and B demonstrates that the energy gap of the $InAs/Ga_{0.75}In_{0.25}Sb$ superlattice is significantly lower than that of an InAs/GaSb superlattice with slightly greater layer thicknesses. It should be noted that the measured energy gap of sample A is in excellent agreement with previously reported optical measurement from InAs/GaSb superlattices with similar layer thicknesses.[8,9] Furthermore, all of the measured energy gaps listed in Table I are consistent with the theoretical predictions of Mailhiot and Smith.[6,7] The shift of the strained-layer superlattice energy gap to longer wavelengths is important because good infrared detection requires thin superlattice layers for strong optical absorption (in a type II superlattice) and good transport properties. It is likely that the shift is due to strain-induced movement of the band edges and/or a favorable valence-band offset between InSb and GaSb. In either case, increasing the value of x should further reduce the $InAs/Ga_{1-x}In_xSb$ superlattice cutoff wavelength. As shown in Table I, the energy gap of sample C is 140 ± 40 meV, or $\sim 9 \mu m$. This result demonstrates that cutoff wavelengths in or approaching the far-infrared range are obtainable for $InAs/Ga_{1-x}In_xSb$ superlattices with thin layers (< 40 Å).

In conclusion, we have successfully grown $InAs/Ga_{1-x}In_xSb$ strained-layer superlattices on GaAs substrates. Excellent surface morphology and x-ray diffraction data were obtained for superlattices grown on GaSb buffer layers at relatively low substrate temperatures (< 400 °C). Samples grown on InAs buffer layers at higher substrate temperatures exhibited rough surfaces and weak x-ray diffraction. Photoluminescence spectra from strained-layer $InAs/Ga_{0.75}In_{0.25}Sb$ superlattices display narrow peaks consistent with direct recombination of electrons and holes in the conduction and valence bands, respectively. The measured energy gaps of the strained-layer superlattices are significantly lower than those of InAs/GaSb superlattices with similar layer thicknesses, in good agreement with the theoretical predictions of Mailhiot and Smith.[6,7] Furthermore, we have demonstrated that $InAs/Ga_{1-x}In_xSb$ superlattices with short periods (< 65 Å) can have cutoff wavelengths in or approaching the far-infrared range. These results suggest that large optical absorption coefficients, which are theoretically obtainable only for thin layers in a type II superlattice, are compatible with far-infrared cutoff wavelengths in this material system.

[1] J. N. Schulman and T. C. McGill, Appl. Phys. Lett. 34, 663 (1979).
[2] D. L. Smith, T. C. McGill, and J. N. Schulman, Appl. Phys. Lett. 43, 160 (1983).
[3] G. C. Osbourn, J. Vac. Sci. Technol. B 2, 176 (1984).
[4] S. R. Kurtz, G. C. Osbourn, R. M. Biefeld, L. R. Dawson, and H. J. Stein, Appl. Phys. Lett. 52, 831 (1988).
[5] S. R. Kurtz, L. R. Dawson, R. M. Biefeld, I. J. Fritz, and T. E. Zipperian, IEEE Electron Device Lett. 10, 150 (1989).
[6] D. L. Smith and C. Mailhiot, J. Appl. Phys. 62, 2545 (1987).
[7] C. Mailhiot and D. L. Smith, J. Vac. Sci. Technol. A 7, 445 (1989).
[8] G. A. Sai-Halasz, L. L. Chang, J.-M. Welter, C.-A. Chang, and L. Esaki, Solid State Commun. 27, 935 (1978).
[9] P. Voisin, G. Bastard, C. E. T. Goncalves da Silva, M. Voos, L. L. Chang, and L. Esaki, Solid State Commun. 39, 79 (1981).
[10] D. K. Arch, G. Wicks, T. Tonaue, and J.-L. Staudenmann, J. Appl. Phys. 58, 3933 (1985).
[11] W. K. Chu, F. W. Saris, C.-A. Chang, R. Ludeke, and L. Esaki, Phys. Rev. B 26, 1999 (1982).
[12] L. L. Chang and L. Esaki, Surf. Sci. 98, 70 (1980).
[13] B. C. DeCooman, C. B. Carter, G. W. Wicks, T. Tanoue, and L. F. Eastman, Thin Solid Films 170, 49 (1989).
[14] J. Bleuse, P. Voisin, M. Voos, H. Munekata, L. L. Chang, and L. Esaki, Appl. Phys. Lett. 52, 462 (1988).
[15] S. Kalem, J. I. Chyi, H. Morkoç, R. Bean, and K. Zanio, Appl. Phys. Lett. 53, 1648 (1988).
[16] J. R. Söderstrom, D. H. Chow, and T. C. McGill, Mater. Res. Soc. Symp. Proc. 145, 409 (1989).
[17] B. M. Clemens and J. G. Gay, Phys. Rev. B 35, 9337 (1987)